ENHANCING THE PROPERTIES OF SPHERICAL NUCLEIC ACIDS

TUNING THE BIOLOGICAL PROPERTIES OF SPHERICAL NUCLEIC ACIDS WITH PHOSPHATE BACKBONE MODIFIED OLIGONUCLEOTIDES

By, JOSEPH MAGGISANO, B.Sc.

A Thesis Submitted to the School of Graduate Studies in Partial Fulfilment of the Requirements for the Degree Master of Science

McMaster University MASTER OF SCIENCE (2023) Hamilton, Ontario (Department of Chemistry and Chemical Biology)

TITLE: Tuning the Biological Properties of Spherical Nucleic Acids with Phosphate Backbone Modified Oligonucleotides

AUTHOR: Joseph Maggisano, B.Sc. (McMaster University)

SUPERVISOR: Dr. Katherine Bujold

NUMBER OF PAGES: xx, 101

LAY ABSTRACT

Oligonucleotides are short synthetic sequences of DNA or RNA that have the capacity to treat diseases at the genetic level. However, they face challenges such as degradation, low cell uptake, and poor tissue distribution. To overcome this issue, we plan to incorporate chemical modifications at the phosphate backbone of oligonucleotides to make them more stable and facilitate more favourable interactions at cell membranes. Conferring oligonucleotides into a 3D arrangement further enhances their stability and cell uptake relative to linear oligonucleotides. By densely functionalizing them onto a nanoparticle core, we can create spherical nucleic acids (SNAs). We hypothesize that the modifications imparted onto the phosphate backbone of linear oligonucleotides will translate their properties into SNAs. The new properties afforded to the SNAs will provide increased cell uptake, alternative uptake mechanisms, and access to cytosolic and nuclear targets, highlighting their potency and therapeutic potential.

ABSTRACT

The increasing number of nucleic acid-based therapeutics demonstrates the potential to treat diseases at the genetic level. Although oligonucleotides show clinical potential, challenges remain including nuclease degradation, rapid clearance when administered systemically, low cell permeability, and limited distribution to tissues of interest. This is largely imparted by the polyanionic phosphate backbone, which produces unfavourable electrostatic interactions at cell membranes. As a result, their clinical translation is dependent on delivery technologies that improve stability, facilitate cell entry, and increase target affinity. Spherical nucleic acids (SNAs) consist of radially orienting linear nucleic acids onto a nanoparticle core, conferring them a three-dimensional, spherical architecture. These structures enter cells readily and display distinct properties that are independent of their nanoparticle core. Accordingly, we decided to replace the intrinsically anionic phosphodiester linkage of DNA with a phosphoramidate linkage (P-N), allowing us to incorporate new functionality at the phosphate backbone. With this handle, we inserted cationic and hydrophobically modified functional groups that were compatible with nanoscale architectures, giving rise to new properties relevant in biological contexts. Specifically, amine and guanidinium derivatized functional groups provided SNAs with a ~10-fold increase in cell uptake at early incubation times compared with unmodified SNAs. This demonstrates that we can tune the behaviour of SNAs with phosphate backbone modifications in a highly controlled manner. We hypothesize that the stringent control over location

and placement of functional groups within the SNA framework will afford them favourable interactions at cell membranes, not only increasing their cell uptake, but also access to alternative uptake mechanisms and potency as therapeutics.

ACKNOWLEDGEMENTS

I would like to express my sincerest gratitude to Dr. Katherine Bujold, my research supervisor, for her invaluable guidance and unwavering support. She exceeded every expectation as a research supervisor and exemplified true mentorship, fostering an environment that nourished me both academically and cordially. I would also like to extend my gratitude to my lab members for their collaborative spirit and insightful discussions that enriched my work. I appreciate every lab member for their contributions, making this academic journey exceptional. To Dr. Bujold and my lab members, your dedication and camaraderie have not only impacted my academic pursuits but also my personal growth significantly.

I would also like to thank the BioInterfaces Institute for granting me access to their instrumentation. Namely, Dr. Yang Yang for training and assisting me with MALDI-TOF MS and Dr. Zeynel Bayindir with DLS. Additionally, I would also like to thank Dr. Carmen Andrei and the Canadian Centre for Electron Microscopy for granting me access to the Talos L120C for all TEM images and Hong Liang of the McMaster Core Flow facility for assisting and training me on the CytoFLEX LX Flow Cytometer.

Moreover, I would like to acknowledge the Brockhouse Institute for Materials Research for granting Rik Chuiko (Ayers group) and I the inaugural Future Materials Innovators Program grant. This grant allowed us to purse an original research idea and gave us a platform to share our research across multiple departments.

Furthermore, I would like to thank my committee members Dr. Alex Adronov and Dr. Ryan Wylie for the critiques and valuable insight they provided me during committee meetings. Lastly, I would like to thank the Wylie lab for generously sharing equipment and reagents during my research.

TABLE OF CONTENTS

LIST OF FIGURES

LIST OF SUPPLEMENTARY FIGURES

LIST OF TABLES

LIST OF ABBREVIATIONS

1D	One dimensional
3D	Three dimensional
ACN	Acetonitrile
APS	Ammonium persulfate
ASO	Antisense oligonucleotide
AuNP	Gold nanoparticle
BBB	Blood-brain barrier
CNS	Central nervous system
CPP	Cell penetrating peptide
Cy5	Cyanine 5
DHAP	2,6-dihydroxyacetophenone
DLS	Dynamic light scattering
DMEM	Dulbecco's modified eagle's medium
DMSO	Dimethyl sulfoxide
DMT	Dimethoxytrityl
DNA	Deoxyribonucleic acid
DTT	Dithiothreitol
EDTA	Ethylenediaminetetraacetic acid
FBS	Fetal bovine serum
HPLC	High performance liquid chromatography
KCN	Potassium cyanide
LNA	Locked nucleic acid
LNP	Lipid nanoparticle
MALDI-TOF MA	Matrix-assisted laser desorption ionization time-of-flight mass spectrometry
mRNA	messenger ribonucleic acid
MW	Molecular weight
NMR	Nuclear magnetic resonance
OD	Optical density
PAGE	Polyacrylamide gel electrophoresis
PBS	Phosphate-buffered saline
P-N	Phosphoramidate
P-O	Phosphodiester
P-S	Phosphorothioate
RNA	Ribonucleic acid
RNase H	Ribonuclease H
SDS	Sodium dodecyl sulfate
SEC	Size exclusion chromatography
siRNA	Small interfering RNA
SNA	Spherical nucleic acid
T	Thymine

TBE	Tris-boric acid-EDTA buffer
TCEP	tris(2-carboxyethyl)phosphine
TEA	Triethylamine
TEAA	Triethylammonium acetate
TEM	Transmission electron microscopy
TEMED	Tetramethylethylenediamine
THF	Tetrahydrofuran
TLC	Thin-layer chromatography
Tris	Tris(hydroxymethyl)aminomethane
UV-Vis	Ultraviolet-visible

DECLARATION OF ACADEMIC ACHIEVEMENT

I, Joseph Maggisano, hereby declare that the thesis entitled "Tuning the Biological Properties of Spherical Nucleic Acids with Phosphate Backbone Modified Oligonucleotides" submitted in partial fulfillment of the requirements for the degree of Master of Science at McMaster University is the result of my original research and has not been previously submitted for any other degree or qualification.

CHAPTER 1 – INTRODUCTION

Oligonucleotide Based Therapeutics

Oligonucleotides are short synthetic oligomers of DNA or RNA, typically less than 100 bases, that can be synthesized using automated protocols with full control over their sequence and position of functional groups. Recently, they have garnered significant interest for clinical applications since they can be tailored to treat a wide variety of genetic and neurodegenerative diseases.[1,2] In the context of therapeutics, the majority of oligonucleotides interact with their biological target via complementary Watson-Crick base pairing to modulate gene expression. This sequence specific complementarity suggests that oligonucleotides need to exhibit unparalleled specificity for their targets, reducing the possibility for off-target and deleterious side effects.[3,4] Stephenson and Zamecnik first elucidated the approach to use oligodeoxyribonucleotides to hybridize with their biological targets and silence gene expression via inhibition of Rous sarcoma viral RNA translation.[5] This pioneering work paved the way for the use of synthetic oligonucleotides to silence or modulate gene expression, and subsequent protein production. Antisense oligonucleotides (ASOs) in particular, can modulate the expression of genes through various mechanisms including RNase H dependent and steric blocking pathways.[6] The RNase H dependent mechanism relies on the recognition of DNA-RNA heteroduplex substrates by RNase H1, an enzyme that catalyzes the degradation of target RNA, effectively silencing or downregulating the expression of disease-causing genes (**Figure 1a**). The steric blocking pathway is typically used for the modulation of alternative splicing, whereby a splice correction is used to either retain or exclude specific exons that encode for proteins (**Figure 1b**).[6–8]

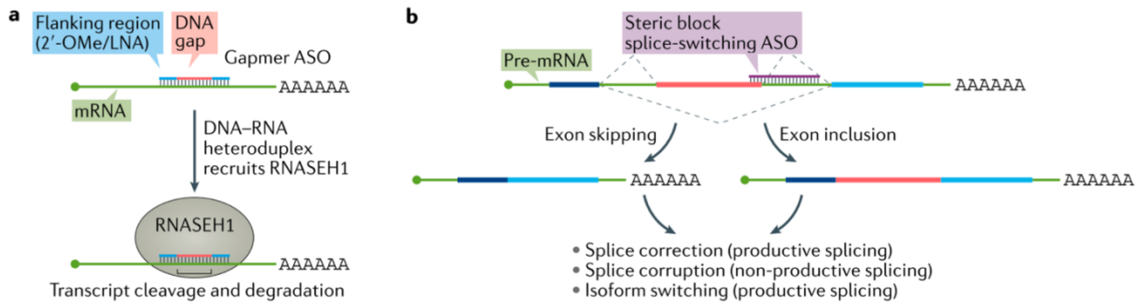

Figure 1. *a) RNase H1 degradation. ASO binds to target mRNA with high affinity. The RNA-DNA duplex is recognized by RNase H1 and degrades the transcript. b) Steric block. ASO binds to pre-mRNA and induces alternative splicing through exon skipping or inclusion.*[6]

An example of a splice modulating ASO is Nusinersin (Spinraza®), an FDA approved oligonucleotide which treats patients with spinal muscular atrophy (SMA) by increasing the amount of functional survival motor neuron (SMN) protein. Additionally, the desirable properties of oligonucleotides including their biocompatibility, programmability, water solubility, and ease of synthesis has highlighted them as an emerging class of biologics for personalized medicine.[9] Since they can be designed to target any gene of interest with high selectivity, oligonucleotides hold the potential to target patient specific sequences associated with rare disease pathologies.[10]

Challenges of Oligonucleotide Drug Delivery

Although oligonucleotides show clinical potential, they still face challenges as they are being translated to the clinic including nuclease degradation, rapid clearance when administered systemically, low cell permeability, and limited distribution to tissues of interest.[1] Additionally, their polyanionic phosphate backbone leads to repulsion at cell membranes due to unfavourable electrostatic interactions, drastically reducing their uptake into various tissues and cell types.[11] Another limitation to the clinical translation of oligonucleotides is their inability to effectively escape endosomal entrapment, limiting access to cytosolic and nuclear targets.[12] To overcome these challenges, many strategies have been implemented including chemical modifications on the nucleobase, sugar modifications at the 2' position (i.e., 2'-O-methoxyethyl, 2'F), backbone modifications (i.e., phosphorothioate), and use of alternate chemistries such as locked nucleic acids (LNAs) and peptide nucleic acids (PNAs) (**Figure 2**).[6]

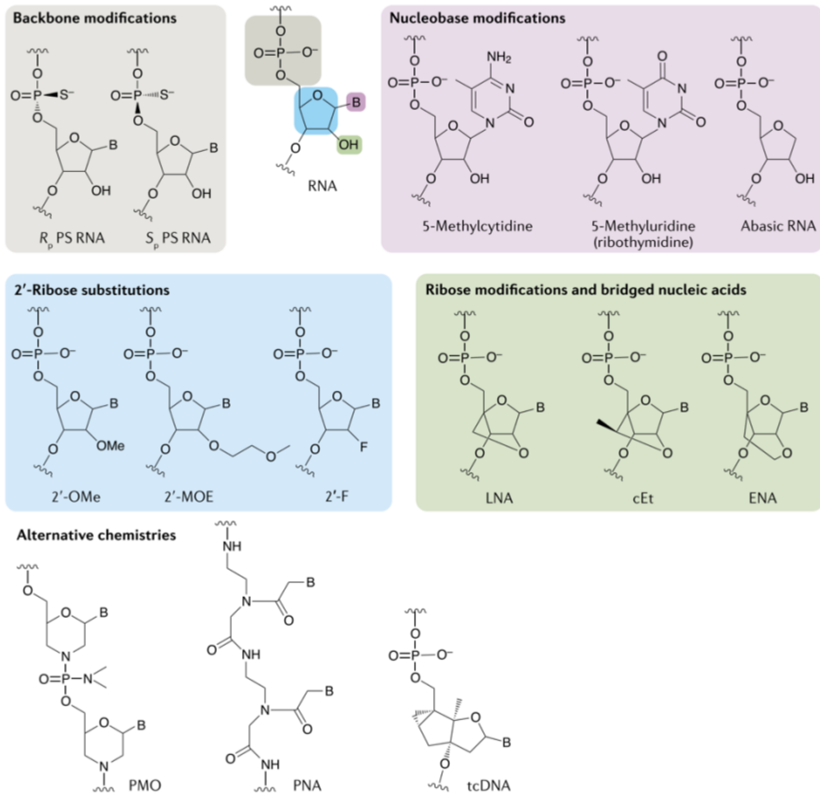

Figure 2. *Chemical modifications used for oligonucleotide-based drugs.[3]*

Additionally, ligands such as N-acetylgalactosamine, dendrimers, and cholesterol have been used as oligonucleotide conjugates to facilitate uptake and promote targeted delivery to specific tissues or cell types.[1] Along with chemical modifications and bioconjugates, the advent of nanocarriers has offered an alternative solution to the delivery of oligonucleotides and other highly charged and polar macromolecules, most notably lipid nanoparticles (LNPs). Lipid nanoparticles can deliver nucleic acid cargos by providing them protection from nuclease digestion and precludes them from renal filtration due to their size.[6] However, difficulties remain stemming from the challenge to precisely control their size and distribution, as well as poor drug loading efficiencies. As a result, the clinical translation of oligonucleotide-based therapeutics is dependent on the delivery technologies that they employ. A system that can facilitate cellular internalization, demonstrate target affinity, maintain stability in vivo, and retain drug potency are key considerations when establishing a relevant platform.

Another important consideration when designing oligonucleotides for neurodegenerative diseases is their administration methods. The blood-brain barrier poses a significant challenge for systemically administered drugs, impeding the uptake of most pharmaceuticals.[13,14] Consequently, to access the central nervous system (CNS), invasive administration methods such as intrathecal injections are required.[15,16] Therefore, it is important to keep exploring strategies that also enhance drug adsorption through less invasive means.

The Effect of Charge on Delivery Efficiency

Charge is another important parameter governing the ability to cross cell membranes and access intracellular compartments. Many transfection reagents such as lipofectamine employ cationic lipids to facilitate cell entry.[17,18] Similarly, cell penetrating peptides (CPPs) such as R9, TAT (48-60), and Penetratin have been widely employed to translocate a wide variety of materials into cells, the latter two being derived from natural proteins.[19] The R9 peptide, a homopolymer of the amino acid arginine, maintains a cationic charge at physiological pH (pKa = 12.48) due to its inherent guanidinium functional groups. Guanidinium-rich molecular transporters have been used to facilitate the uptake of a diverse array of cargos, not limited to peptides, proteins, siRNA, and small molecules across a variety of tissues and barriers.[20] For example, peptide nucleic acids (PNAs) employing guanidinium-based backbones have demonstrated remarkable uptake properties, resistance to nucleases and proteases, and maintenance of their Watson-Crick recognition with complementary sequences.[21] Poly-arginine analogues have not only aided in cell entry, but have also been shown to escape the endosome and access subcellular organelles such as the mitochondria and nucleus.[20,22,23] The ability to escape the endosome and access intracellular compartments is imperative for drugs to interact with their intended targets, demonstrating the utility of cationic polyarginine motifs.

Contrastingly, the phosphodiester (P-O) backbone of oligonucleotides is the main driver of their physiological properties, stemming from the anionic charge carried on the non-bridging oxygen of the phosphate group. Their polyanionic character and hydrophilicity leads to repulsion at cell membranes due to unfavourable electrostatic interactions and differences in hydrophobicity.[6,24] As a direct result, little to no uptake has been reported within the cytoplasm and nucleus when treated with cells, hindering their ability to interact with intracellular DNA or RNA.[25–28] We hypothesize that by replacing the intrinsically anionic phosphodiester backbone with a cationic charge, we can modulate the properties of oligonucleotides and promote favourable electrostatic interactions at cell membranes, leading to an increased cellular uptake and access to other intracellular compartments.

Phosphate Backbone Modifications

Phosphate backbone modifications entail replacing the non-bridging oxygen of an oligonucleotide with alternative atoms. The most common backbone alteration consists of replacing the oxygen atom with a sulfur atom, known as a phosphorothioate (P-S) oligonucleotide. Phosphorothioate oligonucleotides have been widely used as therapeutics due to their improved resistance to nuclease mediated degradation and tissue distribution.[29] Many phosphorothioate oligonucleotides have been clinically approved including Pegaptanib, Spinraza, and Vitravene. This highlights how minimal changes induced to the phosphate backbone can have pronounced effects on oligonucleotide properties and their clinical utility.

More recently, phosphoramidate (P-N) modified oligonucleotides have gained traction and show interesting physiochemical and biological properties, pioneered by the work done by Letsinger and Mungall in 1970.[30] Companies such as Wave Life Sciences have heavily investigated the application of phosphoramidate modified oligonucleotides in the context of gene knockdown for multiple indications. Multiple studies by Wave have demonstrated the pharmacological benefits of the P-N backbone including its increased potency of silencing, duration of response, and access to difficult to reach tissues, expanding the scope of indications amenable to therapeutic oligonucleotides.[31,32] Additionally, replacing the non-bridging oxygen with a nitrogen atom will provide a handle to introduce new functionality at the phosphate backbone (**Figure 3**).

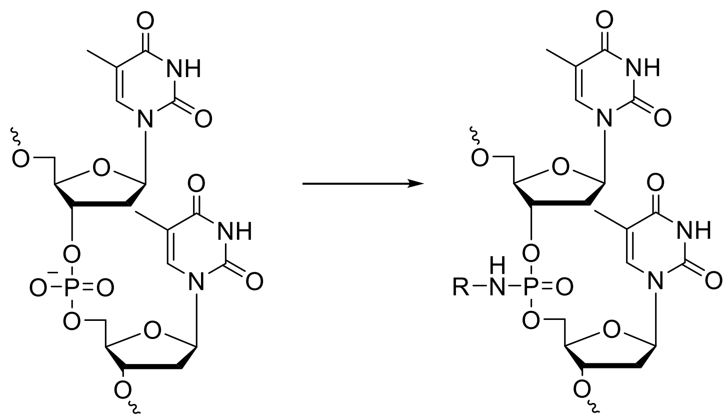

Figure 3. *Exchanging the non-bridging oxygen of the phosphate backbone with a nitrogen atom will provide a handle to introduce new functionality at the phosphate backbone.*

Michel and Vasseur have reported an efficient post synthesis method to introduce several guanidinium motifs to amine derivatized internucleotide phosphoramidate linkages.[33] Alternatively, Skakuj, Bujold and Mirkin have devised a method to replace the phosphate backbone altogether with guanidinium groups using iodine and TMP (2,2,6,6-tetramethylpiperidine), inspired by Dempcy and Bruice.[34,35] This was shown to have a pronounced effect on the uptake properties of oligonucleotides, displaying a ~40 fold increase in uptake relative to their unmodified counterparts.[34] Therefore, the effect of incorporating charged backbone motifs to oligonucleotides, in particular guanidinium modifications, is an effective strategy to not only enhance the stability against degradation by nucleases, but also shown to be an effective way to tailor the cell uptake properties of these drugs. However, while efficient syntheses have been reported, the impact of guanidinium modifications remains largely unexplored in the context of 3D nucleic acid architectures.

Spherical Nucleic Acids (SNAs)

The spherical nucleic acid, invented by Chad Mirkin in 1996, has provided a non-conventional nanoparticle-based approach to the delivery issue of oligonucleotides.[36] The SNA consists of radially orienting linear oligonucleotides onto a nanoparticle core, conferring them a three-dimensional, spherical architecture.[37] Compared with traditional nanoparticle delivery approaches such as LNPs and liposomes, which embed their drugs within the core, SNAs expose oligonucleotides on the surface. The densely functionalized arrangement of oligonucleotides on nanoparticle surfaces gives rise to many of their functional properties, which are independent of their nanoparticle core.[37,38] Compared to their linear counterparts, SNAs have distinct properties that have garnered interest with respect to their use in diagnostics and therapeutics, such as their plasmonic, catalytic, magnetic, and luminescent properties.[37] Work done by Cutler and Mirkin have underscored the advantages of SNAs in a therapeutic setting, including their robust uptake in a multitude of cell lines without transfection, resistant to nuclease degradation afforded by their tightly packed corona, ability to regulate protein expression levels, low cytotoxicity, and have higher affinity constants for complementary nucleic acids compared to their linear counterparts.[37–41] However, a well-known challenge of the SNA is that it precludes endosomal escape, an obstacle that needs to be addressed in order to interact with cytosolic and nuclear targets.[42] Despite the clear advantages that the SNA platform possesses, in conjunction with its well defined structure and control, the exploration of phosphate backbone modifications to further tailor the properties of SNAs has been unexplored.

Context and Scope of This Thesis

We propose to leverage the unique properties of SNAs by exploiting their core independence using 13 nm gold nanoparticles (AuNPs). The choice of nanoparticles 13 nm in size stems from their long-term stability at room temperature, narrow size distribution, extensive surface to volume ratios, and biocompatibility. In this way, we can afford SNAs with new and improved properties, stemming from their phosphate backbone modifications. We hypothesize that the nanoscale arrangement of phosphate backbone modifications will dictate the biological properties of the SNA, driving new interactions at cell surfaces, increasing cell uptake, and providing alternative uptake mechanisms. Additionally, the SNA platform presents a way to rigorously control the presentation of charge and hydrophobics in a nanoscale context (**Figure 4**). The modular design strategy of this approach can potentially be leveraged into a platform technology in which various ASOs can be inserted depending on the target of interest.

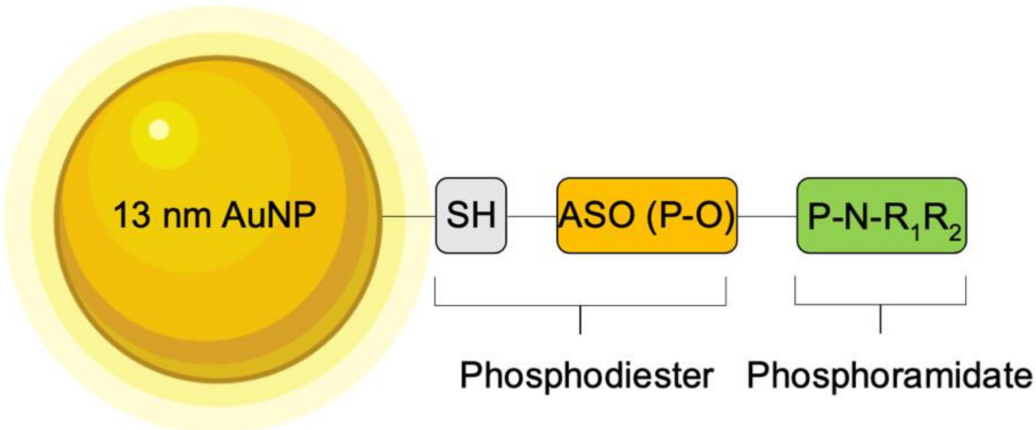

Figure 4. *Oligonucleotide Design & Conjugation Strategy. A thiol tail is placed at either the 3' or 5' terminus of the oligonucleotide to conjugate the strand to AuNPs (13 nm). An antisense oligonucleotide will be placed between the thiol tail and a phosphoramidate modified region.*

Charge Modified SNAs

We expect that the 3D architecture of the SNA will allow us to modulate its surface charge through cationic backbone modifications, specifically using amine and guanidinium derivatized functional groups. In this way, we expect to be able to produce more favourable electrostatic interactions at cell membranes, facilitating their uptake and decoupling the oligonucleotide drug from the uptake mechanism. This may provide unique characteristics including alternative uptake pathways, access to cytosolic and nuclear targets, and more potent therapeutic effects stemming from the stability of the phosphoramidate linkages.

Hydrophobically Modified SNAs

To broaden the scope of targets that can be accessed by SNAs, specifically neurological indications, we proposed to devise hydrophobically modified SNAs with the capacity to traverse the blood-brain barrier (BBB). The backbone modifications were informed by a machine learning model that predicted species with aliphatic character. We hope that the hydrophobically modified oligonucleotides can offer better solutions to current administration methods for treating CNS related diseases with oligonucleotides, which involve intrathecal injections. Additionally, we anticipate that the aliphatic character imposed onto the phosphate backbone will provide the corona of SNAs with lipophilic character, a property notably required for passive BBB transport.[43]

CHAPTER 2 – MATERIALS & METHODS

Materials & Supplies

1,3-diaminopropane, 1-adamantanecarbonyl chloride, isopropyl phosphite, ammonium citrate, sodium citrate, chloroauric acid, boric acid, urea, tris(hydroxymethyl)aminomethane (Tris), ethylenediaminetetraacetic acid (EDTA), O-methylisourea hemisulfate, dithiothreitol, 40% methylamine solution, Tween-20, sodium chloride, potassium cyanide, agarose, all solvents (acetonitrile, methanol, pyridine, tetrahydrofuran (THF)) were purchased from Sigma-Aldrich. Triethylamine, 19:1 acrylamide:bis-acrylamide (40% solution), hydrochloric acid, nitric acid, ammonium persulfate, tetramethylethylenediamine (TEMED), 30% ammonium hydroxide solution, glacial acetic acid, fetal bovine serum, penicillin/streptomycin (10,000 U/mL), trypsin-EDTA (0.25%) and Dulbecco's modified Eagle's medium (DMEM) were obtained from Fisher Scientific. Ethyl trifluoroacetate, and 2,6-dihydroxyacetophenone were obtained from TCI Chemicals. Cy5 maleimide was obtained from Lumiprobe. Column chromatography was performed using SiliaFlash® P60 with a pore diameter of 40-63 µm (50:1 silica: crude mixture) obtained from Silicycle. Desalting columns were obtained from Glen Research (Gel-Pack™ Desalting Column). MDA-MB-231 cells are a generous gift from the Wylie group.

Reagents required for DNA synthesis were made in house using chemicals and solvents purchased from Sigma-Aldrich. Deblock consisted of 3% dichloroacetic acid in dichloromethane. 5-(Ethylthio)-1*H*-tetrazole (ETT) was used as activator and purchased as a 0.25 M solution in acetonitrile from Sigma-Aldrich to which a molecular trap pack (2 g for 200 mL, LGC Genomics) was added to keep it anhydrous. Oxidizer was made from 0.02 M Iodine in tetrahydrofuran/pyridine/water (70:20:10). Cap A consisted of tetrahydrofuran/2,6-Lutidine/Acetic Anhydride (80:10:10) and Cap B was made from 16% 1-Methylimidazole in tetrahydrofuran (16:84). Both capping solutions were kept anhydrous with molecular trap packs (5 g for 450 mL, LGC Genomics). Acetonitrile was used as diluent with a molecular trap pack to keep it anhydrous (20 g for 4 L). All other reagents required for DNA synthesis, including phosphoramidites, solid support (Glen UnySupport^{TM} CPG 1000) and DNA synthesis columns were purchased from Glen Research. H-phosphonate monomers were acquired from ChemGenes (Thymidine H-phosphonate TEA Salt, ANP-3413).

High performance liquid chromatography (HPLC) purifications were conducted using a 100 mM triethylammonium acetate (TEAA) buffer at pH 7 containing 3% acetonitrile. First, 10X TEAA buffer was made by adding 800 mL of Milli-Q water to a flask. 140 mL of triethylamine was added while stirring in an ice bath. Glacial acetic acid was added dropwise to the solution until a pH of 7.00 was reached and the solution was stored at 4 °C. HPLC buffer was then made by combining one part 1 M TEAA with 9 parts autoclaved Milli-Q water, to which 3% acetonitrile (ACN) was added. The entire solution was filtered through a 0.45 μm filter prior to use on the HPLC. Polyacrylamide gel electrophoresis (PAGE) was conducted using 1X tris-boric acid-EDTA (TBE) as running buffer, which consists in 89 mM Tris, 89 mM boric acid, 2 mM EDTA.

Instrumentation

Small molecules were analyzed via ^{1}H-NMR using a 600 MHz NMR spectrometer (AV 600 (2002)) with an auto sampler, processing the data with Bruker TopSpin 3.6.3 software. Oligonucleotide synthesis was carried out on a MerMade 6 (BioAutomation) automated oligonucleotide synthesizer. A SpeedVac ISS100 vacuum concentrator was used to concentrate oligonucleotides. HPLC was conducted on a Shimadzu Prominence instrument equipped with a manual injector (1 mL loop), column oven, and automated fraction collector. Oligonucleotide detection was conducted at 254 nm. PAGE purification was performed at room temperature on Hoefer 600 gel electrophoresis boxes, using 16 x 16 cm gels with 0.75 mm or 1.5 mm thickness and corresponding accessories. Ultraviolet-visible (UV-vis) spectroscopy measurements were acquired on a Cary 50 instrument using the Cary WinUV Scan application. Matrix-assisted laser desorption ionization – time of flight mass spectrometry (MALDI-TOF MS) was performed on a Bruker maXis 4G Mass Spectrometer in positive ion mode using 2,6-dihydroxyacetophenone as the matrix. A Thermo Scientific Talos L120C was used to characterize the 13 nm AuNPs based on their size (diameter) and distribution. ImageJ software was used to determine the nanoparticle size distribution. Dynamic light scattering measurements were conducted on a Zetasizer Nano ZS instrument. A CytoFLEX LX Flow Cytometer (Beckman Coulter) was used to analyze the cellular uptake of SNAs using the red laser to track cyanine 5 (Cy5) emission.

Synthesis of N-Trifluoroacetyl-1,3-propylenediamine

This synthesis was carried out according to the procedure by Michel *et al.* with minor modifications.[33] Briefly, 1,3-diaminopropane and triethylamine (TEA, 2 equiv.) were combined in a round bottom flask and stirred on ice. Ethyl trifluoroacetate (1 equiv.) was added dropwise to the solution over 5 minutes. The mixture was then allowed to warm to room temperature over 16-24 hours. The mixture was concentrated under vacuum to remove the TEA from solution. The crude residue was then purified via column chromatography on silica using 77.5% tetrahydrofuran (THF), 17.5% methanol (MeOH), and 5% TEA as the eluent. The reaction was monitored by TLC using the same solvent system and ninhydrin as the stain. Fractions containing the product were combined and dried. Yields a clear oil in ~15% yield. The product was confirmed by ^{1}H NMR (**Figure 5, Figure S1** and **Figure S2**).

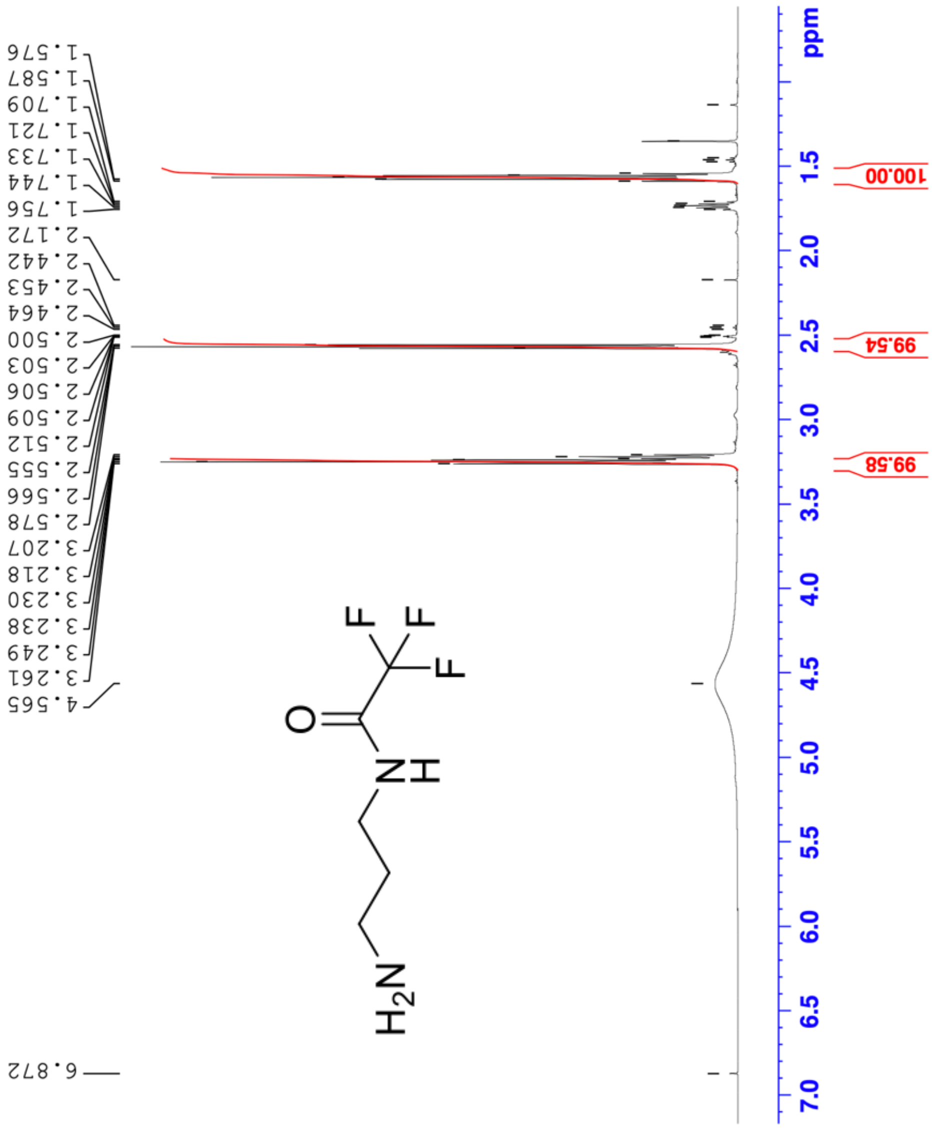

Figure 5. *[1]H-NMR of N-Trifluoroacetyl-1,3-propylenediamine. N-Trifluoroacetyl-1,3-propylenediamine: 1H-NMR (DMSO-d6, 600 MHz): δ 1.56 (quint, 2H), 2.57 (t, 2H), 3.25 (t, 2H).*

Oligonucleotide Synthesis

<u>Phosphoramidite Synthesis (“P-O” Backbone)</u>

DNA oligonucleotides containing phosphate linkages were synthesized using standard solid phase phosphoramidite chemistry protocols[44] at the 1 or 5 µmole scale. Briefly, at each cycle, the trityl group on the solid support or 5’ end of the growing chain was removed using deblock to reveal a 5’ alcohol, which was coupled with an incoming phosphoramidite in 20-fold excess in the presence of ETT activator. The phosphite linkage formed is then oxidized to form a phosphate linkage with oxidizer and unreacted alcohols are capped with Cap A and B prior to restarting the cycle. **Table 1** lists the oligonucleotides synthesized where “-SH” indicates the incorporation thiol-modifier C6 S-S (100 µmoles, Glen Research), “-Cy5” indicates the incorporation of Cyanine 5 phosphoramidite (50 µmoles. Glen Research). Non-standard amidites were incorporated onto the oligonucleotides according to the manufacturer’s specifications.

Table 1. *Sequences of Cy5 labelled oligonucleotides and controls ("P-O" backbone).*

Oligonucleotide	**Sequence (5’-3’)**
T10-Cy5	5’-Cy5-TTTTTTTTTT-SH-3’
T20-Cy5	5’-Cy5-TTTTTTTTTTTTTTTTTTTT-SH-3’
T3 Control	5’-SH-AGGTCTTGTTTCCTTTGCTTTT-3’
T7 Control	5’-SH-GGTCTTGTTTCCTTTGCTTTTTTTT-3’
T10 Control	5’-SH-TTTTTTTTTT-3’

Phosphoramidate Synthesis ("P-N" Backbone)

Oligonucleotides containing phosphoramidate modifications ("P-N") were synthesized at the 1 μmole scale according to the protocol described by Vlaho and Damha, which was automated onto a MerMade 6 oligonucleotide synthesizer. The deblocking solution proposed in the protocol (3% trichloroacetic acid in dichloromethane) was replaced by 3% dichloroacetic acid in dichloromethane to minimize risk of acid-mediated degradation. The activator and Cap A solutions consisted of 0.35 M adamantane carbonyl chloride in 95:5 acetonitrile/pyridine (v/v). The Cap B solution was made from 1% isopropyl phosphite in 95:5 acetonitrile/pyridine (v/v). The amine monomer solution was made by combining 10% N-trifluoroacetyl-1,3-propylenediamine, 10% anhydrous pyridine, and 80% carbon tetrachloride (CCl_4).[45] H-phosphonate building blocks were obtained from a commercial supplier and dissolved in 50:50 pyridine:acetonitrile. All solutions were kept anhydrous using molecular trap packs (0.5 g per 30 mL solution, LGC Genomics). Briefly, at each cycle, the trityl group on the solid support or 5' end of the growing chain was removed using deblock to reveal a 5' alcohol, which was coupled with an incoming thymidine H-phosphonate building block in 10-fold excess in the presence of 1-adamantanecarbonyl chloride activator. The H-phosphonate linkage formed is then oxidized to form a phosphoramidate linkage with the amine monomer solution and unreacted alcohols are capped with Cap A and B prior to restarting the cycle. **Table 2** lists the oligonucleotides synthesized where "n" denotes phosphoramidate linkages.

Table 2. *Sequences of phosphoramidate modified oligonucleotides synthesized. "n" represents phosphoramidate linkages.*

Oligonucleotide	**Sequence (5'-3')**
3X NH_2	5'-SH-AGGTCTTGTTTCCTTTGCT$_n$T$_n$T$_n$T-3'
7X NH_2	5'-SH-AGGTCTTGTTTCCTTTGCT$_n$T$_n$T$_n$T$_n$T$_n$T$_n$T$_n$T-3'
3X Guanidinium	5'-SH-AGGTCTTGTTTCCTTTGCT$_n$T$_n$T$_n$T-3'
7X Guanidinium	5'-SH-AGGTCTTGTTTCCTTTGCT$_n$T$_n$T$_n$T$_n$T$_n$T$_n$T$_n$T-3'
4X Propylamine	5'-SH-TTTTTT$_n$T$_n$T$_n$T$_n$T-3'
4X Hexylamine	5'-SH-TTTTTT$_n$T$_n$T$_n$T$_n$T-3'
4X Octylamine	5'-SH-TTTTTT$_n$T$_n$T$_n$T$_n$T-3'
4X 1-(3-aminopropyl) pyrrolidine	5'-SH-TTTTTT$_n$T$_n$T$_n$T$_n$T-3'

Cleavage & Deprotection of Oligonucleotides

Oligonucleotide synthesis columns were removed from the MerMade6 instrument and any remaining solvent in the synthesis columns was removed under a vacuum pull for a few seconds. A blunt needle was used to disrupt the frit and transfer the solid support to a scintillation vial. For 1 μmol and 5 μmol syntheses, a global deprotection was performed by adding a 1:1 solution of 28-30% ammonium hydroxide (NH_4OH) and 33 wt. % aqueous methylamine (AMA) to the solid support (1 mL total for 1 μmole and 5 mL total for 5 μmole). The mixtures were immediately placed on a heating block set at 55°C for 45 minutes in screw cap vials or tubes. The methylamine and ammonium hydroxide were removed from solution by either gently drying under a stream of nitrogen or at 60 °C on a vacuum concentrator. 1 μmole and 5 μmole syntheses were resuspended in 1 mL and 5 mL of autoclaved Milli-Q water, respectively prior to purification.

Purification of Oligonucleotides

Reverse-Phase High-Performance Liquid Chromatography (HPLC)

The crude deprotected oligonucleotides were filtered through a 0.45 µm polyethersulfone (PES) syringe filter (25 mm diameter). The volume of the filtered oligonucleotides was adjusted to 1 mL with autoclaved Milli-Q water (passed through the same syringe filter to collect any oligonucleotide remaining on the membrane). This buffer was loaded onto line A of the HPLC while line B was loaded with 100% HPLC-grade acetonitrile. Oligonucleotides that retained a 4,4'-dimethoxytrityl (DMT) group at the 5' position were purified out of the crude mixture containing failed sequences using an 8 µm, 100 Å PLRP-S column (4.6 mm x 250 mm, Agilent) pumping at 2.5 mL/min using a linear gradient from 0 to 100% acetonitrile over 30 minutes as described in **Table 3**:

Table 3. *HPLC gradient for oligonucleotide purification.*

Time (minutes)	**[100 mM TEAA, 3% ACN] % (Line A)**	**[ACN] % (Line B)**
0	100	0
5	100	0
35	0	100
45	0	100
46	100	0
60	100	0

Fractions containing the purified oligonucleotide were collected and dried on a SpeedVac vacuum concentrator and stored at 4 °C. The figure below (**Figure 6**) depicts a standard HPLC chromatogram of a phosphoramidate modified oligonucleotides eluting at ~26 minutes.

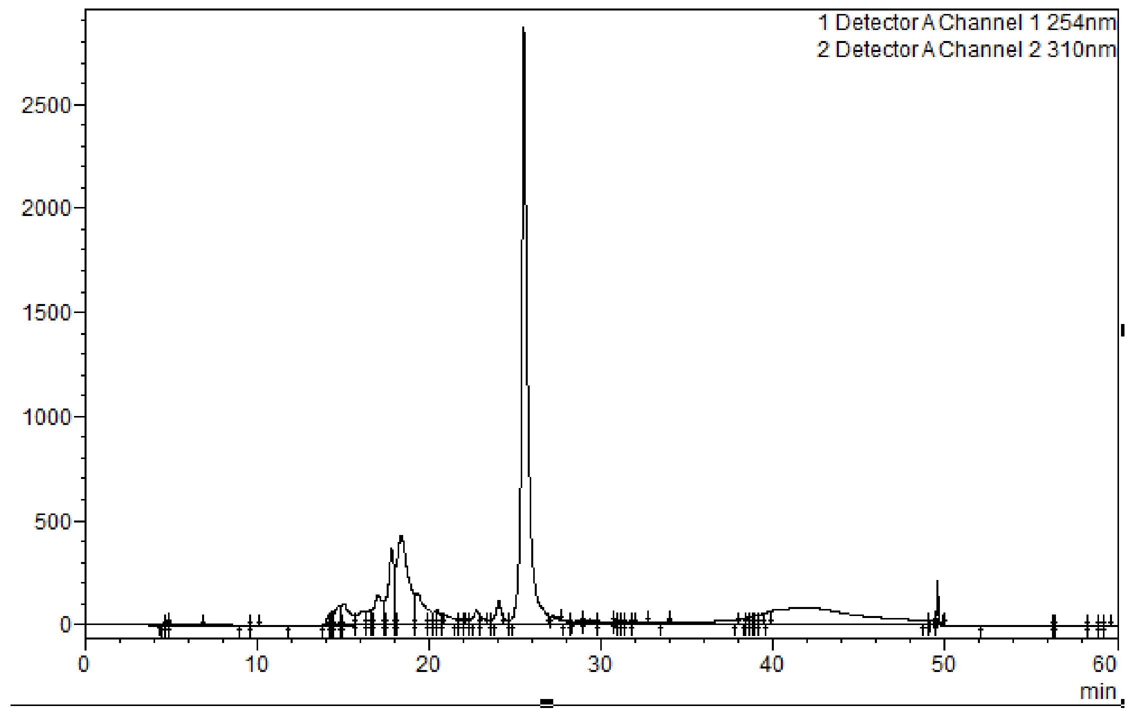

Figure 6. *HPLC chromatogram of a phosphoramidate modified oligonucleotide (4X Propylamine).*

Preparative Denaturing Polyacrylamide Gel Electrophoresis (PAGE)

A 24% acrylamide stock (250 mL) was made by combining 105 grams of urea, 150 mL of 19:1 acrylamide:*bis*-acrylamide 40% solution, and 25 mL of 10X TBE. The 24% acrylamide stock solution was diluted to either 15% or 20% with Milli-Q water depending on the length of the oligonucleotide being purified as per **Table 4**.

Table 4. *Polyacrylamide percentage versus oligonucleotide length.*

Oligonucleotide length (bases)	**Polyacrylamide concentration (%)**
<25	20
25-50	15

The gel was then polymerized by first adding 0.1% (v/v) N,N,N',N'-tetramethylethylenediamine (TEMED) and mixing thoroughly. 0.1% (w/v) ammonium persulfate (APS) was then added rapidly afterwards and mixed thoroughly. The gel was cast between two plates separated by 1.5 mm spacers and allowed to polymerize with a comb inserted to generate a large single well. The well was with water prior to loading the oligonucleotide to be purified as a 1:1 mixture with 8 M urea at a final volume of 500 μL. Gels were run for 2.5 hours at 250 V and 30 mA using 1X TBE as running buffer. Oligonucleotides were visualized on the gel using a UV lamp and the band of interest was excised using a single edge razor blade (typically the most retained band corresponded to the product). The excised bands were placed into a 15 mL falcon tube, crushed to small pieces, and resuspended in ~10 mL of Milli-Q water. The tubes were frozen solid in liquid nitrogen and immediately placed on a heat bock set at 55 °C for 24 hours with intermittent shaking to distribute the crushed gel and facilitate the diffusion of the oligonucleotides out of the gel pieces. Once incubation was completed, the gel was separated from the purified oligonucleotide solution by filtering through a Buchner funnel. The purified oligonucleotides were dried on a SpeedVac vacuum concentrator until they reached a total volume of 1 mL. The oligonucleotides were run through a desalting column according to the protocol described by Glen Research to remove small molecules and salts from solution and stored at 4 °C.

Detritylation & Reduction of Oligonucleotides

Detritylation

For oligonucleotides that retained a 5'-DMT protecting group, acetic acid was added to bring the total volume in solution to 20% (v/v). The solution was allowed to incubate at room temperature for 1 hour to cleave the 5'-DMT protecting group. The acetic acid was removed from solution by either 1) drying it on a SpeedVac vacuum concentrator or 2) subjecting it to a desalting column (buffer exchange) and stored at 4°C.

Reduction of Disulfide Linkages

To reduce the disulfide installed at either the 3' or 5' end of the oligonucleotides, stock solutions of 1 M dithiothreitol (DTT) and 10X Tris-hydrochloride (HCl, pH 8.4) were prepared. The 1 M DTT stock and 10X Tris-HCl (pH 8.4) were added to the oligonucleotides such that their final concentrations in solution were 0.1 M and 1X (v/v), respectively. The solutions were thoroughly mixed and left to react at room temperature for 45 minutes. The oligonucleotides were passed through another round of desalting columns and stored at 4 °C.

Guanidinylation of Amine Functionalized Oligonucleotides

This reaction was adapted according to the procedure by Michel *et al.* with minor modifications.[33] Amine derivatized oligonucleotides (~10 OD) were combined with 28-30% ammonium hydroxide (1:1). A freshly made solution of aqueous O-methylisourea hemisulfate (~4 M) was added to the oligonucleotide solution in a ratio of 1 part salt, 2 parts oligonucleotide. The mixture was allowed to react for 45 minutes at 65 °C. The solution was quenched to 0 °C and partially dried on a SpeedVac vacuum concentrator. The guanidinylated oligonucleotide was corrected to 1 mL with Milli-Q water and run through a desalting column to remove all reaction components and stored at 4 °C.

Characterization of Oligonucleotides

Ultraviolet-Visible Spectroscopy

UV-vis spectroscopy was used to determine the concentration of oligonucleotides, cyanine 5-labeled oligonucleotides, and spherical nucleic acids (SNA), using their maximum absorption bands at 260 nm, 647 nm, and 520 nm respectively. Absorbance spectra were acquired from 800 nm to 200 nm with approximately one reading per nanometer using a 1 cm pathlength microvolume cuvette. For each measurement, the instrument was baselined with Milli-Q water and zeroed. Readings for each sample were acquired using dilution with Milli-Q water to ensure the readings were between 0.1 and 1 absorbance units (a.u.), which is the range where the instrument is the most precise. For oligonucleotides, extinction coefficients were determined using the IDT DNA OligoAnalyzer™ Tool (www.idtdna.com/calc/analyzer). For cyanine 5 labels, an extinction coefficient of 250,000 cm^{-1} M^{-1} was used based on manufacturer's specifications. For spherical nucleic acids, an extinction coefficient of 2.76 x 10^8 cm^{-1} M^{-1} was used based on literature for 13 nm gold nanoparticles.[37] Concentrations were determined using the recorded absorbances, dilution factor, and molar extinction coefficient using the Beer Lambert law ($A = \varepsilon l c$), where A = absorbance, ε = molar extinction coefficient ($M^{-1}\ cm^{-1}$), l = optical path length (cm), and c = molar concentration (M).

Analytical Denaturing Polyacrylamide Gel Electrophoresis

A denaturing polyacrylamide gel was prepared and casted according to the "Preparative Denaturing Polyacrylamide Gel Electrophoresis (PAGE)" section with modifications. Instead, a 20-well comb was inserted after casting the acrylamide solution in between plates separated by 0.75 mm spacers. 10 μL solutions of each oligonucleotide were prepared (~0.1 OD) and combined with 10 μL of 8 M urea. The oligonucleotide solutions were loaded into the wells and run for 2.5 hours at 250 V and 15 mA. The gel was removed and stained in Stains-All solution (0.005% (w/v) Stains-All in 1:1 formamide/water (v/v)) for ~5 minutes to visualize the bands.

MALDI-TOF MS

DHAP matrix was prepared by dissolving 25 mg of 2,6-dihydroxyacetophenone into 300 μL methanol. Saturated ammonium citrate solution (111 μL) was added next, and the matrix was vigorously vortexed and centrifuged until a white precipitate formed at the bottom and the supernatant was a bright yellow solution. 0.5 μL of each oligonucleotide were spotted onto a steel MALDI target plate followed by 0.5 μL of the DHAP matrix supernatant. The oligonucleotides were allowed to dry before they were analyzed by MALDI-TOF MS in positive ion mode.

Stability of Phosphoramidate Linkages in 1X PBS & DMEM

The concentration of a 3X amine derivatized oligonucleotide was determined by UV-vis. Three 30 μM stock solutions (200 μL) of the oligonucleotide were prepared in Milli-Q water. The three oligonucleotide solutions were completely dried down and resuspended in either 200 μL of 1X phosphate-buffered saline (PBS), 1X Dulbecco's Modified Eagle Medium (DMEM), or Milli-Q water. The oligonucleotides were incubated for 4 hours at 37°C and run through a desalting column. MALDI-TOF MS was used to analyze the oligonucleotides.

Synthesis of 13 nm gold nanoparticles (AuNPs)

13 nm gold nanoparticles were synthesized according to the protocol outlined by Liu and Lu using aqua regia-cleaned glassware.[46] Briefly, 2 mL of a 50 mM chloroauric acid ($HAuCl_4$) solution was added to 98 mL of Milli-Q water. The solution was brought to a reflux while stirring on a mineral oil bath, then 10 mL of a 38.8 mM sodium citrate solution was added rapidly and directly into the solution. When a deep red colour became apparent (~1 minute), the solution was allowed to reflux for another 20 minutes. The gold nanoparticles were collected in aqua regia-cleaned glassware and stored at room temperature in the dark.

TEM Analysis of 13 nm AuNPs

13 nm citrate capped AuNPs were sonicated for ~5 minutes and spotted onto a 300 nm copper mesh with holey carbon film purchased from Ted Pella. The AuNPs were left to dry for ~2 hours. The grid containing dried AuNPs was placed on a single tilt sample holder and inserted into the goniometer. Alignment procedures were followed according to CCEM (Canadian Centre for Electron Microscopy) and images were required using Velox acquisition software. Particle size and distribution was analyzed by ImageJ software.

Dual Layer Spherical Nucleic Acid (SNA) Synthesis

<u>Cyanine 5 SNA Monolayer Synthesis</u>

The concentration of a T_{20} cyanine 5 (Cy5) labelled oligonucleotide was determined by UV-vis by measuring its absorbance at 260 nm (A_{260}) and using the extinction coefficient of a 20-base poly-thymine sequence (162,600 M^{-1} cm^{-1} determined using the OligoAnalyzer Tool from IDT DNA, www.idtdna.com/calc/analyzer) and the Beer-Lambert equation. Similarly, the concentration of the 13 nm AuNPs was determined by UV-vis by measuring their extinction at 520 nm (Ext_{520}) using an extinction coefficient of 2.76 x 10^8 M^{-1} cm^{-1}.[37] Using these concentrations, SNAs with a low-density T_{20} Cy5 monolayer were synthesized by incubating DNA with AuNPs at a ratio of 85:1 for 16-24 hours at a final concentration of 10 nM AuNPs and 850 nM DNA, diluting with Milli-Q water as required. The AuNPs, Milli-Q water, and DNA were combined, vortexed, and left on an inverting mixer for ~5 minutes. Tween-20 was then added to a final volume of 0.25% in solution. Salt aging was performed by adding sodium chloride (NaCl) every 30 minutes in 0.01 M increments until the final concentration in solution was 0.05 M, mixing thoroughly between each addition. The Cy5 monolayer SNAs were then allowed to mix for 16 to 24 hours. After the incubation was completed, the excess DNA and salts were removed through 3 rounds of pelleting (45 min, 14,800 rpm) and aspirating the supernatant, replacing it with an equal volume of Milli-Q water. The final concentration of SNAs with a low density of T_{20} Cy5 was then assessed using UV-visible spectroscopy, monitoring their extinction at 520 nm with typical concentrations ranging from 50-100 nM. SNAs functionalized with a low density of Cy5 T_{20} are transiently stable and were used immediately in a second DNA functionalization assay.

Dual Layer SNA Synthesis with Modified Oligonucleotides

The concentration of the Cy5 monolayer SNA (Ext_{520}) and the modified oligonucleotides (A_{260}) were determined by UV-vis. To assemble dual layer SNAs, the protocol from the section “Cyanine 5 SNA Monolayer Synthesis” was used. The ratio of modified oligonucleotide to Cy5-SNA used was either 500 or 750:1. The Cy5-SNA stock, Milli-Q water, and modified oligonucleotides were combined and left to mix on an inverting mixer for 16-24 hours. Tween-20 was added to a final volume of 0.25% in solution. The dual layer SNAs were salt aged in 0.1 M increments to a final concentration of 0.5 M NaCl in solution. The dual layer SNAs were allowed to mix for another 16 to 24 hours. The excess DNA and salts were removed via 3 rounds of pelleting (45 min, 14,800 rpm), aspirating the supernatant, and replacing with Milli-Q water. SNAs were then assessed for their concentration using their extinction at 520 nm and stored at 4 °C.

SNA Characterization

Cy5 Monolayer SNA Functionalization Assay

This assay was conducted to determine the number of Cy5-labeled oligonucleotides were functionalized onto the Cy5 monolayer SNAs. A 1 µM stock of cyanine 5 labelled oligonucleotide (200 µL) and a 1 nM stock of the corresponding Cy5 monolayer SNA (200 µL) were prepared. A 40 mM potassium cyanide (KCN) solution and a 20 mM KCN solution were prepared. 160 µL of 40 mM KCN was added to the Cy5 monolayer SNA sample (1:1) and thoroughly mixed to dissolve the AuNPs. 100 µL of the mixture was dispensed into 3 adjacent wells (rows 9-11) on a 96-well plate. A calibration curve for Cy5 signal was established by dispensing 100 µL of 40 mM KCN in a well (row 8) followed by 100 µL of 1 µM Cy5 DNA stock. 100 µL of 20 mM KCN was dispensed into 7 adjacent wells (rows 1-7). A 1:2 serial dilution was performed starting from row 8 and stopping at row 2. The fluorescence of the Cy5 dye was measured on a microplate reader using an excitation of 651 nm and an emission of 670 nm. The number of T_{20} Cy5 oligonucleotides per AuNP was determined from the Cy5 reading on the Cy5 monolayer SNA samples, dividing by their known gold concentration.

Oligreen Total DNA Functionalization Assay

This assay was conducted to determine the number of DNA strands per AuNP were found on average on SNAs after both DNA strands were functionalized (Cy5 label and strand of interest). The Oligreen total DNA functionalization assay was prepared according to the protocol described in the section above using a separate calibration curve for each different oligonucleotide that was assessed. Prior to measuring fluorescence, a 0.5% Oligreen stock solution was made in water (v/v). 100 μL of Oligreen solution was dispensed in each well and the fluorescence was measured within 5 minutes on a plate reader using an excitation of 480 nm and an emission of 520 nm. The number of oligonucleotides per AuNP was determined from the Oligreen reading on the Cy5 monolayer SNA samples, dividing by their known gold concentration.

Agarose Gel Electrophoresis

A 1% agarose gel (w/v) was prepared by combining 0.5 g of agarose with 50 mL of 1X TBE buffer. The mixture was microwaved in 30 second intervals until the solution became clear. The volume was corrected back to 50 mL with water and poured into a gel box. A 10-well comb was inserted, and the gel was allowed to solidify for 30 minutes at room temperature. The gel was then placed in 1X TBE running buffer. The SNAs were loaded at a final concentration of ~20 nM with 10% glycerine (v/v). The gel was run for 1 hour at 100 V and 50 mA.

Dynamic Light Scattering (DLS)

For measurements of hydrodynamic diameter, 3 nM solutions of SNAs were prepared at a volume of 1 mL in disposable cuvettes and filtered. Measurements were carried out at a temperature of 25°C. For each SNA, three replicates were performed with 11 acquisitions each.

Bioconjugation of Thiolated Oligonucleotides with Cy5 Maleimide

A stock solution of Cy5 maleimide (Lumiprobe) was made by suspending it in dimethyl sulfoxide (DMSO) at a concentration of 10 mg/mL. A fresh solution of Tris(2-carboxyethyl) phosphine hydrochloride (TCEP) was made (0.5 M) and corrected to a pH of 7 with 10 M sodium hydroxide (NaOH). 100 μM solutions of thiolated oligonucleotides (100 μL) were prepared. 2 μL of the TCEP solution was added to the oligonucleotides and left to react for ~5 minutes. 10X PBS was added to each oligonucleotide to bring its concentration to 1X in solution. A 10X molar excess of Cy5 maleimide was added to each oligonucleotide and thoroughly mixed. DMSO was used as a cosolvent if the Cy5 maleimide did not fully dissolve in solution (~10 μL increments). The solutions were vigorously vortexed and allowed to mix at room temperature for 2 hours. The oligonucleotide solutions were corrected to 1 mL with milli-Q water and run through a desalting column, eluting with 1 mL fractions. RP-HPLC was performed on the oligonucleotides according to the standard protocol described above.

Octanol-Water Partitioning of Oligonucleotides

Oligonucleotides were prepared at a final concentration of 100 μM (100 μL). 100 μL of octanol was added to each oligonucleotide, mixed thoroughly, and allowed to settle for ~20 minutes. An aliquot of the water layer was analyzed by UV-vis. To determine the ratio of oligonucleotide partitioned into the octanol phase versus the water phase, the following equation was used: $P_{o/w} = \frac{[Oligonucleotide]_o}{[Oligonucleotide]_w}$, where P represents the *n*-octanol-water partition ratio.

SNA Uptake by Flow Cytometry

MDA-MB-231 cells were plated at 50,000 cells/well in 24-well plates one day before the experiment. To assess cellular uptake of different SNAs, first, the media was aspirated out of each well and replaced with 1X DMEM (1% penicillin-streptomycin) without FBS (300 μL per well for a 24-well plate). Wells were then treated with SNAs incubated at a final concentration of 2 nM or 1X PBS (negative control). The SNAs were incubated at 37 °C and 5% CO_2 for varying lengths of time. For samples incubated longer than 4 hours, the media was supplemented with 10% FBS at the 4-hour mark. Once the incubation was completed, the media in each well was aspirated and 200 μL of trypsin was added to each well and incubated at 37°C and 5% CO_2 for 5 minutes. 300 μL of 1X DMEM FULL was added to each well and thoroughly combined. The mixtures were transferred into round bottom tubes and centrifuged for 5 minutes at 1400 rpm. The media was carefully aspirated to not disturb the cell pellet. The cells were resuspended in 500 µL of 1X PBS and transferred and filtered into 5 mL round-bottom polystyrene tubes with a 35 µm strainer for analysis by flow cytometry. The fluorescence intensity was determined using a red laser (638 nm) to excite the Cy5 fluorescent dye conjugated to the SNAs. Data analysis was performed using FlowJo software to determine the relative fluorescence intensity of each SNA.

Processing Flow Cytometry Data with FlowJo

Data analysis was performed using FlowJo software to determine the relative fluorescence intensity of each SNA in live MDA-MB-231 cells. The following two examples demonstrate how fluorescence intensities were acquired for unstained cells and cells incubated with a dual layer SNA derivatized with seven guanidinium residues per oligonucleotide. A plot of forward versus side scatter was generated to identify live MDA-MB-231 cells (**Figure 7**).

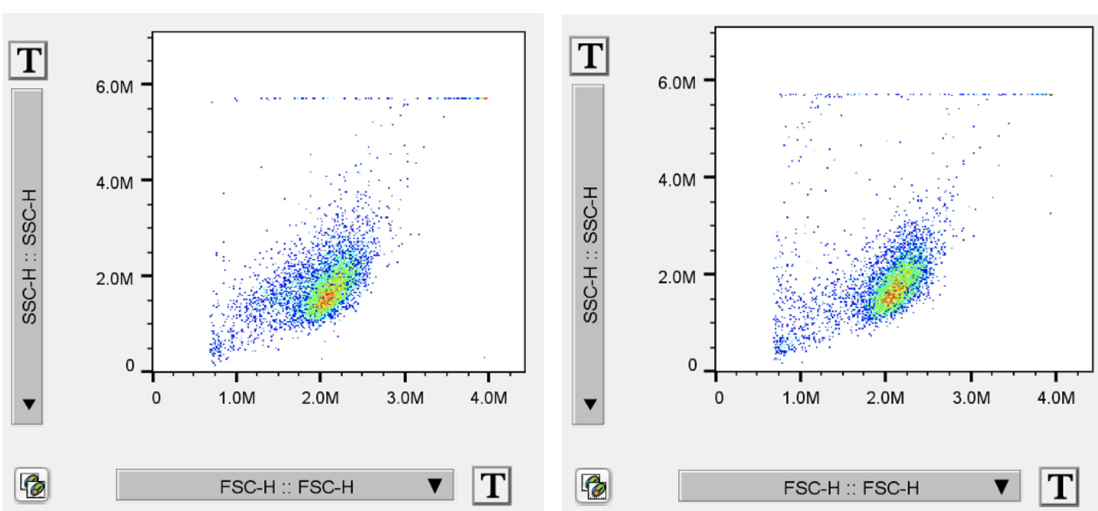

Figure 7. *Plot of forward scatter versus side scatter for a) Unstained MDA-MB-231 cells and b) 7X Guanidinium SNA incubated with MDA-MB-231 cells.*

The live cells were gated and a second plot of forward scatter (area) versus forward scatter (height) was generated to show single cells (**Figure 8**).

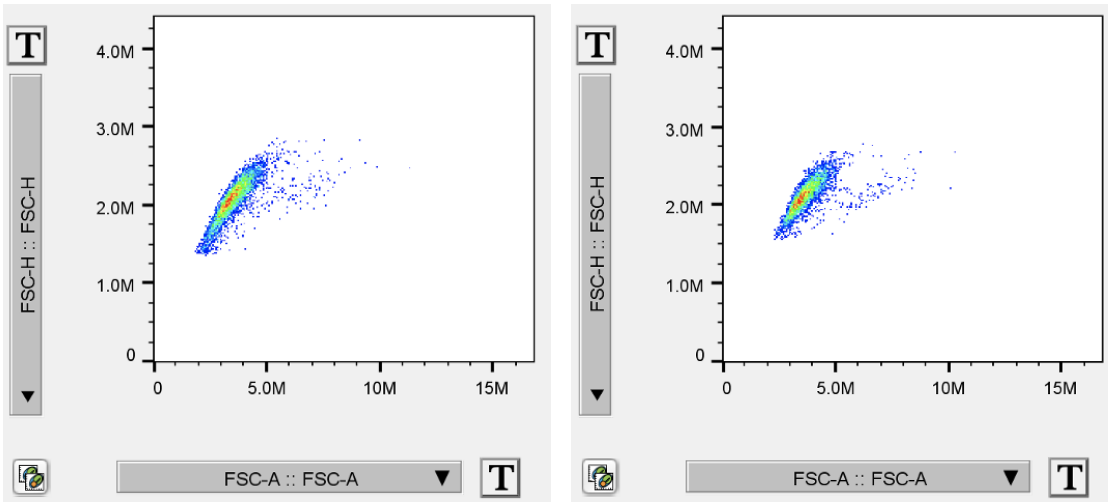

Figure 8. *Plot of forward scatter (area) versus forward scatter (height) for a) Unstained MDA-MB-231 cells and b) 7X Guanidinium SNA incubated with MDA-MB-231 cells.*

The single cells were further gated and a plot of side scatter (height) versus side scatter (area) was created to separate the single cells based on granularity (**Figure 9**).

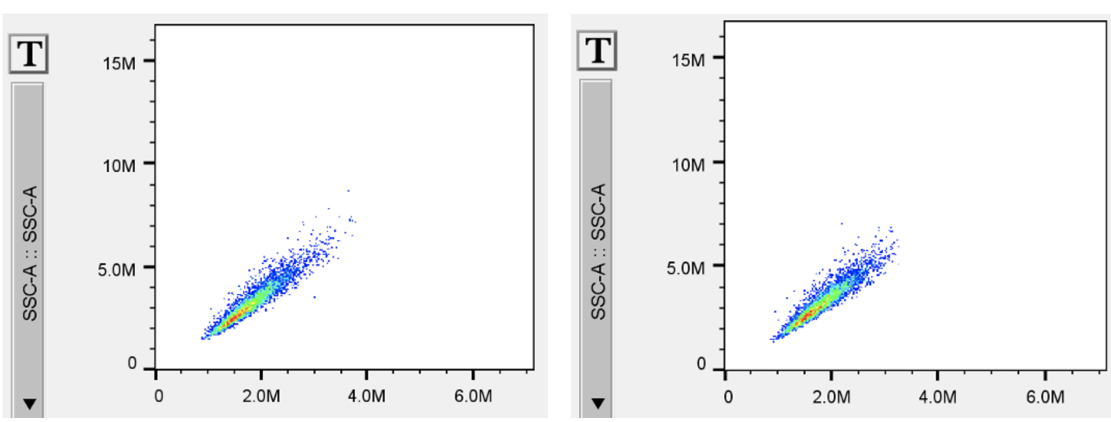

Figure 9. *Plot of side scatter (height) versus side scatter (area) for a) Unstained MDA-MB-231 cells and b) 7X Guanidinium SNA incubated with MDA-MB-231 cells.*

The single cells separated by granularity were gated and a histogram of Cy5 fluorescence intensity was plotted (**Figure 10**).

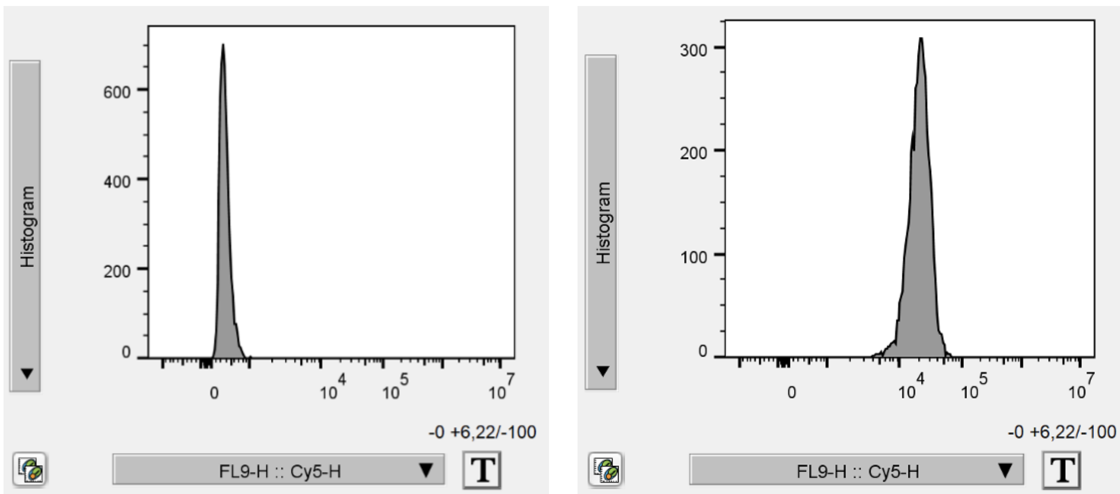

Figure 10. *Histogram of Cy5 fluorescence intensity for a) Unstained MDA-MB-231 cells and b) 7X Guanidinium SNA incubated with MDA-MB-231 cells.*

The histograms were overlayed in layout editor and the mean fluorescence intensity was determined by adding the mean Cy5 intensity statistic (**Figure 11**).

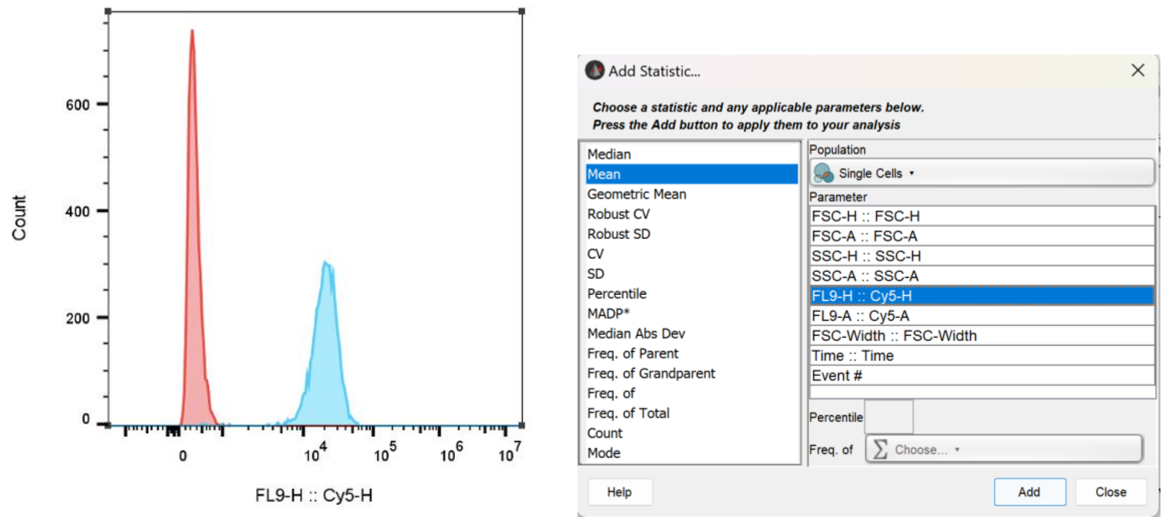

	Sample Name	Subset Name	Count	Mean : FL9-H
	Guan2.fcs	Single Cells	5661	20936
	Unstained.fcs	Single Cells	6004	379

Figure 11. *a) Overlayed histogram of unstained MDA-MB-231 cells with 7X Guanidinium SNA incubated with MDA-MB-231 cells. b) Mean fluorescence intensity statistic was applied to all samples.*

CHAPTER 3 – SYNTHESIS OF GUANIDINIUM FUNCTIONALIZED SNAS

Synthesis & Purification of N-Trifluoroacetyl-1,3-Propylenediamine

We hypothesized that phosphate backbone modifications could be used at the nanoscale to facilitate the cell entry of spherical nucleic acids and improve their localization to compartments of interest (e.g., cytoplasm). To test this, we first elected to synthesize SNAs functionalized with cationic modifications, such as guanidiniums, due to their demonstrated ability to facilitate transport of nanoscale objects across membranes.[20] To achieve this, we synthesized oligonucleotides derivatized with guanidiniums according to the protocol by Michel *et al*. In their approach, guanidinium groups are incorporated post-synthetically onto the phosphate backbone of oligonucleotides derivatized with primary amines in a 3 step process where 1) a diamine is protected with a base-labile protection group, 2) this protected diamine is introduced on the phosphate backbone of oligonucleotides using H-phosphonate chemistry to form a phosphoramidate-derivatized oligonucleotide that contains primary amine groups and 3) the amines are converted into guanidiniums post synthesis and deprotection to give the oligonucleotide of interest (**Figure 12**).

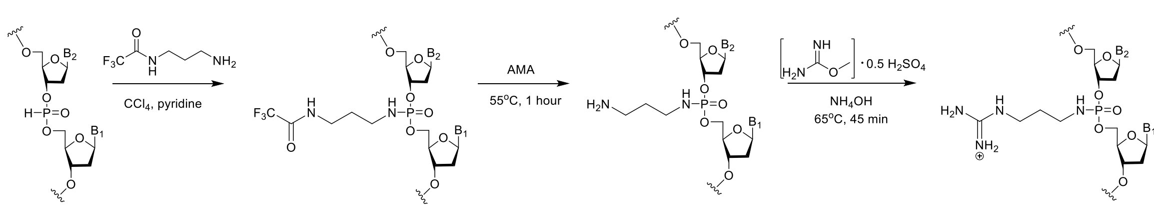

Figure 12. *Synthesis of guanidinium-functionalized oligonucleotides.*

As a first step, 1,3-diaminopropane was protected using ethyl trifluoroacetate, a protecting group that is conveniently removed during global deprotection of oligonucleotides under basic conditions.[45] By using a 1:1 stoichiometric ratio of 1,3-diaminopropane to ethyl trifluoroacetate, one amino group can be protected while the other amino group is left free to react (**Figure 13**).

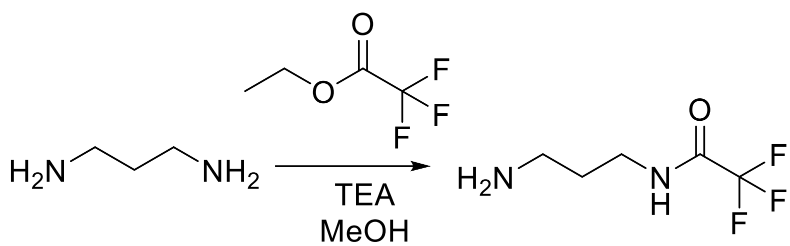

Figure 13. *Schematic of the Synthesis of N-Trifluoroacetyl-1,3-propylenediamine.*

This was done to avoid having the diamine starting material react from both ends, which would leave a nucleophilic group on the growing oligonucleotide chain, which can produce undesirable crosslinks between strands during solid phase synthesis. The amine protection reaction proceeds through a nucleophilic acyl substitution mechanism, producing ethanol as a by-product, which can be removed through rotary evaporation. To achieve effective separation of the mono-protected product from the starting material and di-protected product, column chromatography was performed using a silica column with an eluent composition of 77.5% THF, 17.5% MeOH, and 5% TEA. Typical yields of ~15% were achieved after purification due to loss of product on the silica column. This is because silica is slightly acidic while the primary amine of N-trifluoroacetyl-1,3-propylenediamine is slightly basic. This creates a strong interaction that requires a competing amine, hence the use of TEA during the separation, and reduces the overall yield of synthesis. Although the yield is poor, minimal product is required for oxidative amination onto the phosphate backbone of oligonucleotides and all starting material were cheap to acquire, facilitating gram scale syntheses. Another convenient aspect of this synthesis was its applicability to diamines of different lengths (e.g., ethyl and butyl), which provided a handle to modulate the hydrophobic character of the modified oligonucleotides. Successful synthesis of the product was confirmed using ^{1}H NMR, which showed three strong resonances corresponding to an integration of 2 protons each (**Figure 5**, **Figure S1** and **Figure S2**).

Oligonucleotide Synthesis

Oligonucleotides were then synthesized using a combination of automated protocols using phosphoramidite and phosphoramidate chemistry.[44,45] Phosphoramidite chemistry was used to synthesize unmodified oligonucleotide sequences on a solid support that contain phosphate internucleoside linkages. The phosphoramidite cycle entails a stepwise addition of nucleotides in the 3’ to 5’ direction until the desired sequence is achieved (**Figure 14**). Briefly, the 5’ DMT group is removed on the growing oligonucleotide chain, revealing a 5’ hydroxyl group. An incoming phosphoramidite is activated by a tetrazole catalyst and the 5’ hydroxyl group of the growing chain attacks the phosphorous. An oxidation step is then performed using iodine to generate a phosphorus(V) centre from a phosphorus(III) centre. The cycle is repeated until the desired oligonucleotide sequence is achieved. Phosphoramidite chemistry has been well established and is the gold standard method for producing synthetic DNA/RNA due to its nearly quantitative yields at each coupling step (typically >99.5%).[47]

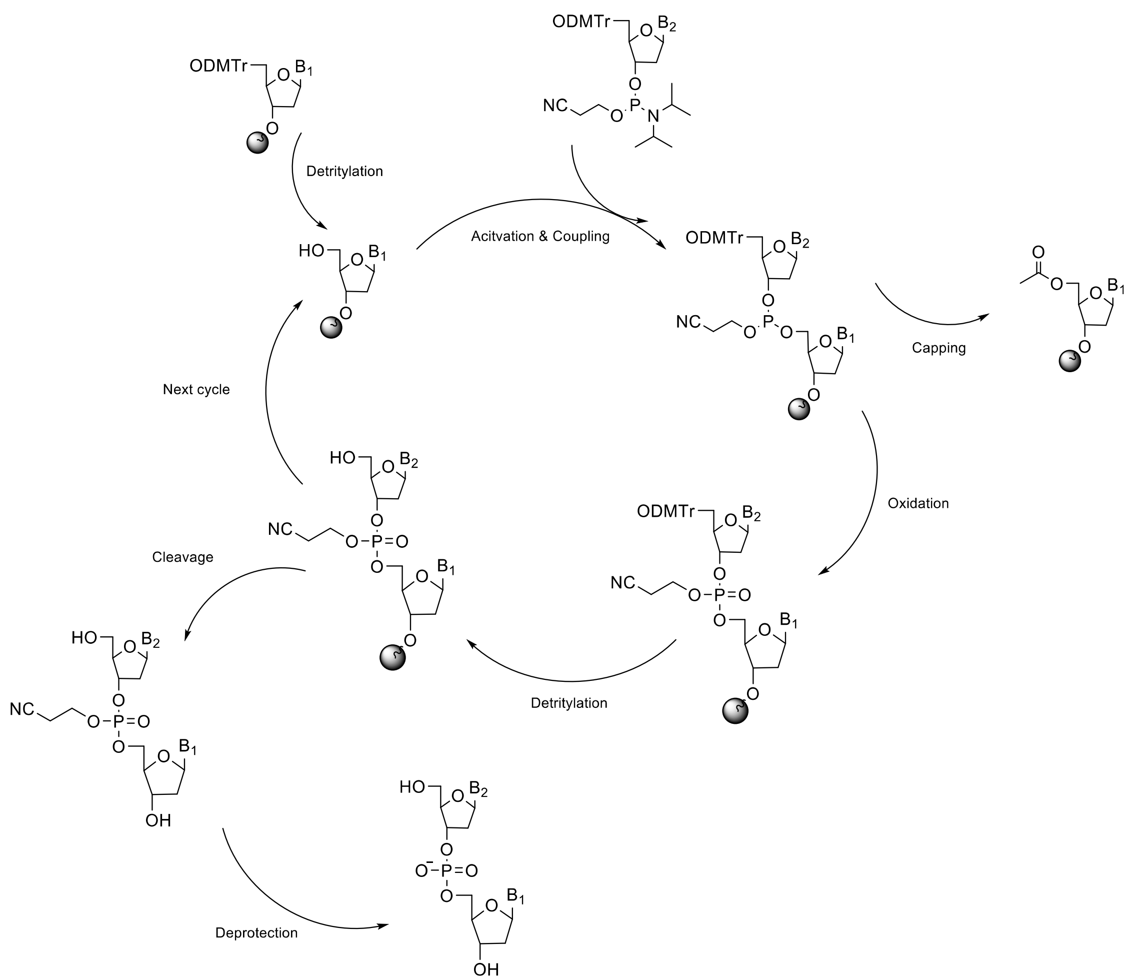

Figure 14. *Phosphoramidite cycle used to generate oligonucleotides.*

In contrast, phosphoramidate chemistry was used to amidate the phosphorus atom, effectively replacing the typical phosphodiester bond with a P-

N linkage instead, allowing for chemical manipulation and introduction of new functionality at the phosphorus atom directly (**Figure 15**). Introducing modifications to the phosphate backbone of oligonucleotides is not as accessible when compared to other chemical modifications such as deoxyribose sugar or nitrogenous base alterations. This is because the typical phosphoramidite synthesis cycle is disrupted and new coupling chemistry needs to be adapted, including the introduction of different precursors. Vlaho and Damha have optimized phosphoramidate synthesis using an automated solid-phase synthesis approach that employs H-phosphonate nucleosides as precursors to establish internucleoside phosphoramidate linkages, with coupling yields of >97% per step.[45] Compared to phosphoramidite synthesis, the H-phosphonate approach has a distinct set of advantages, including access to a broad scope of biologically relevant phosphate analogues through changes in oxidation conditions.[48] Despite the longer synthesis times and the modified building blocks needed to introduce P-N linkages, they induce pronounced changes to the properties of oligonucleotides, providing them with new utility in a biological setting. Conveniently too, all standard DNA nucleosides can be purchased as H-phosphonate derivatives, further reducing access barriers to these types of modified oligonucleotides.

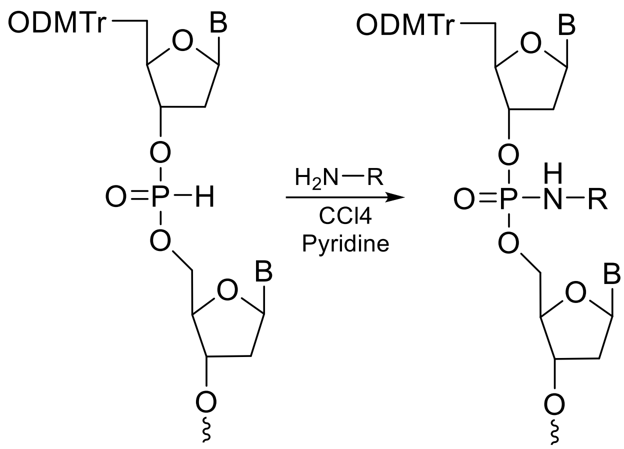

Figure 15. *H-Phosphonate approach to phosphoramidate linkages.*

To successfully incorporate phosphoramidate internucleoside backbone linkages, commercial H-phosphonate nucleoside derivatives were coupled in sequence to establish oligonucleotides of various lengths, using adamantane carbonyl chloride as an activator. An additional oxidative amination step was then performed to create P-N linkages at the phosphorus using primary amines derivatized with different substituents (**Figure 16**).[33,45] Briefly, the 5' DMT group on the growing oligonucleotide chain is removed to expose a 5' hydroxyl group. An incoming thymidine H-phosphonate nucleoside derivative is activated with adamantane carbonyl chloride and coupled onto the growing chain. An oxidative amination step is performed using carbon tetrachloride to effectively amidate the phosphorus, generating P-N linkages. The cycle is repeated to achieve as many phosphoramidate linkages as required. Both synthetic methods (phosphoramidite and phosphoramidate) were carried out in an automated fashion on an oligonucleotide synthesizer (MerMade 6).

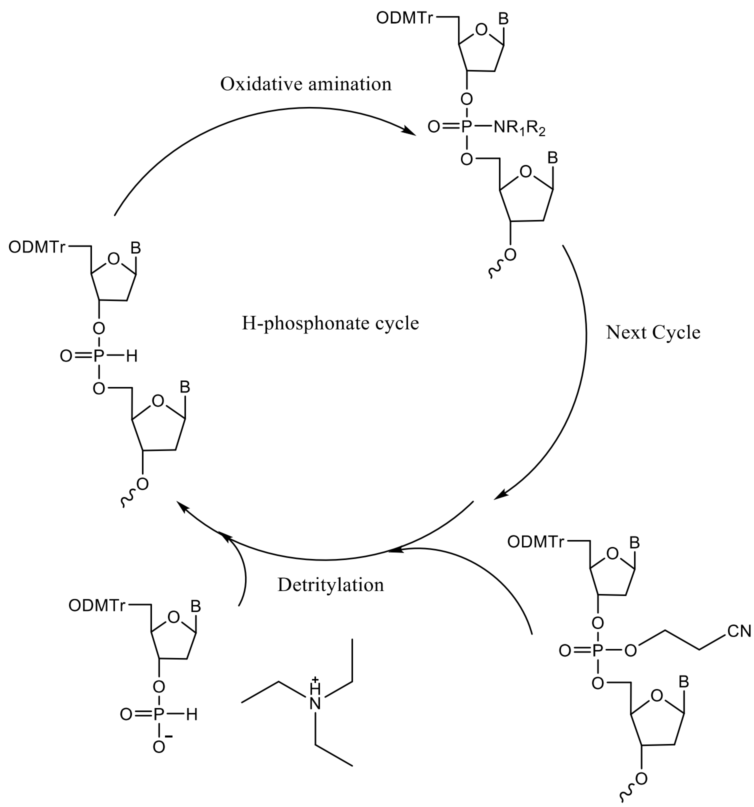

Figure 16. *Complete H-phosphonate cycle to introduce phosphoramidate linkages.*

Synthesis of Oligonucleotides Containing Phosphoramidate Linkages

The protected monomer (N-trifluoroacetyl-1,3-propylenediamine) was introduced onto the phosphate backbone of H-phosphonate nucleoside derivatives. Specifically, N-trifluoroacetyl-1,3-propylenediamine was functionalized either 3 times or 7 times onto thymidine H-phosphonate nucleosides at the 3’ end using phosphoramidate synthesis protocols as described in the Materials & Methods section. As controls, oligonucleotides of the same length and sequence were synthesized using unmodified phosphate linkages. Following these couplings, an antisense oligonucleotide was synthesized using phosphoramidite chemistry, thereby creating mixed backbone oligonucleotides where the phosphoramidate was introduced at the 3' end to facilitate cell entry, and the 5' end carries the ASO for a therapeutic effect (**Figure 17**). To incorporate these strands into spherical nucleic acids, each strand was provided with a thiol tail at the 5' end using phosphoramidite chemistry, introduced during synthesis as a disulfide. This allows the bioconjugation of oligonucleotides to gold nanoparticles through a covalent (Au-S) bond. The thiol was incorporated on the ASO side to ensure the therapeutic oligonucleotide was clustered near the core of the nanoparticles and thereby protected from nucleases in serum. In contrast, the phosphoramidate linkages were placed on the other end of the strand (3' end) to ensure they ended up on the surface of the SNAs and facilitate their interactions with cell membranes. The modular design strategy of this approach ensured the number and type of phosphoramidate modifications were controlled, enabling the study of structure-function relationships with these backbone modifications in the context of cell uptake. This approach could also potentially be leveraged into a platform technology in which various ASOs can be inserted depending on the target of interest, highlighting its addressability to a broad scope of indications.

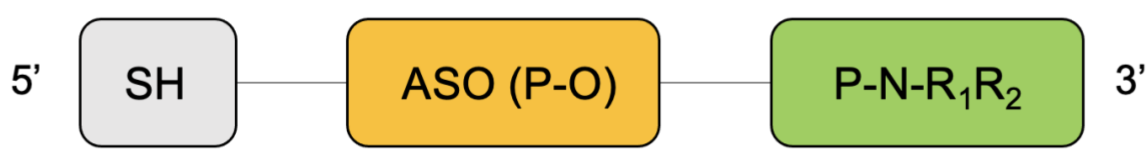

Figure 17. *Oligonucleotide Design Strategy. Phosphoramidate linkages are placed at the 3' end to facilitate cell entry. A thiol tail is placed at the 5' end for bioconjugation to AuNPs along with an ASO for therapeutic effect.*

Oligonucleotide Deprotection & Purification

Post-synthesis, a global deprotection step was carried out in basic conditions to cleave 1) the protecting groups from the nitrogenous bases, 2) the solid support from the oligonucleotides, 3) the cyanoethyl protection groups on phosphate linkages and 4) the ethyl trifluoroacetate protecting groups on the primary amines. The phosphoramidate linkages remained stable under these basic conditions while being heated at a temperature of 55°C for 45 minutes, indicating no cleavage of the phosphoramidate linkage when analyzed by MALDI-TOF MS. At the 5' end, a 4,4'dimethoxytrityl (DMT) group was maintained on each oligonucleotide during the synthesis cycle to enable purification by RP-HPLC. The DMT group is a bulky and hydrophobic protecting group that interacts with the hydrophobic stationary phase of RP-HPLC columns, allowing separation from sequences that do not carry this handle. As a result, the fully synthesized oligonucleotide sequences containing a final 5'-DMT group have a higher affinity for the hydrophobic stationary phase of the RP-HPLC column and be retained longer in the column as failed sequences are eluted earlier. This approach facilitated the synthesis of mixed backbone oligonucleotides in high purity as evidenced by MALDI-TOF MS.

Detritylation, Reduction & Desalting

Following purification of the oligonucleotides, the 5'-DMT (DMT) group is typically cleaved in acidic conditions, followed next by a reduction of the disulfide to obtain a primary thiol for AuNP conjugation, thus giving rise to the fully purified and deprotected oligonucleotide. However, for amine-derivatized oligonucleotides, a slightly altered protocol was used. They were first detritylated in acid, followed by a guanidinylation reaction to introduce guanidium groups and they were reduced to thiols as the last step. This order of reaction was used since primary thiols are strong nucleophiles and can become guanidinylated as well by attacking the electrophilic carbon of the primary imine of O-methylisourea hemisulfate. As a result, there would be no handle to covalently attach the oligonucleotides to the AuNPs, disrupting SNA formation. Importantly, under the acidic conditions used to remove the DMT group, the phosphoramidate linkages remained completely intact, highlighting their resistance to acidic environments. To remove any remaining salts and small molecules from solution, including the cleaved DMT group, desalting columns made of Sephadex G20 resin were used. Sephadex is a cross-linked dextran gel that effectively serves as a form of size exclusion chromatography (SEC) and can perform buffer exchanges. Overall, the approach used to complete the deprotection of the modified oligonucleotides was successful and enabled the preparation of highly pure mixed backbone oligonucleotides.

Guanidinylation Reaction of Primary Amines

Oligonucleotides bearing free amines from phosphoramidate linkages were subjected to a guanidinylation reaction using O-methylisourea hemisulfate.[33] O-methylisourea hemisulfate was the guanidylating reagent of choice as previous procedures have shown its improved guanidinylation efficiency relative to other reagents.[33,49] The reaction mechanism most likely proceeds through a nucleophilic attack initiated by the primary amine derivatized on the phosphate backbone of the oligonucleotide. The amine can attack the electrophilic carbon centre of the primary imine of O-methylisourea hemisulfate to form a tetrahedral intermediate. Upon reforming the guanidinium, methanol is lost as a leaving group in the process. This provides the oligonucleotides with inherently cationic guanidinium residues at physiological pH (pKa = 12.48). Due to the intrinsic acidity of O-methylisourea hemisulfate in solution, ammonium hydroxide was used to correct the reaction to a pH of >11. It is imperative that the reaction is maintained above or equal to a pH of 11 as primary amines and lysine have a pKa ranging from ~9.5-11 and require deprotonation to activate them as potent nucleophiles.[50] We found that pH was the most important parameter governing the efficiency of the guanidinylation reaction, as decreasing the O-methylisourea hemisulfate concentration still provided full guanidinylation of the amine derivatized backbone linkages compared with concentrations used in literature.[33,49] The oligonucleotides were stable under the reaction conditions (65°C) and no deleterious effects were observed including P-N cleavage or depurination by MALDI-TOF MS, confirming the synthesis of mixed charge oligonucleotides carrying guanidinium groups.

MALDI-TOF MS Analysis of Oligonucleotides

The exact mass of the oligonucleotides was determined using MALDI-TOF MS in positive ion mode. MALDI-TOF MS analyzes the oligonucleotides based on the time they take to fly through a time-of-flight tube or “drift” region to the detector which provides the exact mass of the oligonucleotides. **Figure 18**, **Figure 19**, **Figure 20** and **Figure 21** show the MALDI-TOF MS spectra of phosphoramidate modified oligonucleotides and depict sharp and narrow peaks associated with the expected masses of the strands. These results are also tabulated in **Table 5** which show excellent match between expected values and found masses by MALDI-TOF MS for mixed backbone oligonucleotides. This demonstrates the feasibility of our synthetic approach and the ability to maintain rigorous control over the placement of charged motifs within the phosphate backbone of oligonucleotides. Additionally, we can effectively and selectively saturate all the free amines derivatized on the oligonucleotide backbone with guanidinium residues, eliminating the need for a subsequent purification step.

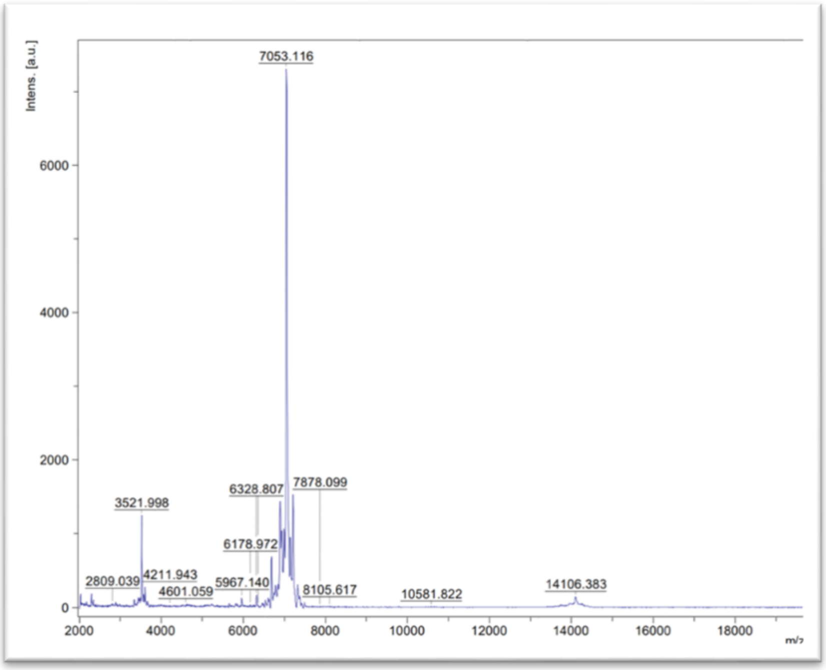

Figure 18. *3X NH2 oligonucleotide MALDI-TOF MS spectrum.*

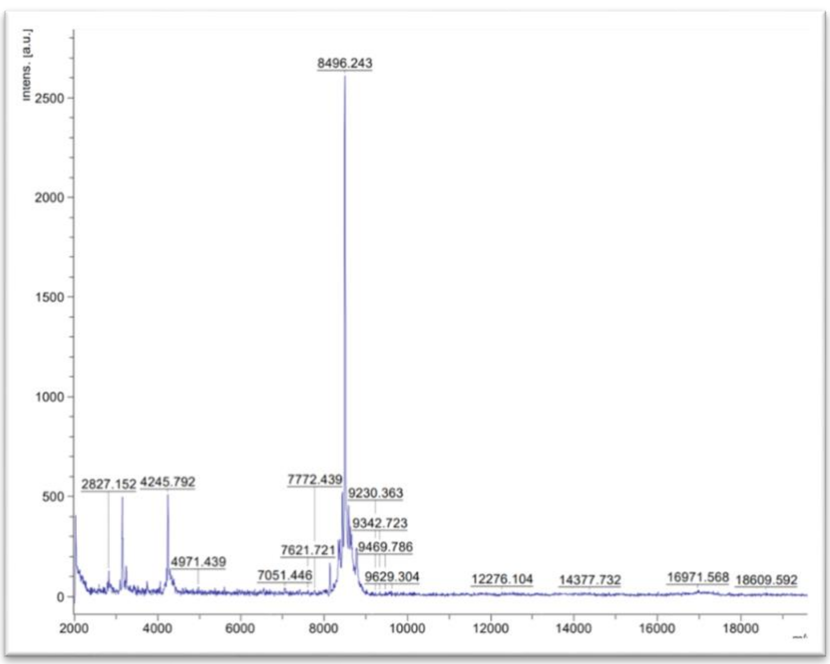

Figure 19. *7X NH_2 oligonucleotide MALDI-TOF MS spectrum.*

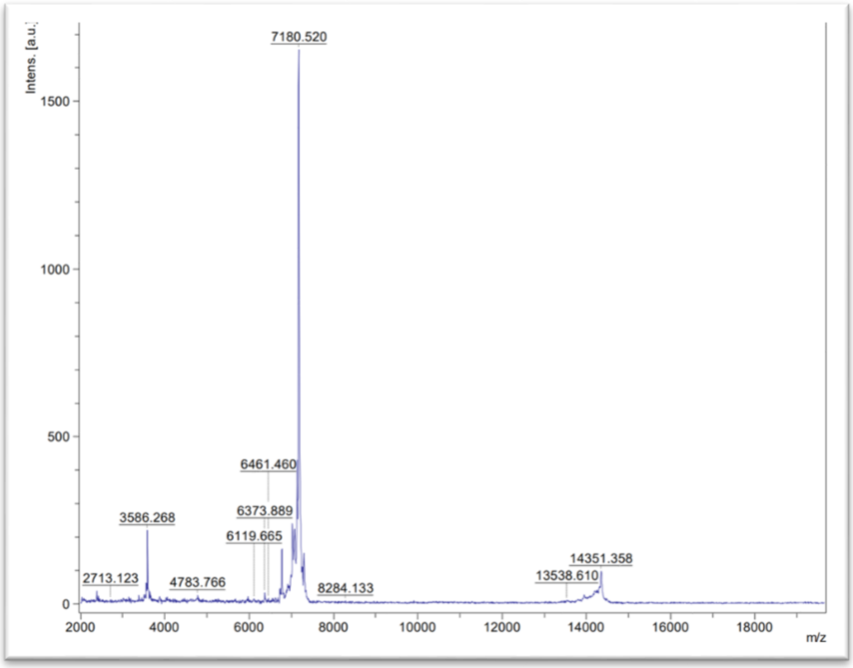

Figure 20. *3X Guan oligonucleotide MALDI-TOF MS spectrum.*

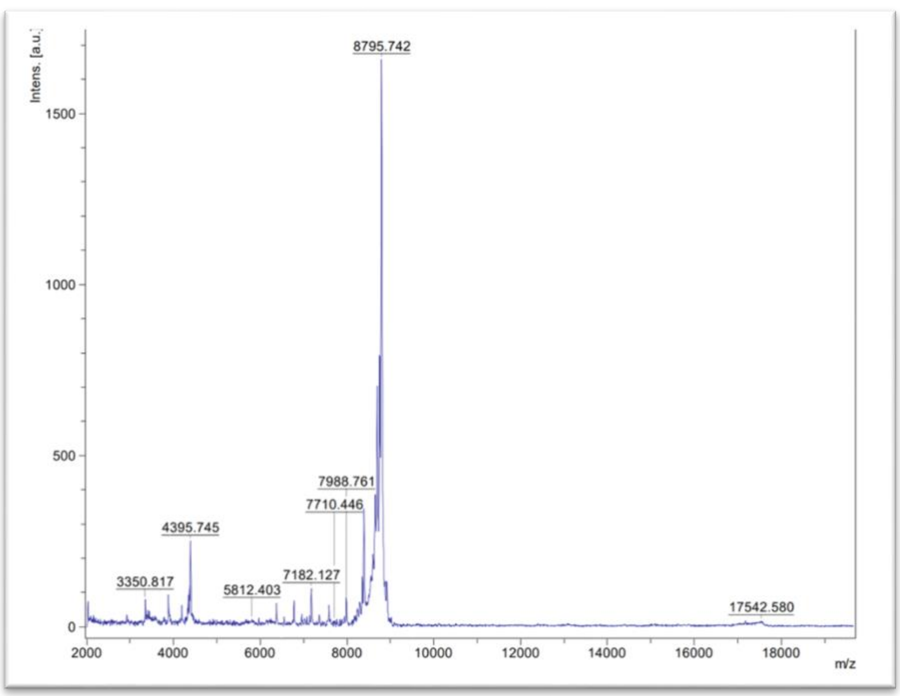

Figure 21. *7X Guan oligonucleotide MALDI-TOF MS spectrum.*

Table 5. *Oligonucleotide masses found by MALDI-TOF MS compared to their exact masses.*

Oligonucleotide	Exact Mass (Da)	Found Mass (Da)	Δ
T10-Cy5	3710.8	3712.4	+1.6
T20-Cy5	6752.8	6757.3	+4.5
3T Control	6572.4	6586.3	+13.9
7T Control	8093.3	8101.6	+8.3
3X NH_2	7050.6	7053.1	+2.5
7X NH_2	8499.3	8496.2	-3.1
3X Guanidinium	7176.6	7180.5	+3.9
7X Guanidinium	8793.2	8795.7	+2.5

Guanidinium Oligonucleotides Display Strong Electrostatic Interactions

A purification gel was performed on a 3X guanidinium functionalized oligonucleotide with 8 M urea. Three bands were excised from the gel and the oligonucleotides were extracted and analyzed by MALDI-TOF MS for exact mass determination (**Figure 22a**).

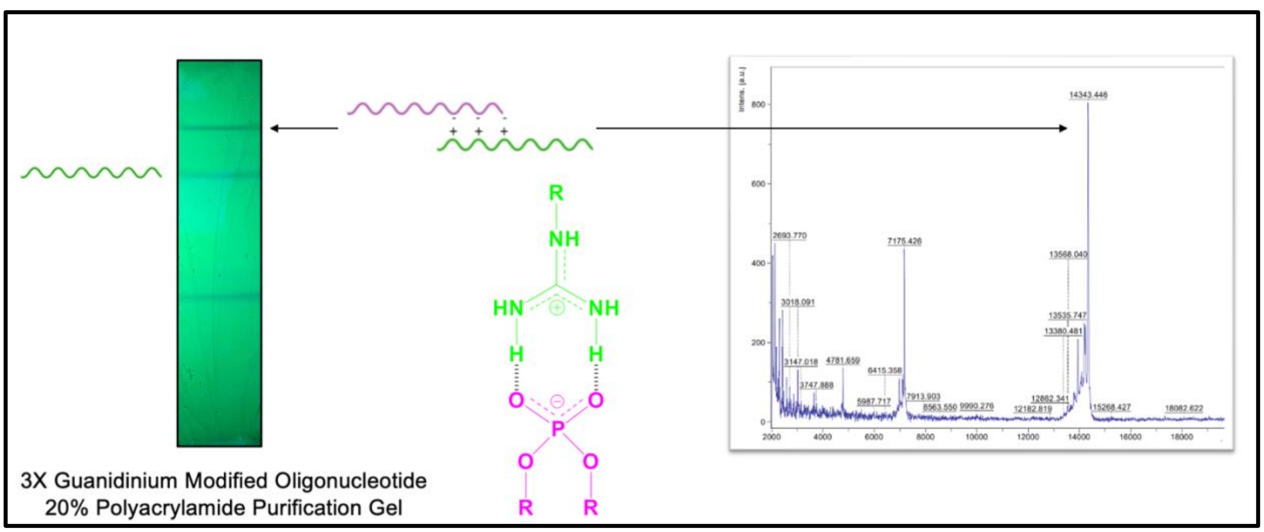

Figure 22. *(a) 20% polyacrylamide purification gel (8 M urea) of 3X Guan oligonucleotide. (b) Electrostatic interaction between guanidinium motifs and phosphate groups. (c) MALDI-TOF MS spectra showing dimer of guanidinium oligonucleotides.*

PAGE separates oligonucleotides based on their size and charge, allowing smaller and more negatively charged oligonucleotides to migrate further down the gel towards the cathode. Additionally, the gel was conducted in 8 M urea, which functions as a denaturant and will disrupt hydrogen bonding between the nucleobases, linearizing the oligonucleotides. As a result, electrostatic forces are governing the interactions between the oligonucleotides. Specifically, the guanidinium groups carry a positive charge at physiological pH and are forming electrostatic interactions with the phosphate groups, which are negatively charged at physiological pH (**Figure 22b**). An analysis by MALDI-TOF MS confirms that a dimer had formed, indicated be a peak that is approximately twice in mass relative to the single stranded oligonucleotide (**Figure 22c**). This demonstrates that guanidinium derivatized oligonucleotides display strong electrostatic interactions, even with minimal guanidinium motifs. Molecular dynamics simulations by Deglane and Vasseur support these findings by revealing interactions between the anionic backbone of nucleic acid targets and the cationic backbone of modified oligonucleotides, enhancing their affinity for complementary targets and duplex formation.[51]

Stability of Phosphoramidate Linkages

An oligonucleotide containing three phosphoramidate linkages (3X NH_2) was incubated with either water, 1X PBS, or 1X DMEM media at a final concentration of 30 μM. The mixtures were incubated for 4 hours at 37°C to determine if the phosphoramidate linkages were stable under relevant physiological conditions. The oligonucleotides were analyzed by MALDI-TOF MS to determine if there was any cleavage of the phosphoramidate linkages (**Figure 23**, **Figure 24** and **Figure 25**). Analysis by MALDI-TOF MS revealed that under all three conditions, phosphoramidate linkages remained intact and no cleavage was observed. A consistent mass of ~7044 Da was observed for all 3 samples, consistent with the expected mass of the strand (**Table 5**). As discussed above, the phosphoramidate-modified oligonucleotides displayed stability over a broad pH and temperature range. In addition to that. we observed no degradation or loss of linkages at temperatures of 4°C and -20°C for months at a time. Moreover, reactions conducted at elevated temperatures (~65°C) and in pH ranges from ~2.5-11.5 did not induce any degradation or cleavage of the phosphoramidate linkages. Their stability over a broad range of conditions not only makes their handling and manipulation facile, but also validates their utility in various biomedical applications.

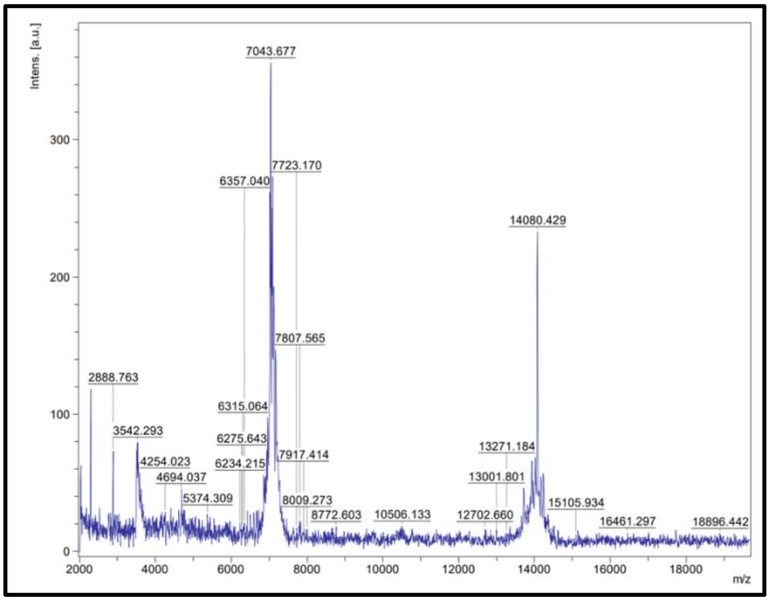

Figure 23. *3X NH_2 incubated with water for 4 hours at 37°C.*

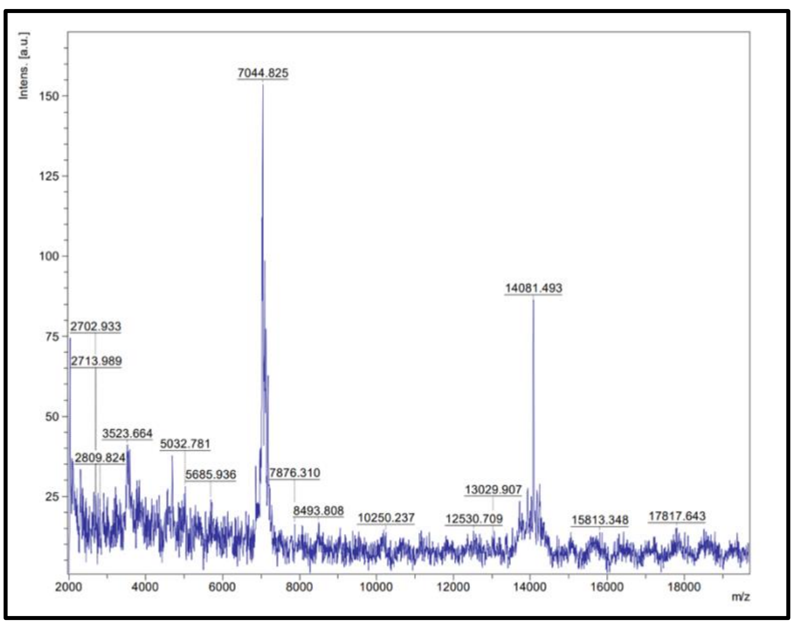

Figure 24. *3X NH2 incubated with 1X PBS for 4 hours at 37°C.*

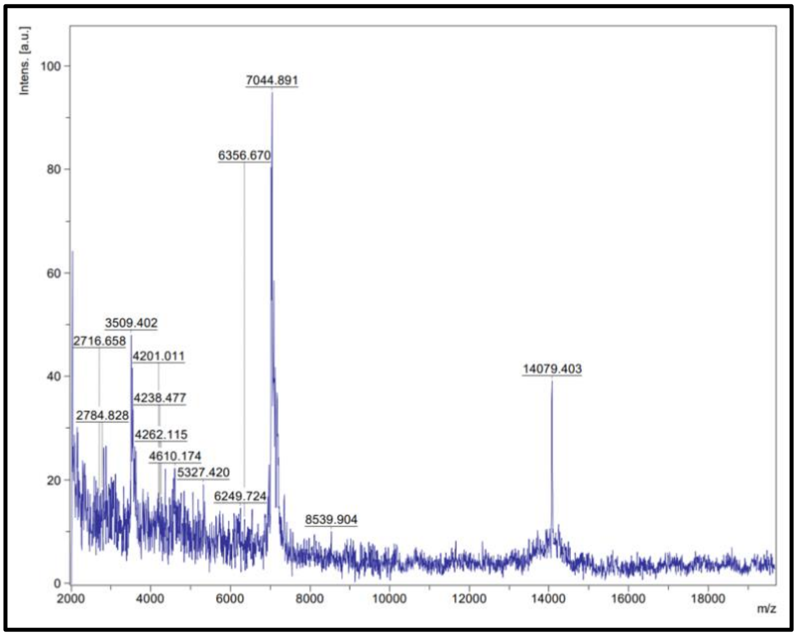

Figure 25. *3X NH2 incubated with 1X DMEM for 4 hours at 37°C.*

Dual Layer Spherical Nucleic Acid Synthesis

Synthesis & Characterization of 13 nm AuNPs

13 nm citrate capped AuNPs were synthesized according to Liu and Lu (2006).[46] The nanoparticles were analyzed by transmission electron microscopy (TEM) to determine their size, shape, and distribution (**Figure 26**).

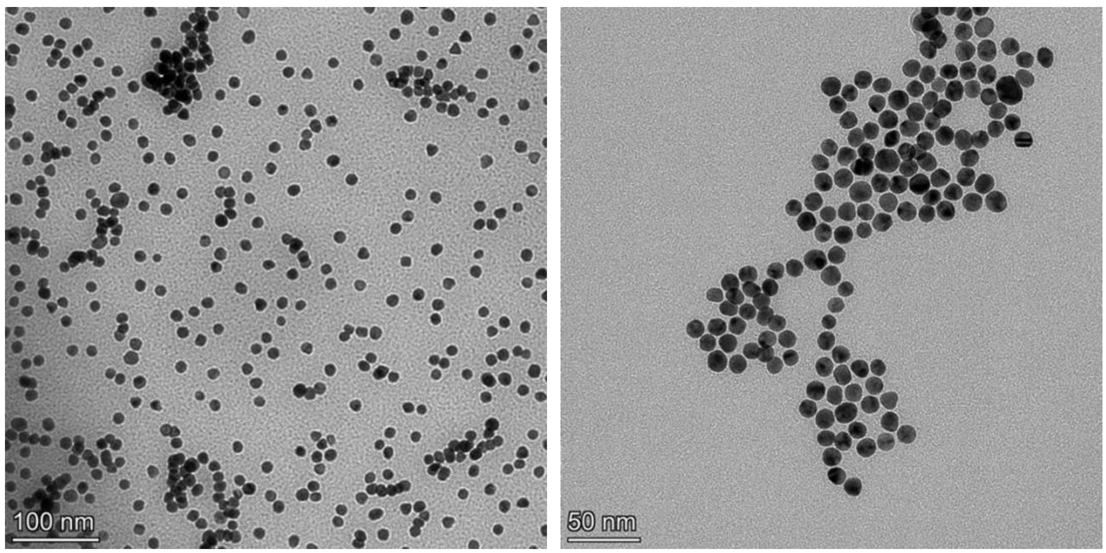

Figure 26. *13 nm gold nanoparticles observed by TEM.*

The nanoparticles were found to have an average size of 13.48 nm with a standard deviation of 1.41 nm based off 100 measurements using ImageJ software. The size of the nanoparticles is directly correlated with their properties and cellular interactions. The uniform size distribution of the 13 nm citrate capped gold nanoparticles will ensure the control, predictability, and reliability of their behaviours across different batches of SNAs and in biological assays.

Cy5 Monolayer SNA Synthesis

To track and quantify SNAs in biological systems, a fluorescent label is required to visualize and quantify them. Therefore, we synthesized oligonucleotides with Cy5 fluorescent dyes and generated spherical nucleic acids with an initial layer of Cy5 dye. We chose to incubate the Cy5 labelled DNA and AuNPs at a ratio of 85:1, as increasing the loading density would saturate the surface of the AuNPs, leaving limited space for the second layer of backbone modified oligonucleotides. Conversely, lowering the loading density of Cy5 DNA to AuNPs was found to cause aggregation and instability of the monolayer. The aggregation can be attributed to the instability of the nanoparticles in highly ionic environments[52], a requirement when functionalizing them with biomolecules. We found that at a ratio of 85:1, the surface charge imparted by the negatively charged oligonucleotides can repel neighbouring particles, imparting higher nanoparticle stability. Therefore, this ratio provides a nice compromise between nanoparticle stability while minimizing surface functionalization.

Dual Layer SNA Synthesis

After the Cy5 SNA monolayer had been established, it was used as the new stock to synthesize dual layer SNAs. The remainder of the Cy5 monolayer SNA surface was saturated with backbone modified oligonucleotides and the salt concentration in solution was gradually increased to achieve densely functionalized surfaces, a process known as salt-aging (**Figure 27**).[53] Salt-aging is a technique that promotes a high loading density of oligonucleotides onto the surface of gold nanoparticles by gradually increasing the concentration of salt in solution. The electrostatic repulsion of neighbouring oligonucleotides is effectively screened, enabling an increased packing density on the nanoparticle surface until steric constraints prevent further adsorption.[37] Because phosphate backbone modifications have been largely unexplored in the context of nanoscale architectures, we used a variety of techniques to characterize them including ultraviolet visible spectroscopy (UV-vis), agarose gels, fluorescence based functionalization assays, and dynamic light scattering (see next chapter).

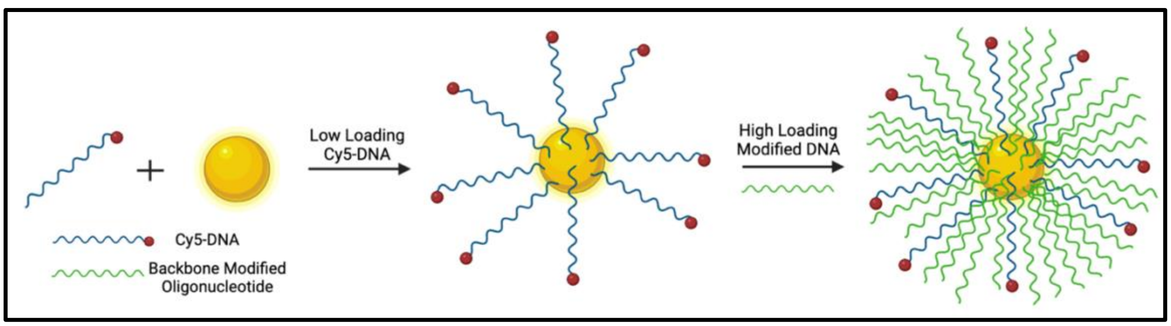

Figure 27. *Synthesis of dual-layer SNAs.*

Characterization of Dual Layer SNAs

<u>UV-visible Spectroscopy</u>

At a specific wavelength/frequency of light, electron oscillation on gold nanoparticle surfaces causes a phenomenon called surface plasmon resonance (SPR), resulting in a strong adsorption and scattering of light. For 13 nm spherical AuNPs, this wavelength is 520 nm. Therefore, UV-vis can provide us important information regarding the size, shape, and concentration of our dual layer SNAs.

Figure 28 highlights a series of dual layer SNAs with absorbances between ~522-523 nm, consistent with 13 nm AuNPs functionalized with a DNA corona. Additionally, the SNAs remained a deep red colour, consistent with the colour of naked gold nanoparticles, and did not exhibit a colour change from red to purple. Aggregation was not observed as a colour change from red to purple would ensue, in accordance with a shift in the SPR peak from ~520 nm to ~600 nm.[37]

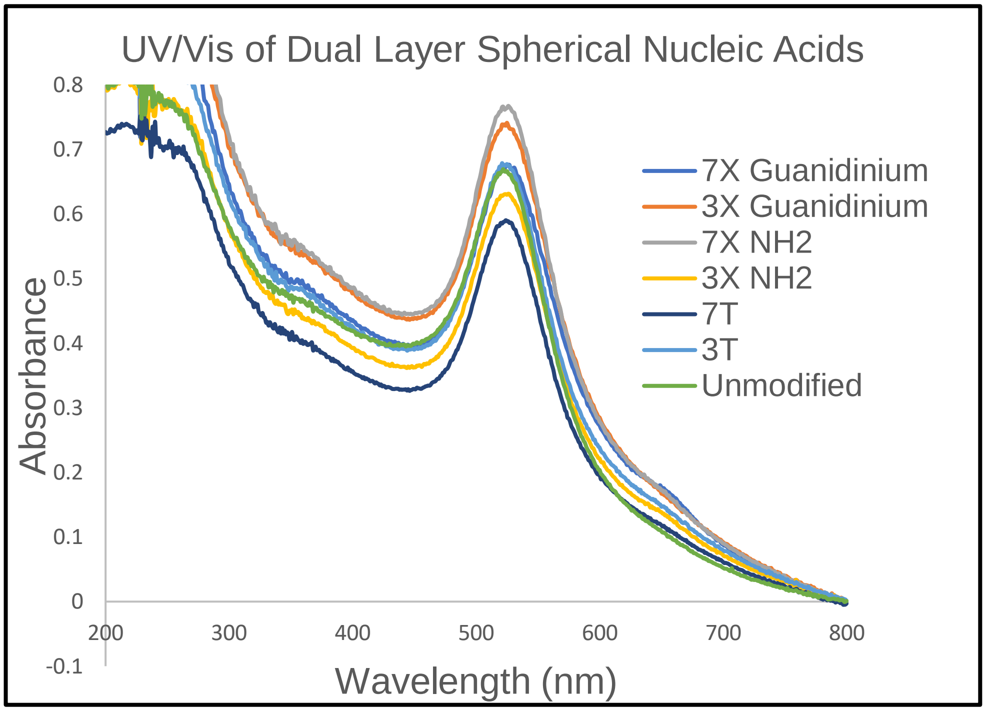

***Figure 28**. UV-vis analysis of dual layer SNAs.*

Agarose Gels

Dual layer SNAs were subjected to 1% agarose gels run in 1X TBE buffer (**Figure 29** and **Figure 30**) to determine their monodispersity as well as to verify that a second layer of phosphate backbone modified oligonucleotides was functionalized.

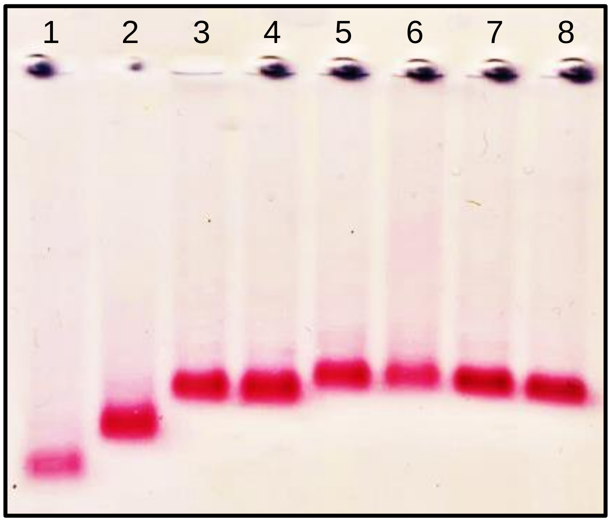

SNA	Lane
Cy5 Monolayer	1
Unmodified	2
3T	3
7T	4
3X NH2	5
7X NH2	6
3X Guanidinium	7
7X Guanidinium	8

Figure 29. *1% Agarose (1X TBE) 500:1 DNA: AuNP*

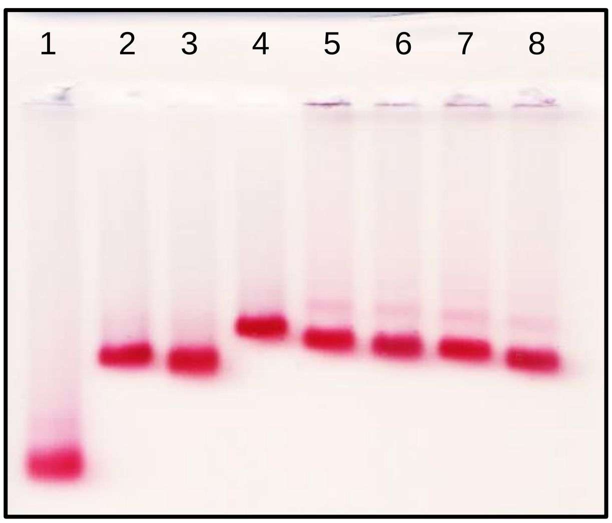

SNA	Lane
Cy5 Monolayer	1
Unmodified	2
3T	3
7T	4
3X NH2	5
7X NH2	6
3X Guanidinium	7
7X Guanidinium	8

Figure 30. *1% Agarose (1X TBE) 750:1 DNA: AuNP*

Dual layer SNAs were assembled using a ratio of either 500:1 or 750:1 backbone modified oligonucleotide: Cy5 SNA monolayer. The dual layer SNAs have a reduced mobility through the gel compared with the Cy5 monolayer, indicative of an increased oligonucleotide loading density on the nanoparticle surfaces. Additionally, the extent of oligonucleotide functionalization on the AuNPs can be controlled by varying the loading ratio between the two. Oligonucleotides loaded with a ratio of 750:1 (**Figure 30**) strands per Cy5 SNA monolayer display an even greater separation from the Cy5 monolayer, compared to a ratio of 500:1 (**Figure 29**). Furthermore, the SNAs appear as sharp bands on the gel with minimal to no streaking, representative of monodisperse SNAs. This indicates that we can incorporate positively charged phosphate backbone modifications into well-defined SNA architectures.

DLS (Dynamic Light Scattering)

DLS was performed on dual layer SNAs to determine their size distribution profile, which provides more quantitative measurements compared with UV-vis and agarose gels. 13 nm AuNPs were analyzed by DLS as a control (**Figure 31**, **Figure 32** and **Figure 33**) and were found to have a diameter of ~13 nm, consistent with the size measured by TEM.

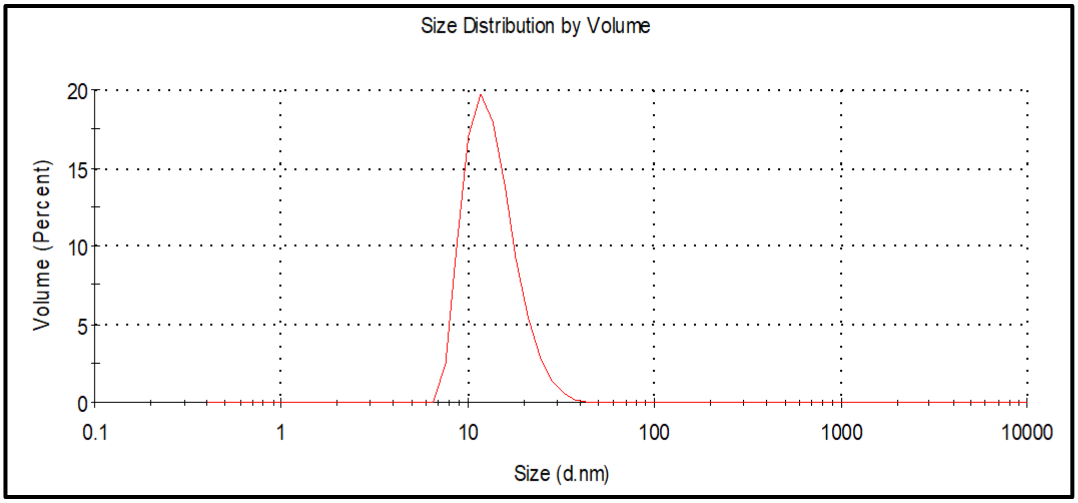

Figure 31. *13 nm AuNPs size distribution by volume*

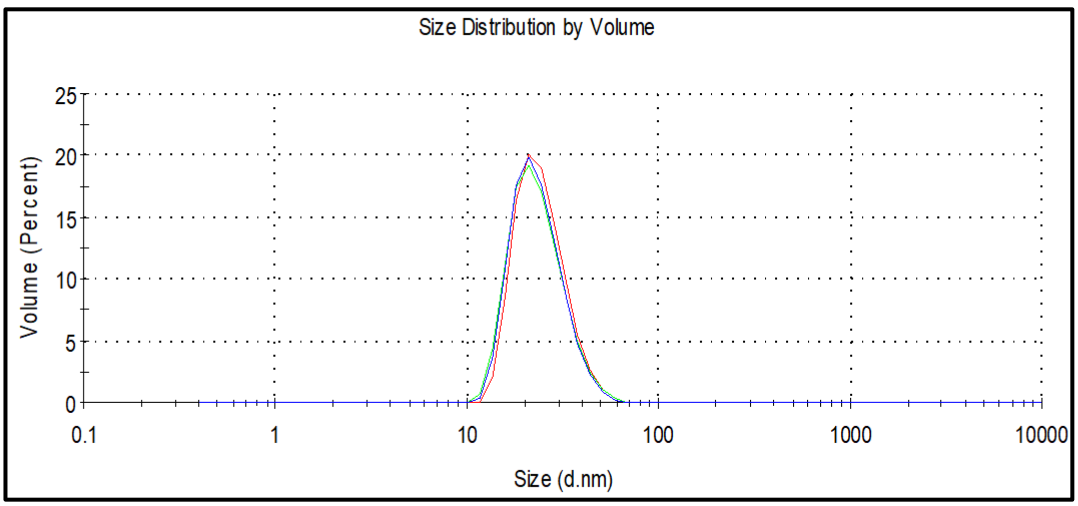

Figure 32. *4X NH_2 dual layer SNA size distribution by volume*

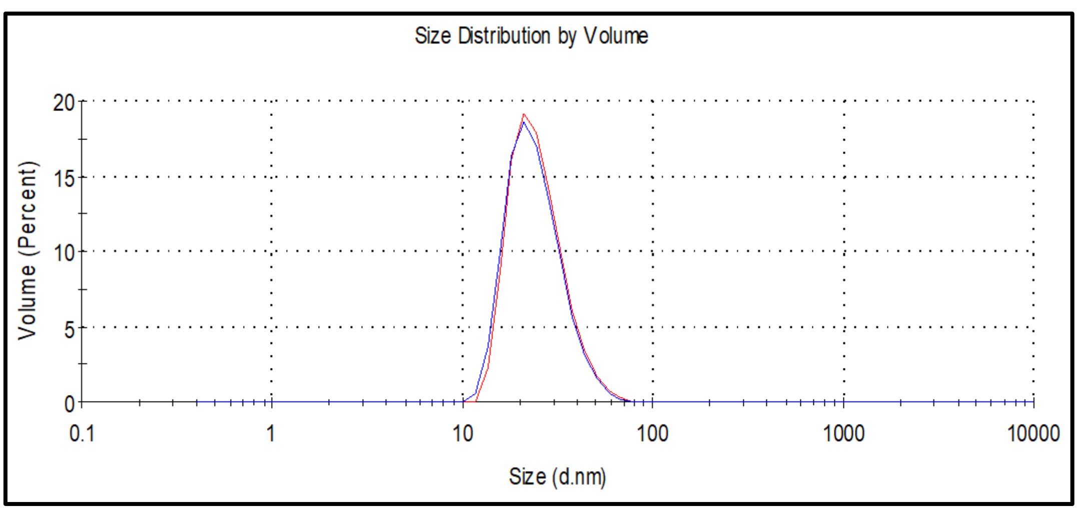

Figure 33. *8X NH2 dual layer SNA size distribution by volume*

Additionally, 4X and 8X NH_2 modified dual layer SNAs were analyzed by DLS and were found to have diameters of ~28 nm and ~31 nm, respectively. The found diameters were very close to their expected diameters (**Table 6**).

Table 6*. Expected versus found diameters of dual layer SNAs measured by DLS.*

Dual Layer SNA	Expected Diameter (nm)	Found Diameter (nm)
13 nm AuNP	~ 13	12.99 ± 0.37
4X NH_2	~ 28	28.02 ± 0.33
8X NH_2	~ 31	30.00 ± 0.40

The DLS data demonstrates that monodisperse dual layer SNAs can be assembled from phosphoramidate modified oligonucleotides, corroborating the data seen with agarose gels and UV-vis.

AuNP Functionalization Assays

To accurately determine the extent of oligonucleotide functionalization on the gold nanoparticles, fluorescent based assays were used to provide quantitative assessments of how many oligonucleotides were functionalized per AuNP. A calibration curve was established by performing a 2-fold serial dilution on a Cy5 labelled oligonucleotide, the strand used to assemble the Cy5 SNA monolayer (**Figure 34**). By dividing the recorded absorbances for the SNAs by the slope of the calibration curve, we can determine the concentration of Cy5-DNA in the monolayer. Dividing this concentration of Cy5-DNA by the concentration of initial

AuNPs in the assay, we can establish the number of strands/AuNP. Typical monolayer functionalization was found to be between ~69-75 strands per AuNP.

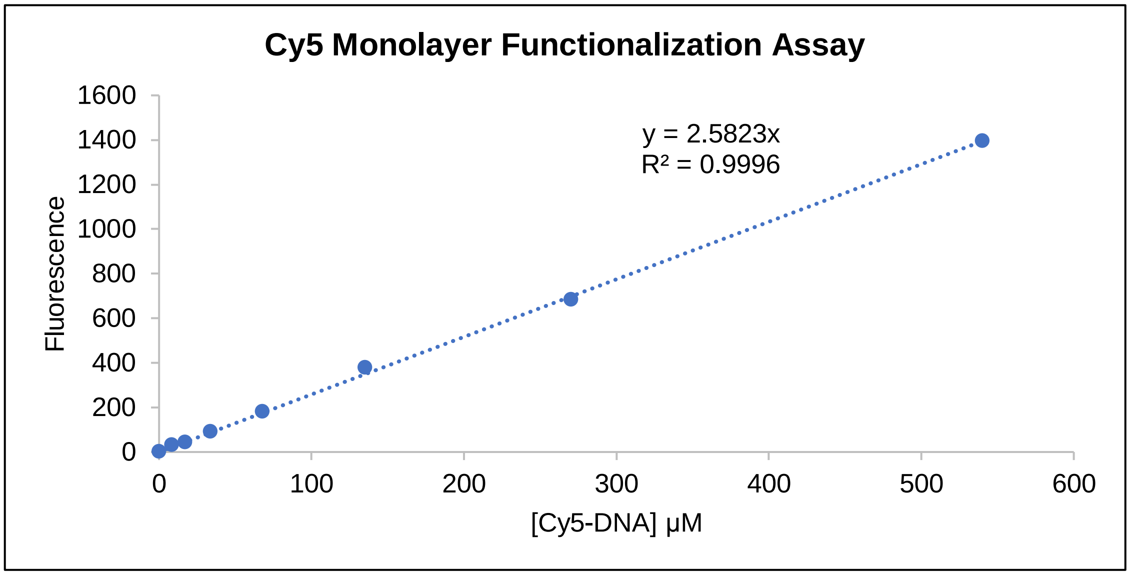

Figure 34. *Calibration curve for Cy-5 labelled DNA. Excitation (651 nm), Emission (670 nm).*

When measuring the functionalization of dual layer SNAs, a calibration curve was established as previously described using an excitation (480 nm) and emission (520 nm) for Oligreen® (**Figure 35**). Oligreen is an ultrasensitive nucleic acid stain for quantitating oligonucleotides and single-stranded DNA in solution.

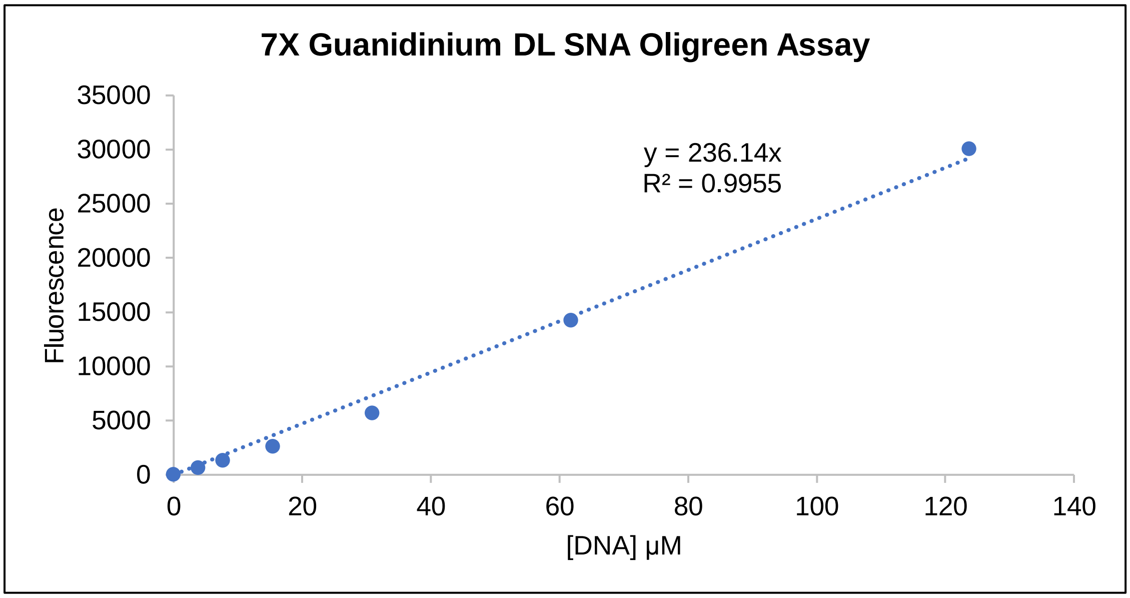

Figure 35. *Calibration curve for 7X guan oligonucleotide. Excitation (480 nm), Emission (520 nm).*

The Oligreen fluorophore will provide the total number of oligonucleotides on the SNA surfaces. To determine how many modified oligonucleotides are on the AuNP surfaces, the total number of oligonucleotide strands was subtracted by the amount of Cy5 labelled strands determined using the Cy5-DNA calibration curve (**Table 7**). For every strand of Cy5 DNA functionalized, ~2 more strands of backbone modified oligonucleotides were functionalized. This suggest that the SNAs will be more likely to exhibit the properties of the charge modified oligonucleotides, compared to the Cy5 labelled strands.

Table 7. *The number of modified oligonucleotides on each SNA was determined by subtracting the number of Cy5 strands per SNA.*

Dual Layer SNA	Total DNA/NP	(Total DNA/NP) – (Cy5 Monolayer)
Scram	344	275
Scram3T	113	44
Scram7T	233	165
3XNH2	236	167
7XNH2	186	118
3XGuan	228	159
7XGuan	232	164

Calibration curves for all the dual layer SNAs can be found in the supplementary section (**Figure S10** - **Figure S15**).

Live Cell Uptake Assays of Dual Layer SNAs (7X Series)

A 7X series of dual layer SNAs were incubated in MDA-MB-231 cells at a final concentration of 2 nM in serum free media (non-transfected). The mean fluorescence intensity (MFI) of each SNA was determined using flow cytometry, which is correlated with the relative uptake of the SNAs into the cells. The uptake of each SNA was measured at incubation times of 30 minutes, 1 hour, and 6 hours. At all 3 time points, the amine and guanidinium derivatized SNAs displayed an increased uptake relative to the unmodified SNAs and the PBS negative control (**Figure 36**, **Figure 37** and **Figure 38**). The mean fluorescence intensity of the amine and guanidinium modified SNAs were ~10X higher than the unmodified SNAs at all three time points, indicating a rapid cellular uptake at early time points when introduced to cells (**Figure 39**). These results suggest that the new functionality introduced at the phosphate backbone of oligonucleotides affords SNAs with distinct properties at the nanoscale level, demonstrated by the rapid and increased cellular uptake relative to unmodified SNAs in live MDA-MB-231 cells. These results indicate that the new functionality incorporated at the phosphate backbone through P-N linkages may be providing the SNAs with alternative uptake mechanisms, potentially governed by more favourable electrostatic interaction at cell surfaces. To further explore this rapid uptake at early time points, receptor blocking assays should be employed with confocal microscopy to determine both the uptake mechanism of these charge modified SNAs as well as their intracellular fate.

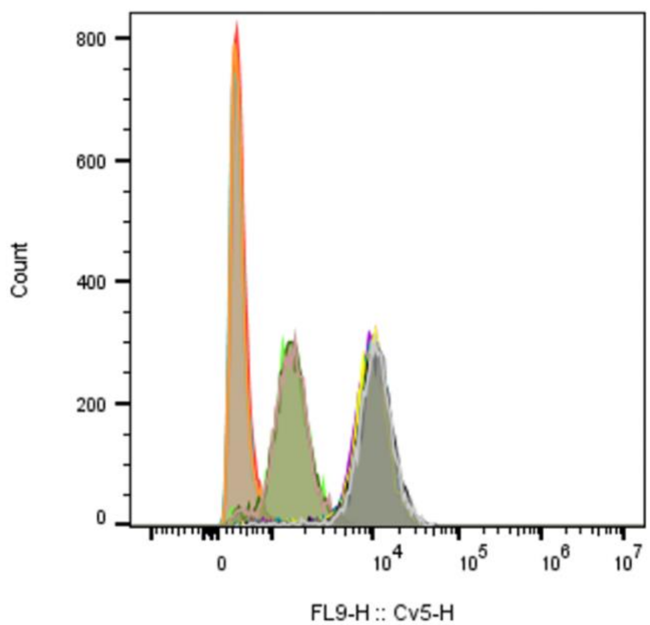

	Sample Name	Subset Name	Count
	Guan30mins3.fcs	Single Cells	6261
	Guan30mins2.fcs	Single Cells	6351
	Guan30mins1.fcs	Single Cells	6351
	NH230mins3.fcs	Single Cells	6309
	NH230mins2.fcs	Single Cells	6281
	NH230mins1.fcs	Single Cells	6486
	8T30mins3.fcs	Single Cells	6368
	8T30mins2.fcs	Single Cells	6485
	8T30mins1.fcs	Single Cells	6382
	PBS30min1.fcs	Single Cells	6656
	PBS30min2.fcs	Single Cells	6567
	UNS30min.fcs	Single Cells	7193

Figure 36. *Histogram of Cy5 fluorescence intensities of SNAs containing unmodified backbones (8T), amine derivatized backbones (NH_2), and guanidinium derivatized backbones (Guan) incubated for 30 minutes with MDA-MB-231 cells.*

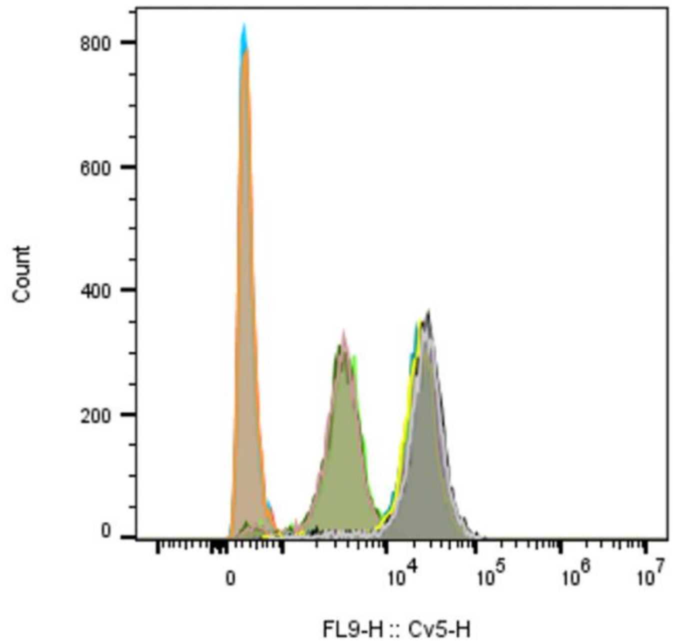

	Sample Name	Subset Name	Count
	Guan1hr3.fcs	Single Cells	6685
	Guan1hr2.fcs	Single Cells	6474
	Guan1hr1.fcs	Single Cells	6685
	NH21hr3.fcs	Single Cells	6568
	NH21hr2.fcs	Single Cells	6481
	NH21hr1.fcs	Single Cells	6510
	8T1hr3.fcs	Single Cells	6591
	8T1hr2.fcs	Single Cells	6625
	8T1hr1.fcs	Single Cells	6499
	PBS1hr2.fcs	Single Cells	6785
	PBS1hr1.fcs	Single Cells	6587
	UNS1hr.fcs	Single Cells	6838

Figure 37. *Histogram of Cy5 fluorescence intensities of SNAs containing unmodified backbones (8T), amine derivatized backbones (NH_2), and guanidinium derivatized backbones (Guan) incubated for 1 hour with MDA-MB-231 cells.*

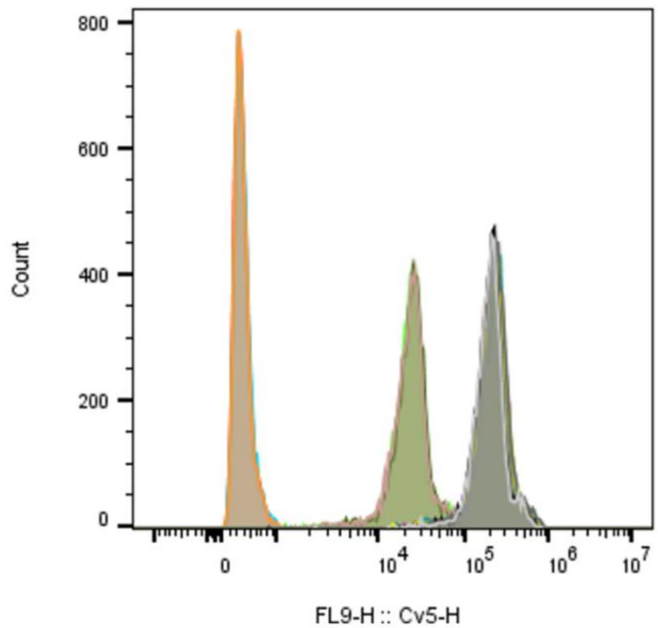

	Sample Name	Subset Name	Count
	Guan6hr3.fcs	Single Cells	6741
	Guan6hr2.fcs	Single Cells	6938
	Guan6hr1.fcs	Single Cells	6835
	NH26hr3.fcs	Single Cells	6907
	NH26hr2.fcs	Single Cells	6747
	NH26hr1.fcs	Single Cells	6648
	8T6hr3.fcs	Single Cells	6628
	8T6hr2.fcs	Single Cells	6575
	8T6hr1.fcs	Single Cells	6601
	PBS6hr2.fcs	Single Cells	6380
	PBS6hr1.fcs	Single Cells	6487
	UNS6hr.fcs	Single Cells	6502

Figure 38. *Histogram of Cy5 fluorescence intensities of SNAs containing unmodified backbones (8T), amine derivatized backbones (NH2), and guanidinium derivatized backbones (Guan) incubated for 6 hours with MDA-MB-231 cells.*

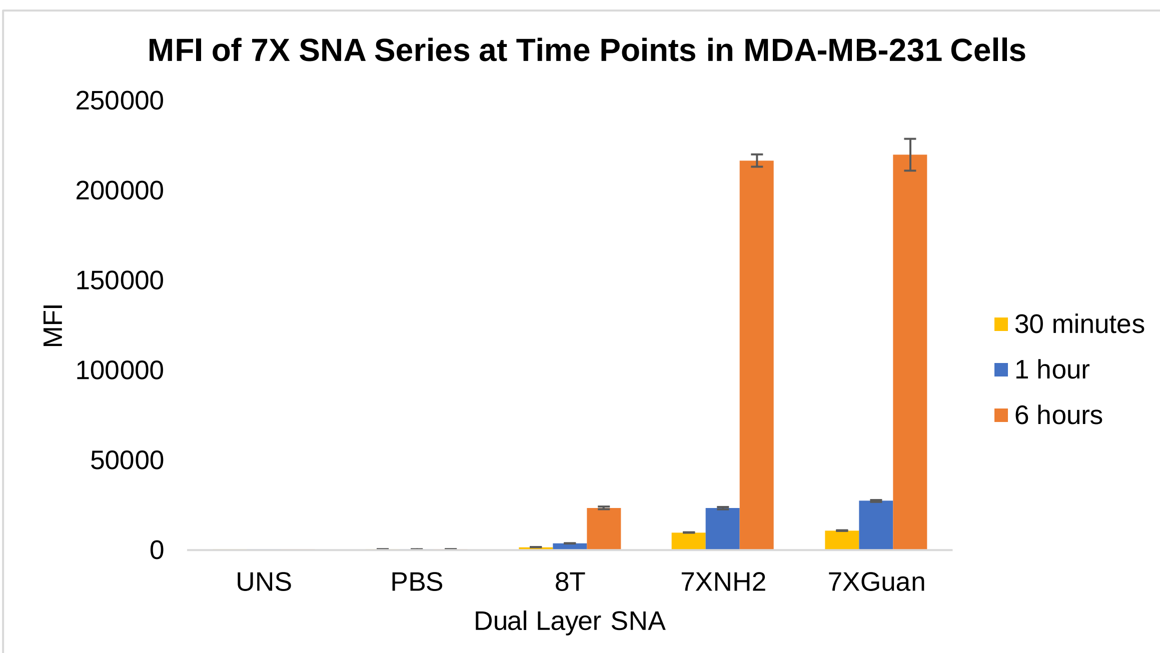

Figure 39. *Mean fluorescence intensity of dual layer SNAs at 30 minutes, 1 hour, and 6 hours.*

CHAPTER 4 – DESIGN OF SNAS FOR BLOOD-BRAIN BARRIER CROSSING

The properties of oligonucleotides at the nanoscale have been shown to be independent of their nanoparticle core.[38] We hypothesize that by introducing hydrophobic modifications to the phosphate backbone of SNAs, we can open the door for more favourable interactions at the blood-brain barrier by facilitating hydrophobic interactions with the lipid membranes of cells. Currently a challenge with the intravenous delivery of biological molecules to the brain is their low ability to elicit either passive or active transport mechanisms that will deliver them across the blood-brain barrier (BBB) and into the interstitial fluid towards the brain.[13,54–56] As a direct consequence, invasive administration methods such as intranasal and intrathecal delivery are the only effective means to address this problem.[57,58] We aim to circumnavigate this challenge by synthesizing hydrophobically modified SNAs that we hypothesize will elicit new uptake mechanisms afforded by their backbone functionality, possibly enabling passive transport or diffusion through the BBB.

Synthesis of Hydrophobically Modified Oligonucleotides

Oligonucleotides (10mers) were synthesized with different phosphoramidate backbone modifications derivatized with either propylamine, hexylamine, octylamine, and 1-(3-aminopropyl) pyrrolidine (**Figure 40**) to introduce hydrophobic character at each internucleoside linkage. The oligonucleotides were synthesized, purified by HPLC and analyzed by MALDI-TOF MS for exact mass determination (**Figure 41**, **Figure 42**, **Figure 43** and **Figure 44**) according to the protocols described in Materials & Methods. The expected masses of the oligonucleotides were corroborated by MALDI-TOF MS as shown in **Table 8**.

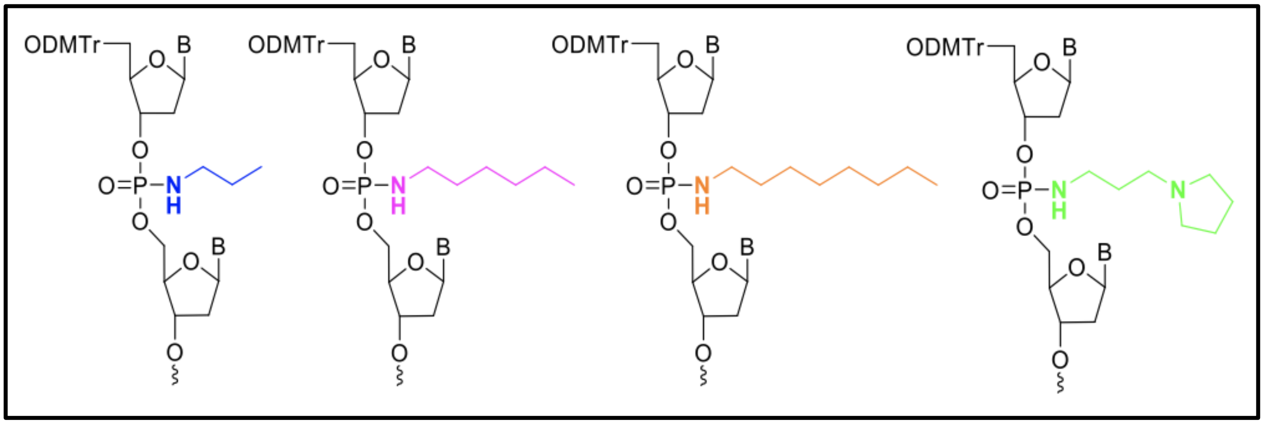

Figure 40. *Oligonucleotides synthesized with different backbone modifications; blue = propylamine, pink = hexylamine, orange = octylamine, green = 1-(3-aminopropyl) pyrrolidine.*

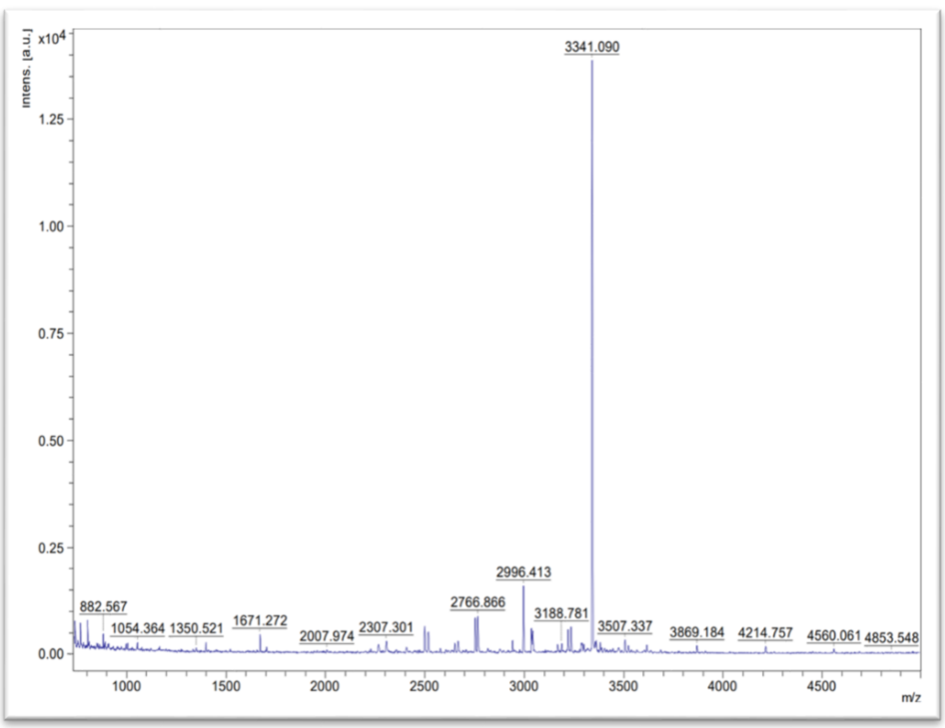

Figure 41. *MALDI-TOF MS spectrum of 4X Propylamine.*

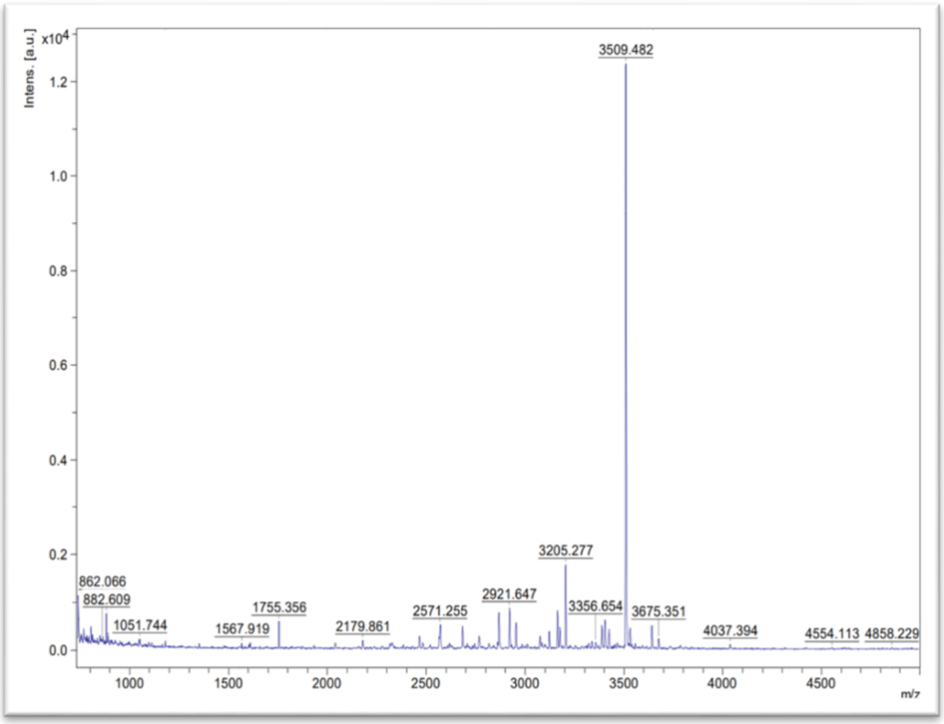

Figure 42. *MALDI-TOF MS spectrum of 4X Hexylamine.*

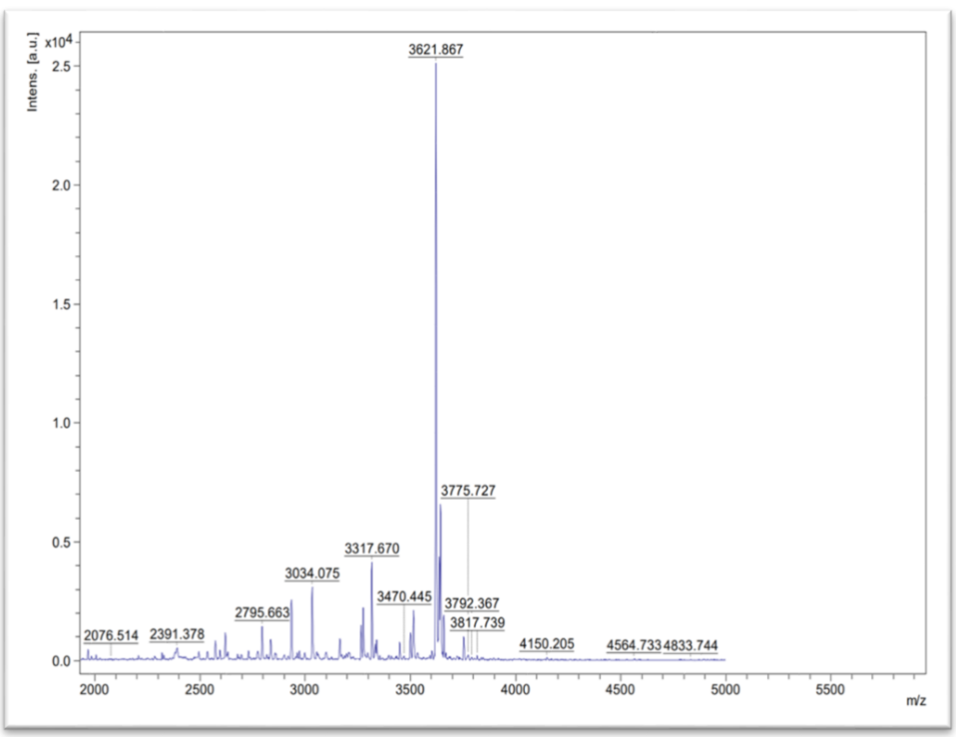

Figure 43. *MALDI-TOF MS spectrum of 4X Octylamine.*

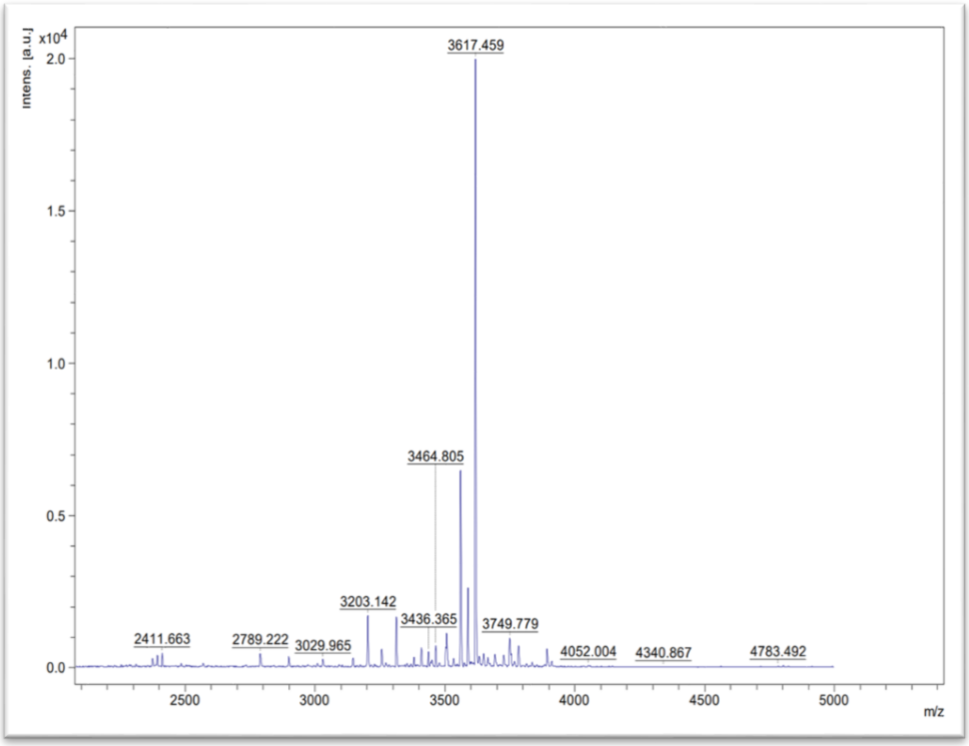

Figure 44. *MALDI-TOF MS spectrum of 4X 1-(3-aminopropyl) pyrrolidine.*

Table 8. *Oligonucleotide masses found by MALDI-TOF MS.*

Oligonucleotide	Exact Mass (Da)	Found Mass (Da)	Δ
4X Propylamine	3344.2	3341.1	-3.1
4X Hexylamine	3512.2	3509.5	-2.7
4X Octylamine	3624.2	3621.8	-2.4
4X 1-(3-aminopropyl) pyrrolidine	3620.2	3617.5	-2.7

The results indicate that using H-phosphonate chemistry to introduce hydrophobic phosphoramidate linkages onto oligonucleotides is applicable to a large scope of functional groups.

Synthesis of Hydrophobic Dual Layer SNAs

Dual layer SNAs were assembled according to the protocols previously described in Chapters 2 and 3. When salt-aging the SNAs, a salting out effect was observed due to the hydrophobic nature of the backbone modifications, causing the SNAs to aggregate. The amount of salt (NaCl) that could be added to the SNAs was directly proportional to the hydrophobicity of the modification. For the propylamine, hexylamine, and octylamine SNAs, final salt concentrations of 0.4 M, 0.3 M, and 0.1 M were achieved, respectively. For the 1-(3-aminopropyl) pyrrolidine, a final salt concentration of 0.5 M could be achieved, most likely due to the tertiary amine which can accept hydrogen bonds from water, making it slightly more soluble than the other modifications, and therefore less likely to salt-out.

The dual layer SNAs appeared to be monodisperse when run on a 1% agarose gel in 1X TBE (**Figure 45**). The monolayer was functionalized with ~78 strands of Cy5 labelled DNA (**Figure S16**) and the dual layer SNAs were functionalized with a second layer of hydrophobically modified oligonucleotides as seen with the increased retention time through the agarose gel. The intrinsic salt concentration within the gel was strong enough to induce a salting out effect of the most hydrophobically modified SNA (octylamine), leading to aggregation and a complete halt in mobility through the gel.

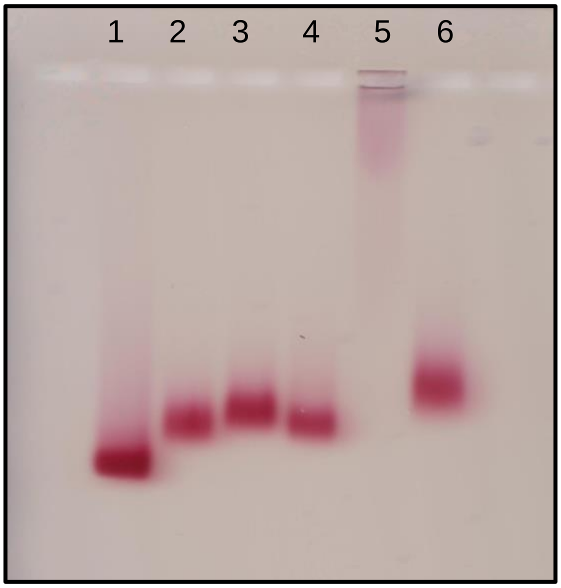

SNA	Lane
Cy5-Monolayer	1
P-O	2
4X Propyl	3
4X Hexyl	4
4X Octyl	5
4X 1-(3-aminopropyl) pyrrolidine	6

Figure 45. *1% Agarose (1X TBE) of Hydrophobically modified dual layer SNAs.*

Octanol-Water Partitioning of Hydrophobically Modified Oligonucleotides

An octanol-water partitioning experiment was performed to determine the relative lipophilicity of the linear oligonucleotides as well as their respective SNAs. Lipophilicity is one of the most important parameters associated with the ability to cross the BBB for small molecule drugs less than 600 Da.[14] We hypothesize that the modifications imparted onto the phosphate backbone of the oligonucleotides and subsequent SNAs will confer their properties to the these larger structures, providing them with an increased lipophilicity. UV-vis was used to determine the concentration of the modified oligonucleotides in the water phase relative to an unmodified (P-O) oligonucleotide control (**Figure 46**). Increasing the aliphatic length of the backbone modification favours the oligonucleotides to partition into the octanol phase, demonstrating that the modifications imparted onto the oligonucleotides maintain their properties at the macromolecular level.

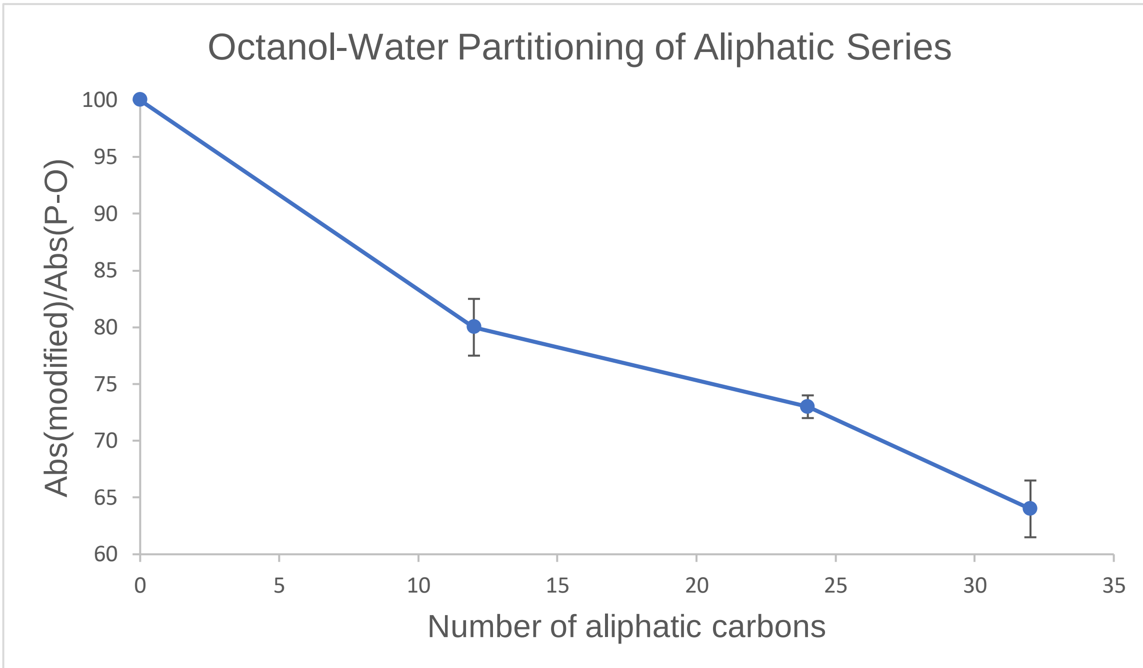

Figure 46. *Octanol-water partitioning of linear oligonucleotides.*

Octanol-Water Partitioning of Hydrophobically Modified SNAs

The hydrophobically modified dual layer SNAs, regardless of the backbone modification imposed, did not show any partitioning into the octanol layer. To establish the properties of the aliphatic functional groups at the nanoscale, we propose to fully saturate every available phosphate linkage available with a P-N linkage, allowing us to introduce more functionality, and subsequently more hydrophobicity to each oligonucleotide. Additionally, decreasing the AuNP size is another avenue to explore because the size of AuNPs can be rigorously controlled.[59–62] In this way, we can (1) reduce the total size of the SNAs and (2) allow the backbone modifications to dominate their properties, attributed by the larger ratio between modifications to nanoparticle size.

Bioconjugation of Thiolated Oligonucleotides with Cyanine5 Maleimide

To further explore the properties of linear oligonucleotides containing hydrophobic modifications, we decided to react the 5' thiol on each strand with a cyanine5 maleimide, effectively clicking on a fluorescent label to them. This will allow us to track and quantify them in more biologically relevant systems, such as permeability assays and potentially in vivo models. To maximize the specificity and reactivity of the thiol-maleimide bioconjugation reaction, we determined that the two most important parameters were the reducing reagent chosen and the pH. As a result, we conducted the reaction at a pH of ~7, in accordance with literature values for various thiol-maleimide reactions.[63,64] As for the reducing reagent, we chose TCEP instead of DTT as the free thiols in DTT may compete with the 5' thiol on each oligonucleotide, and would need to be removed from solution prior to conjugation. Moreover, TCEP does not regenerate during reduction like DTT, which exists in equilibria and can directly catalyze thiol-disulfide exchange reactions.[65,66] The MALDI-TOF MS spectra for the oligonucleotide-Cy5 conjugates can be seen in **Figure 47**, **Figure 48**, **Figure 49**, and **Figure 50**. The spectra display sharp and narrow peaks, associated with the expected masses of the conjugates as summarized in **Table 9** below.

Table 9. *Expected versus found masses of oligonucleotide-Cy5 conjugates by MALDI-TOF MS.*

Oligonucleotide-Cy5 Conjugate	Exact Mass (Da)	Found Mass (Da)	Δ
4X Propylamine-Cy5	3950	3947.754	-2.246
3X Hexylamine-Cy5	4034	4029.270	-4.73
5X-Octylamine-Cy5	4342	4339.706	-2.294
4X 1-(3-aminopropyl) pyrrolidine	4226	4224.005	-1.995

The results indicate that we can selectively label thiolated oligonucleotides containing hydrophobic phosphoramidate linkages. However, yields of ~30% were achieved for the conjugates, necessitating improved reaction conditions to increase the efficiency of labelling. The low yields may be attributed to the poor water solubility of the Cy5 maleimide, crashing out of solution and decreasing the extent of labelling. To overcome the solubility issue, sulfo-cyanine5 maleimides should be considered as they confer an increased water solubility stemming from their sulfonate groups.

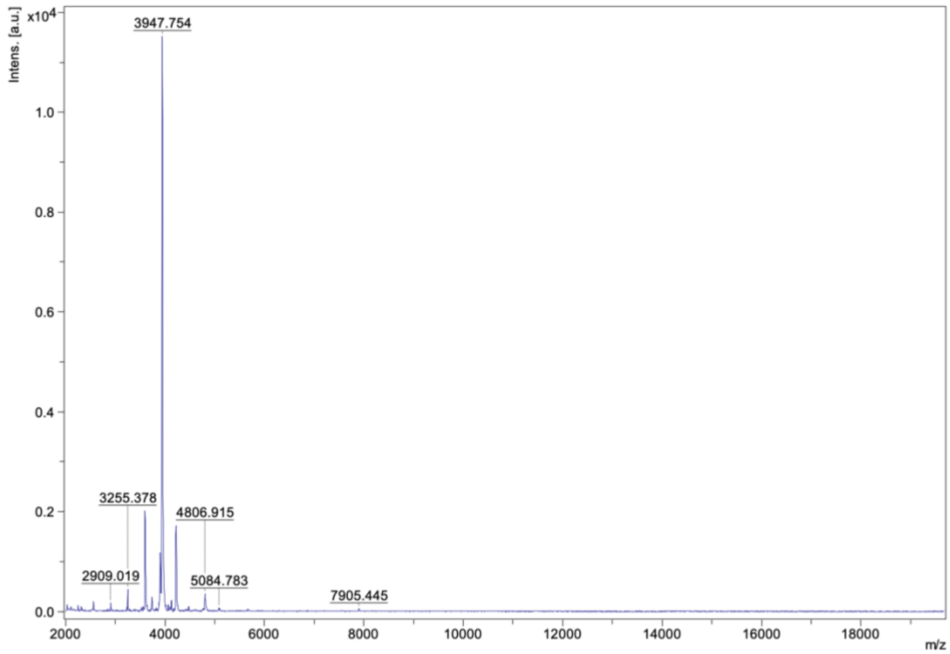

Figure 47. *MALDI-TOF MS spectrum of 4X Propylamine-Cy5 conjugate.*

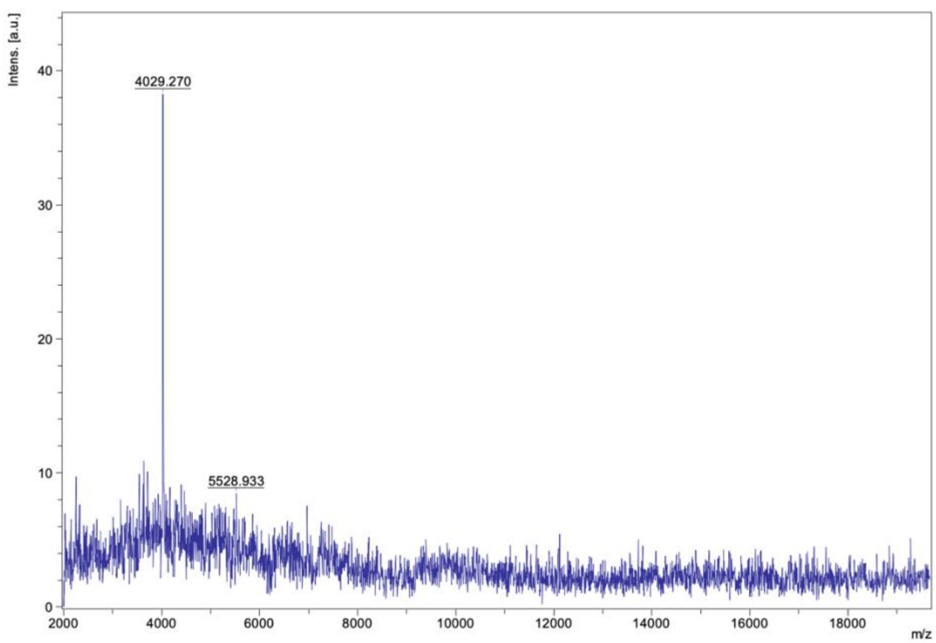

Figure 48. *MALDI-TOF MS spectrum of 3X Hexylamine-Cy5 conjugate.*

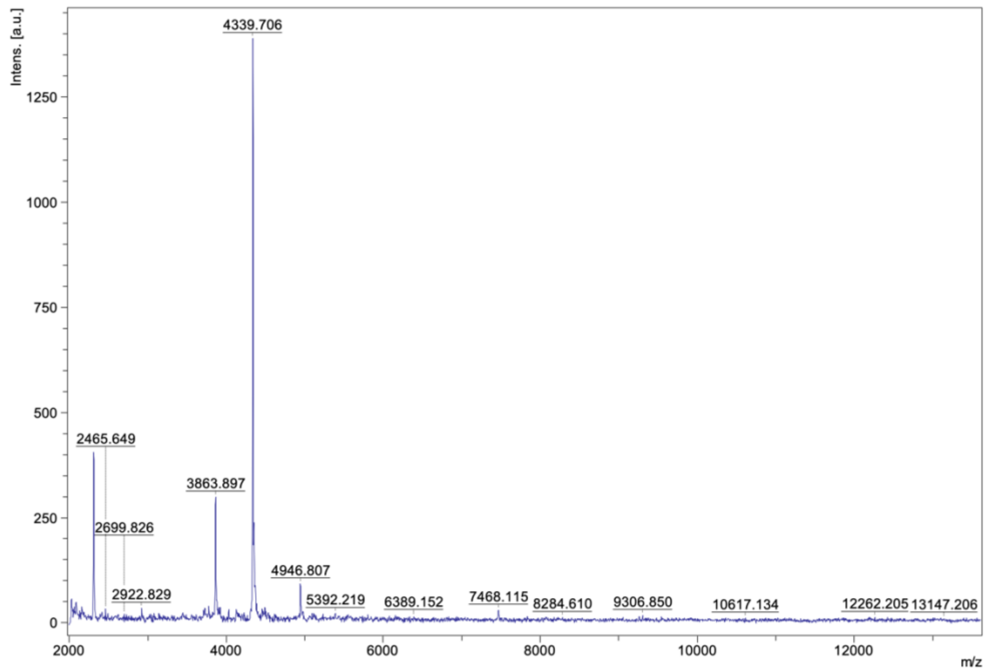

Figure 49. *MALDI-TOF MS spectrum of 5X Octylamine-Cy5 conjugate.*

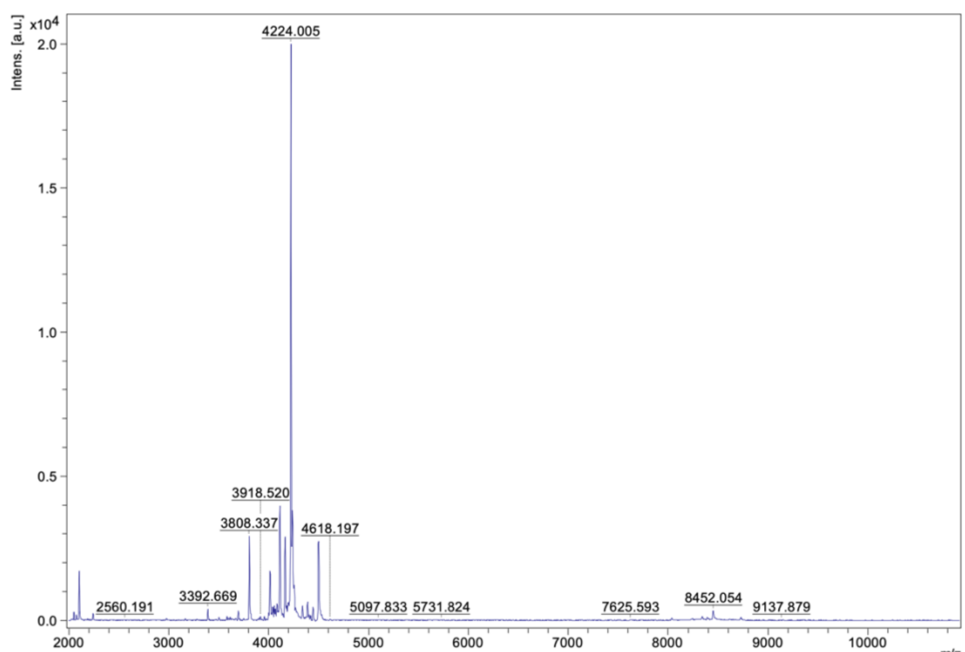

Figure 50. *MALDI-TOF MS spectrum of 4X 1-(3-aminopropyl) pyrrolidine conjugate.*

CHAPTER 5 – CONCLUSIONS AND FUTURE OUTLOOK

The main objective of this thesis was to tune the properties of spherical nucleic acids with phosphate backbone modifications, taking advantage of the core independent properties elicited by the SNA architecture. Specifically, we attempted to dictate the biological properties of SNAs by driving new interactions at cell surfaces with charged and hydrophobically modified functional groups introduced through phosphoramidate linkages. In this way, we aimed to provide them stability over a broad range of conditions, increased cellular uptake, and alternative uptake mechanisms compared to traditional SNAs.

We demonstrated that phosphoramidate modified oligonucleotides can be readily synthesized in high yields in an automated fashion using H-phosphonate nucleoside precursors and are stable under relevant physiological conditions. Additionally, they can be stored for months at a time at -20°C and tolerate broad temperature and pH ranges, making their handling facile and convenient. Post synthesis, oligonucleotides containing amine derivatized internucleotide phosphoramidate backbone linkages can be saturated with guanidinium residues without a subsequent purification step, demonstrating the efficiency of the guanidinylation reaction above a pH of 11 with O-methylisourea hemisulfate. These synthetic approaches enabled the synthesis of oligonucleotide bearing both negatively charged phosphate linkages and cationic guanidinium groups.

We were also able to tailor the lipophilicity of oligonucleotides by introducing aliphatic modifications, increasing their partitioning into the octanol phase. This indicates that the functional group imposed onto the phosphate backbone of oligonucleotides retain their properties at the macromolecular level. Similarly, integrating cationic guanidinium motifs to the backbone of linear oligonucleotides exhibited strong electrostatic interactions, even with minimal modifications per strand. This highlights the stringent control we have over the placement of modifications along the phosphate backbone and underscores the use of various functional groups to tune their properties for specific purposes.

We were able to incorporate the charge and hydrophobically modified oligonucleotides into well-defined spherical nucleic acid architectures. Fluorescence assays, DLS, and agarose gels demonstrated that we could effectively synthesize monodisperse SNAs with consistent size distributions. The new functionality incorporated at the phosphate backbone affords these SNAs new properties distinct from their nanoparticle core, demonstrated by their high cellular uptake relative to unmodified SNAs in MDA-MB-231 cells without transfection.

It is widely known that unmodified SNAs are taken up into cells through scavenger receptors and endocytosis, an energy-dependent process, and sorted into early endosomes.[67] As a result, they have difficulty interacting with their cytosolic and nuclear targets[67], hindering their efficacy as drugs. Therefore, future work should be geared toward determining the uptake mechanism and intracellular fate of the phosphate backbone modified SNAs. Specifically, receptor blocking assays should be employed to block specific cell uptake pathways to determine if the phosphate backbone modified SNAs exhibit new uptake mechanisms, driven by their new functionality. Confocal microscopy should be implemented to track their intracellular fate and determine if the modified SNAs can access new compartments and penetrate the nuclear envelope. This information would reveal how SNA architecture and composition can regulate uptake pathways and escape endosomal entrapment.

Lastly, to determine their efficacy as therapeutic agents of gene regulation, these modified SNAs should be evaluated on their ability to silence gene expression and protein production through Wester blots. Specifically, ASOs should be evaluated in the context of linear oligonucleotides and SNA architectures to verify the therapeutic potential of this approach for multiple targets.

SUPPLEMENTARY FIGURES

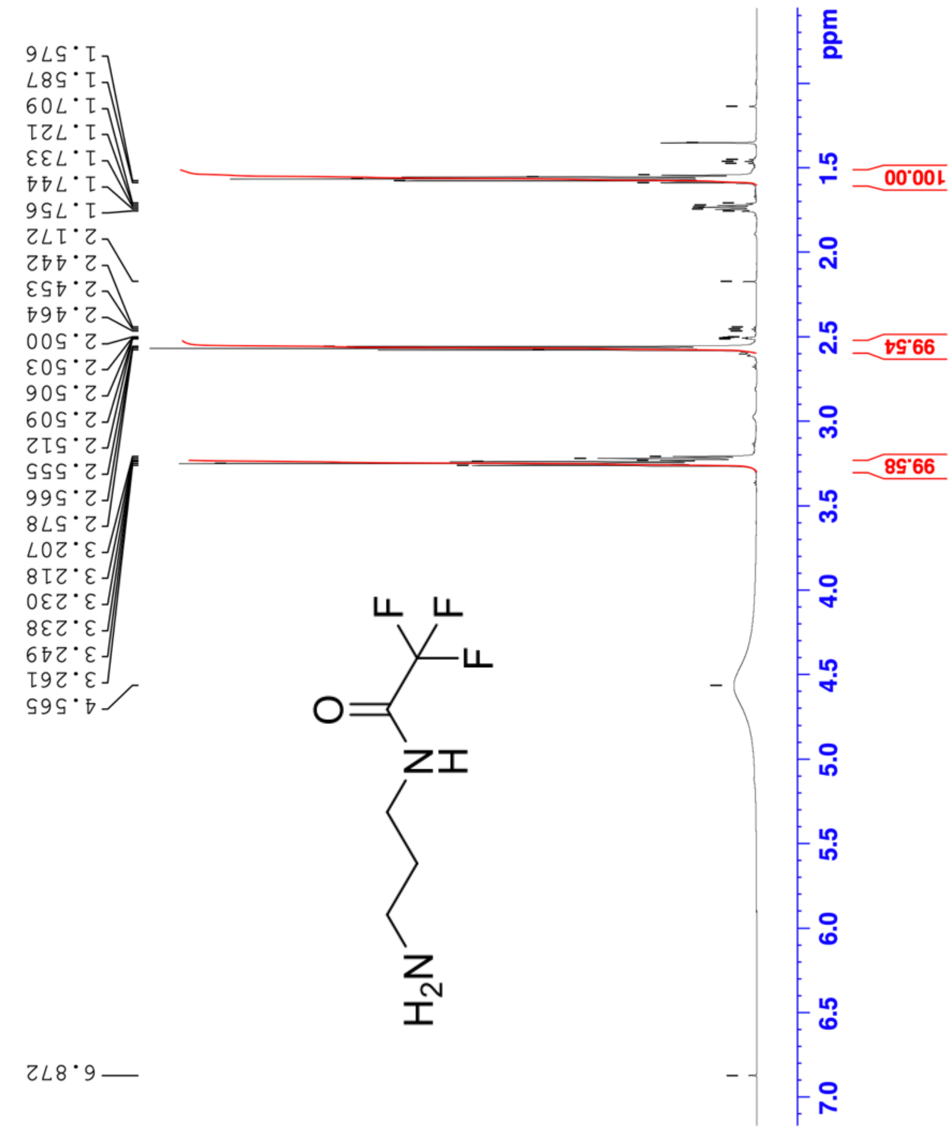

Figure S1. *[1]H-NMR of N-Trifluoroacetyl-1,3-propylenediamine. N-Trifluoroacetyl-1,3-propylenediamine: [1]H-NMR (DMSO-d_6, 600 MHz): δ 1.56 (quint, 2H), 2.57 (t, 2H), 3.25 (t, 2H).*

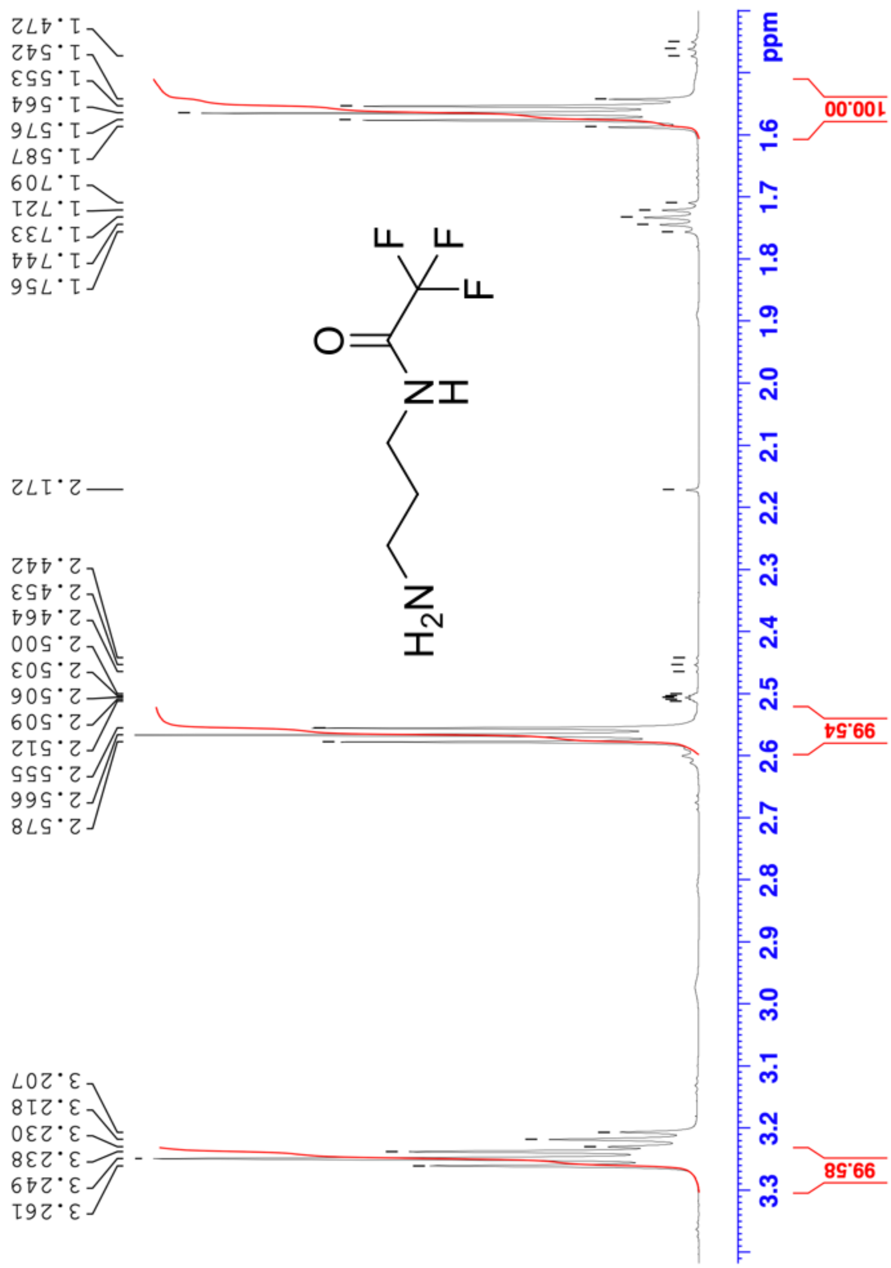

Figure S2. *[1]H-NMR of N-Trifluoroacetyl-1,3-propylenediamine. N-Trifluoroacetyl-1,3-propylenediamine: [1]H-NMR (DMSO-d_6, 600 MHz): δ 1.56 (quint, 2H), 2.57 (t, 2H), 3.25 (t, 2H).*

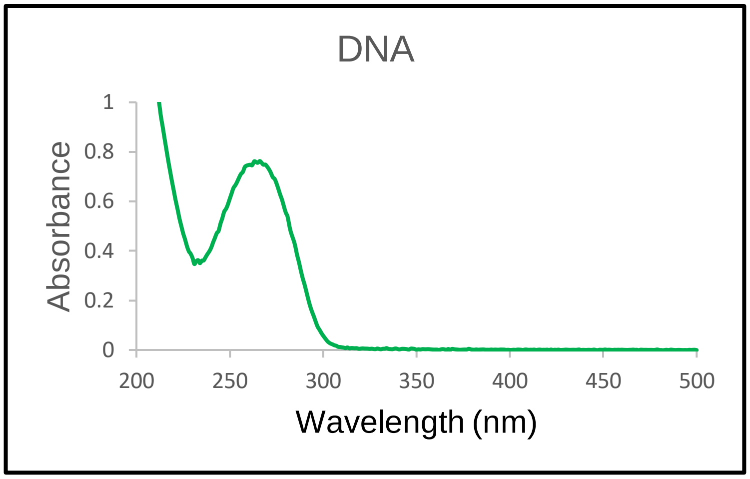

Figure S3. *UV-vis of oligonucleotides (A260).*

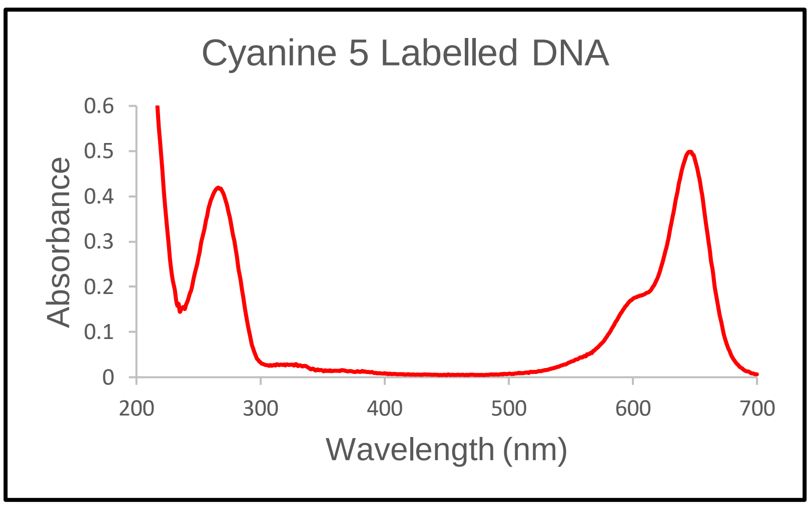

Figure S4. *UV-vis of Cy5 labelled DNA (A647).*

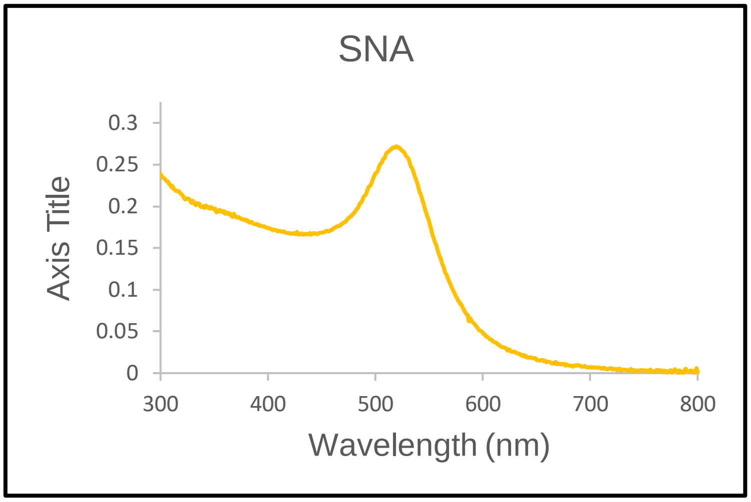

Figure S5. *UV-vis of SNAs (A520).*

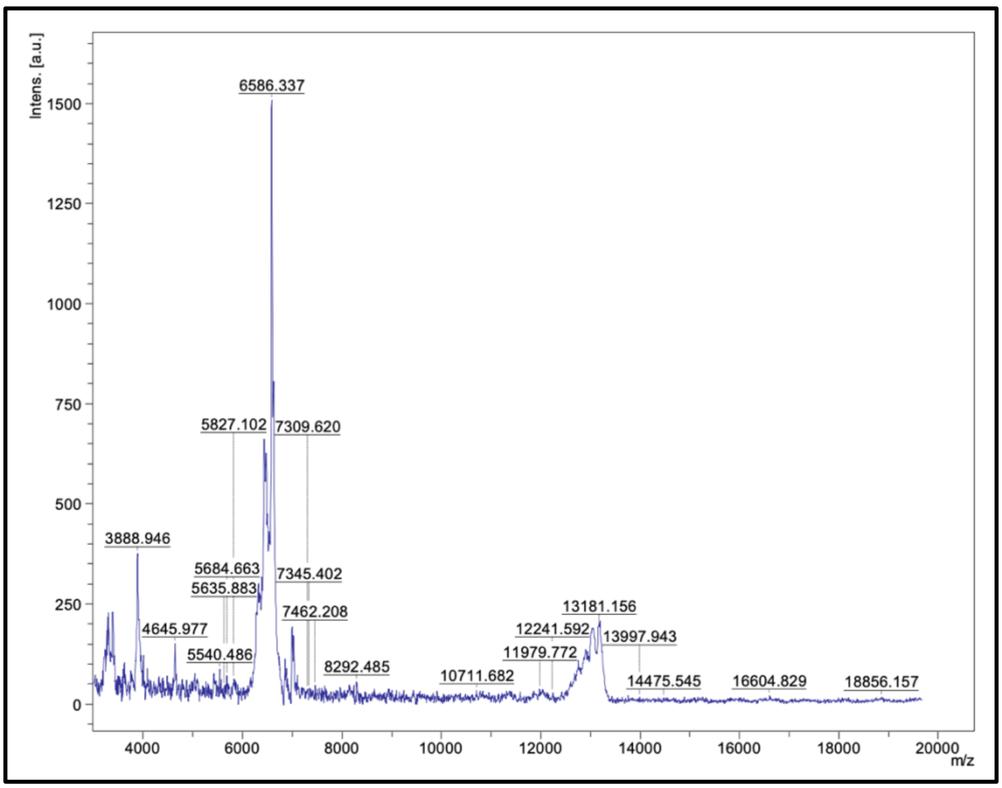

Figure S6. *3T control oligonucleotide MALDI-TOF MS spectra.*

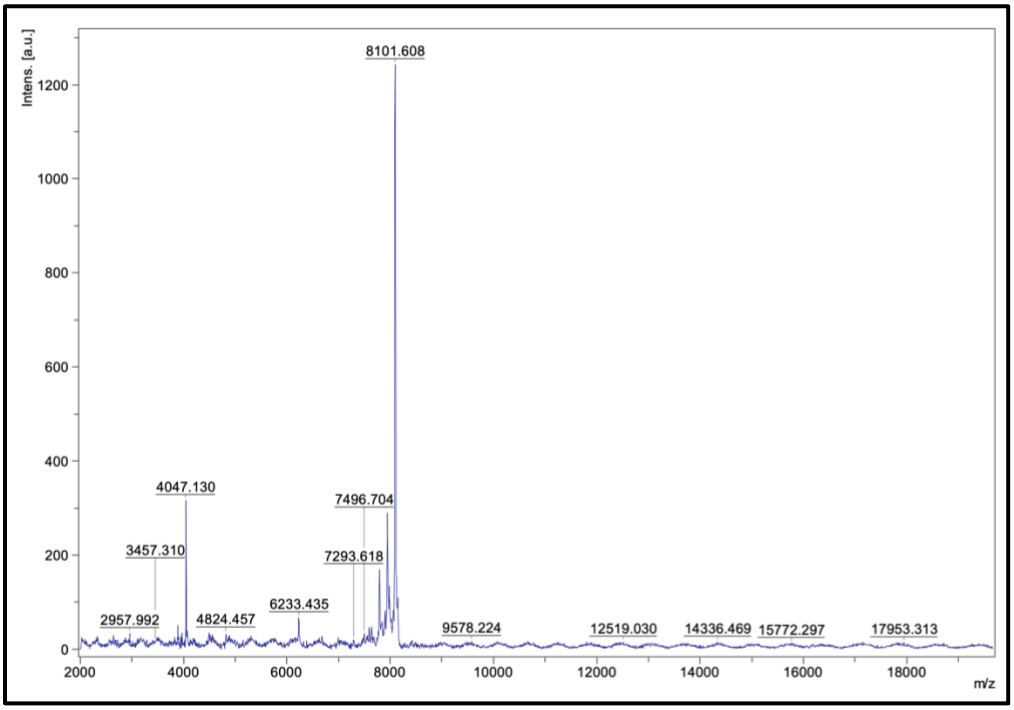

Figure S7. *7T control oligonucleotide MALDI-TOF MS spectra.*

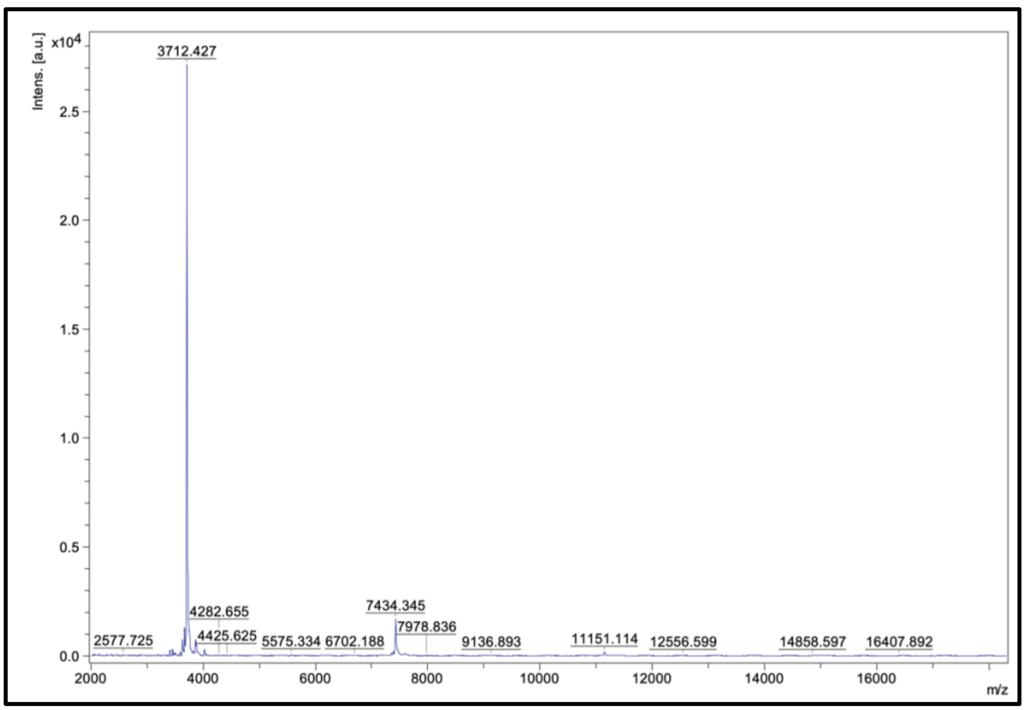

Figure S8. *T10-Cy5 oligonucleotide MALDI-TOF MS spectra.*

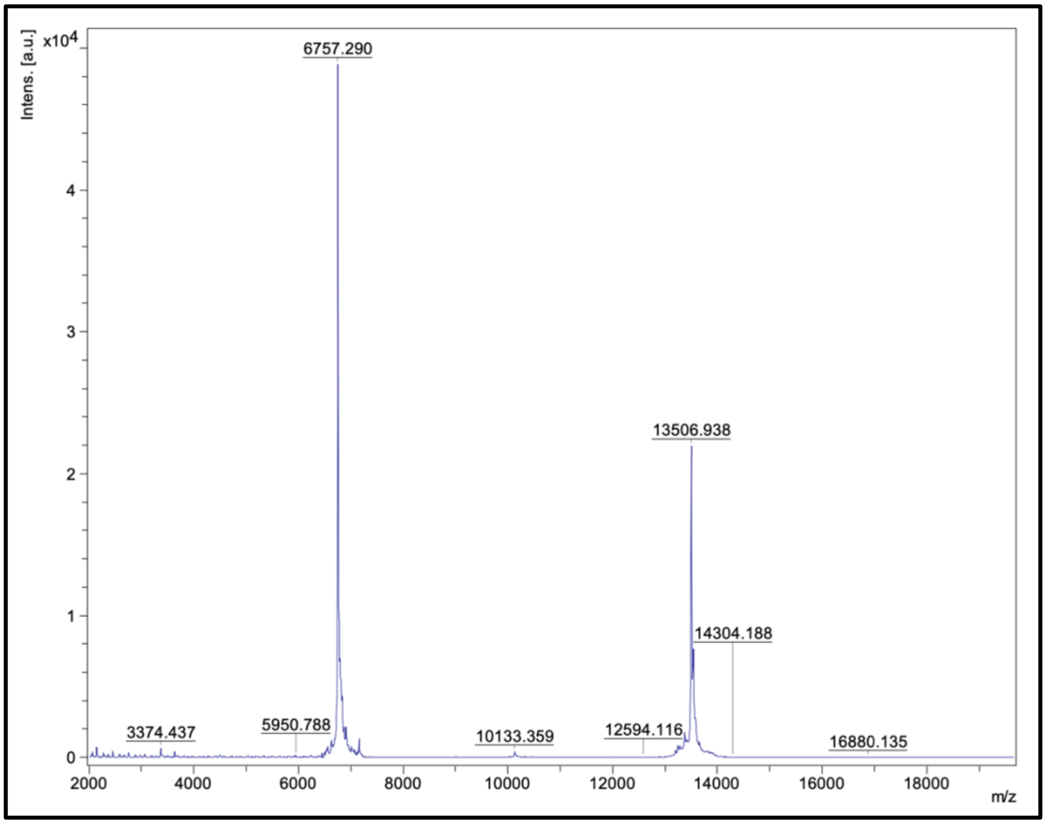

Figure S9. *T20-Cy5 oligonucleotide MALDI-TOF MS spectra.*

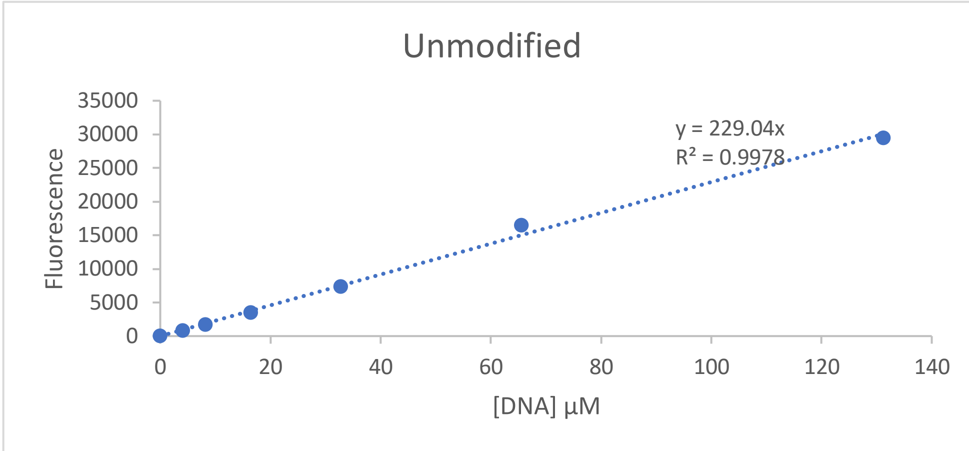

Figure S10. *Calibration curve for an unmodified oligonucleotide. Excitation (480 nm), Emission (520 nm).*

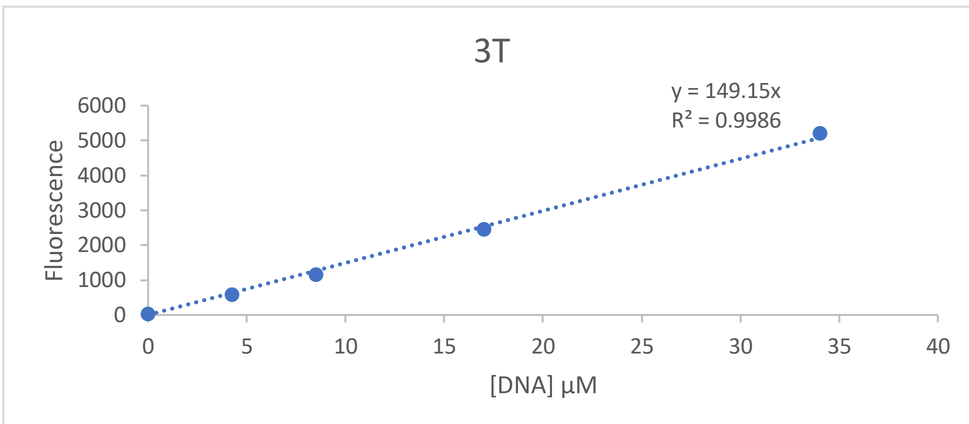

Figure S11. *Calibration curve for 3T oligonucleotide. Excitation (480 nm), Emission (520 nm).*

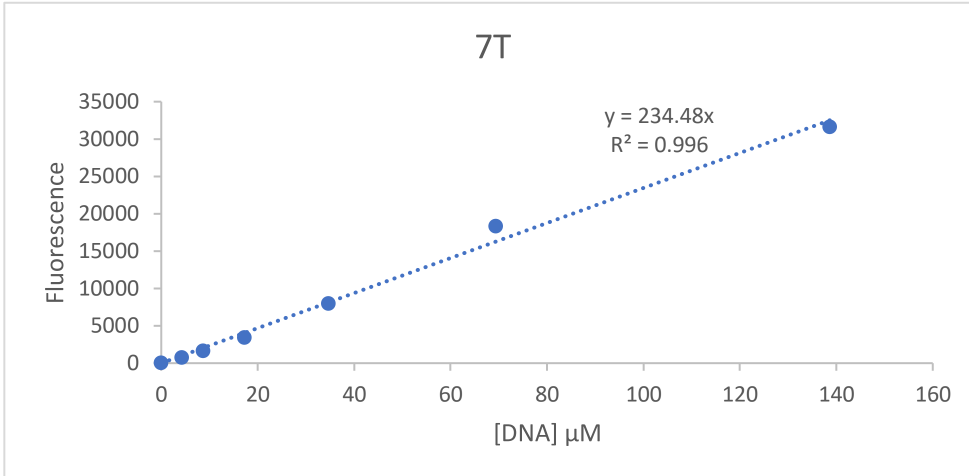

Figure S12. *Calibration curve for 7T oligonucleotide. Excitation (480 nm), Emission (520 nm).*

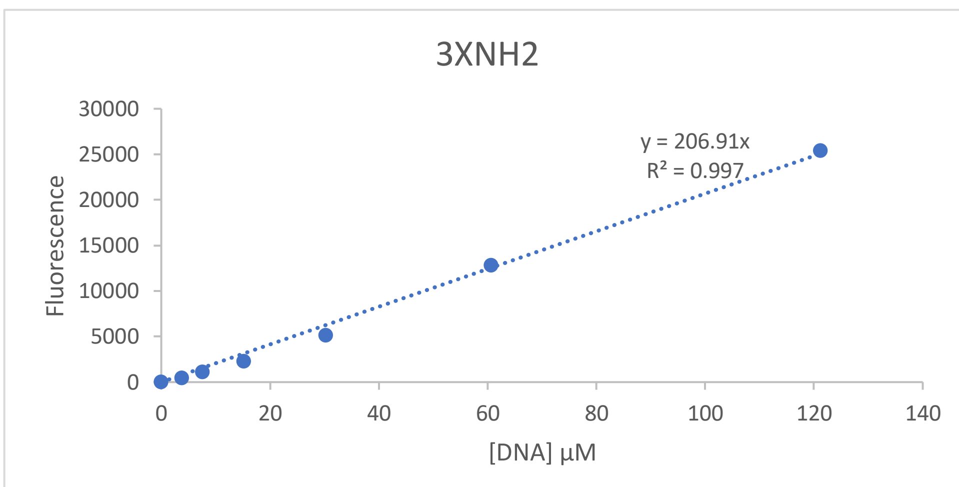

Figure S13. *Calibration curve for a 3X NH2 modified oligonucleotide. Excitation (480 nm), Emission (520 nm).*

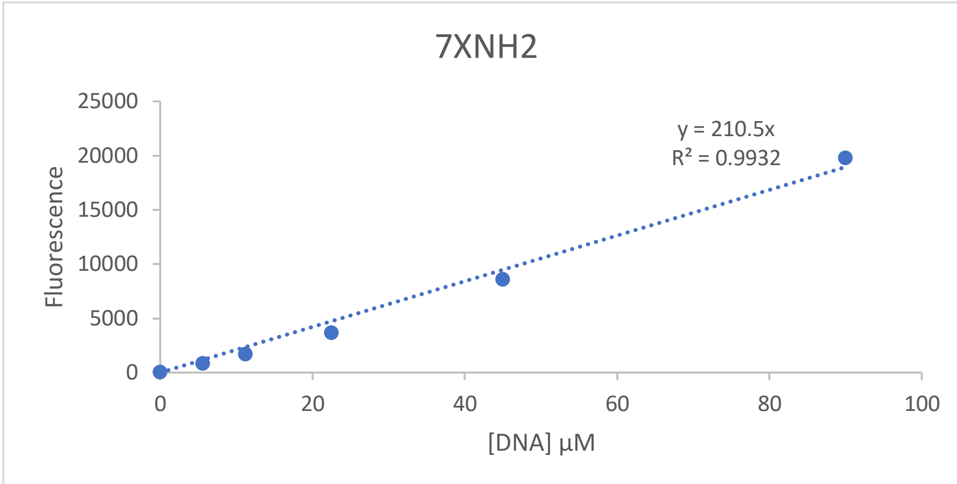

Figure S14. *Calibration curve for a 7X NH2 modified oligonucleotide. Excitation (480 nm), Emission (520 nm).*

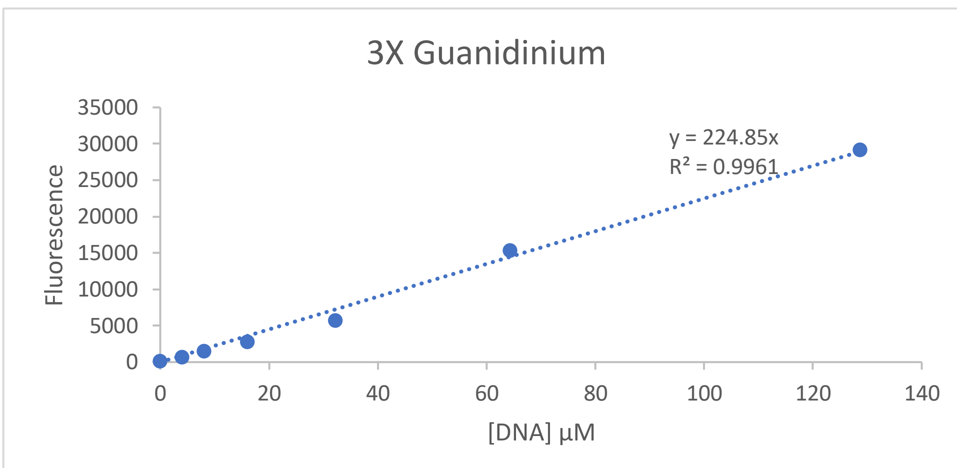

Figure S15. *Calibration curve for 3X guanidinium modified oligonucleotide. Excitation (480 nm), Emission (520 nm).*

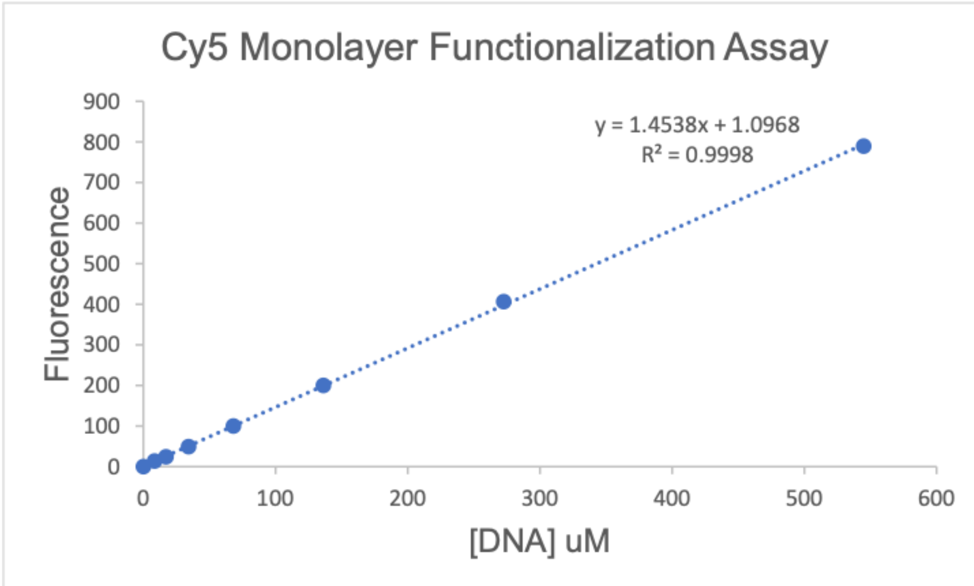

Figure S16. *Calibration curve for Cy5-labelled DNA used for hydrophobically modified SNAs. Excitation (651 nm), Emission (670 nm).*

REFERENCES

(1) Kulkarni, J. A.; Witzigmann, D.; Thomson, S. B.; Chen, S.; Leavitt, B. R.; Cullis, P. R.; van der Meel, R. The Current Landscape of Nucleic Acid Therapeutics. *Nat. Nanotechnol.* **2021**, *16* (6), 630–643. https://doi.org/10.1038/s41565-021-00898-0.

(2) Sun, J.; Roy, S. Gene-Based Therapies for Neurodegenerative Diseases. *Nat. Neurosci.* **2021**, *24* (3), 297–311. https://doi.org/10.1038/s41593-020-00778-1.

(3) Radhakrishnan, M. L.; Tidor, B. Specificity in Molecular Design: A Physical Framework for Probing the Determinants of Binding Specificity and Promiscuity in a Biological Environment. *J. Phys. Chem. B* **2007**, *111* (47), 13419–13435. https://doi.org/10.1021/jp074285e.

(4) Moumné, L.; Marie, A. C.; Crouvezier, N. Oligonucleotide Therapeutics: From Discovery and Development to Patentability. *Pharmaceutics* **2022**, *14* (2). https://doi.org/10.3390/pharmaceutics14020260.

(5) Stephenson, M. L.; Zamecnik, P. C. Inhibition of Rous Sarcoma Viral RNA Translation by a Specific Oligodeoxyribonucleotide. *Proc. Natl. Acad. Sci. U. S. A.* **1978**, *75* (1), 285–288. https://doi.org/10.1073/pnas.75.1.285.

(6) Roberts, T. C.; Langer, R.; Wood, M. J. A. Advances in Oligonucleotide Drug Delivery. *Nat. Rev. Drug Discov.* **2020**, *19* (10), 673–694. https://doi.org/10.1038/s41573-020-0075-7.

(7) Dominski, Z.; Kole, R. Restoration of Correct Splicing in Thalassemic Pre-MRNA by Antisense Oligonucleotides. *Proc. Natl. Acad. Sci. U. S. A.* **1993**, *90* (18), 8673–8677. https://doi.org/10.1073/pnas.90.18.8673.

(8) Lin, X.; Chen, H.; Lu, Y. Q.; Hong, S.; Hu, X.; Gao, Y.; Lai, L. L.; Li, J. J.; Wang, Z.; Ying, W.; Ma, L.; Wang, N.; Zuo, E.; Yang, H.; Chen, W. J. Base Editing-Mediated Splicing Correction Therapy for Spinal Muscular Atrophy. *Cell Res.* **2020**, *30* (6), 548–550. https://doi.org/10.1038/s41422-020-0304-y.

(9) Gleeson, J. G.; Bennett, C. F.; Carroll, J. B.; Cole, T.; Douville, J.; Glass, S.; Tekendo-Ngongang, C.; Williford, A. C.; Crooke, S. T. Personalized Antisense Oligonucleotides 'for Free, for Life' — the n-Lorem Foundation. *Nat. Med.* **2023**, *29* (6), 1302–1303. https://doi.org/10.1038/s41591-023-02335-2.

(10) Kim, J.; Hu, C.; Moufawad El Achkar, C.; Black, L. E.; Douville, J.; Larson, A.; Pendergast, M. K.; Goldkind, S. F.; Lee, E. A.; Kuniholm, A.; Soucy, A.; Vaze, J.; Belur, N. R.; Fredriksen, K.; Stojkovska, I.; Tsytsykova, A.; Armant, M.; DiDonato, R. L.; Choi, J.; Cornelissen, L.; Pereira, L. M.; Augustine, E. F.; Genetti, C. A.; Dies, K.; Barton, B.; Williams, L.; Goodlett, B. D.; Riley, B. L.; Pasternak, A.; Berry, E. R.; Pflock, K. A.; Chu, S.; Reed, C.; Tyndall, K.; Agrawal, P. B.; Beggs, A. H.; Grant, P. E.; Urion, D. K.; Snyder, R. O.; Waisbren, S. E.; Poduri, A.; Park, P. J.; Patterson, A.; Biffi, A.; Mazzulli, J.

R.; Bodamer, O.; Berde, C. B.; Yu, T. W. Patient-Customized Oligonucleotide Therapy for a Rare Genetic Disease. *N. Engl. J. Med.* **2019**, *381* (17), 1644–1652. https://doi.org/10.1056/nejmoa1813279.
(11) Juliano, R. L. Intracellular Trafficking and Endosomal Release of Oligonucleotides: What We Know and What We Don't. *Nucleic Acid Ther.* **2018**, *28* (3), 166–177. https://doi.org/10.1089/nat.2018.0727.
(12) Bost, J. P.; Ojansivu, M.; Munson, M. J.; Wesén, E.; Gallud, A.; Gupta, D.; Gustafsson, O.; Saher, O.; Rädler, J.; Higgins, S. G.; Lehto, T.; Holme, M. N.; Dahlén, A.; Engkvist, O.; Strömstedt, P. E.; Andersson, S.; Edvard Smith, C. I.; Stevens, M. M.; Esbjörner, E. K.; Collén, A.; El Andaloussi, S. Novel Endosomolytic Compounds Enable Highly Potent Delivery of Antisense Oligonucleotides. *Commun. Biol.* **2022**, *5* (1), 1–14. https://doi.org/10.1038/s42003-022-03132-2.
(13) Pardridge, W. M. Drug Transport across the Blood-Brain Barrier. *J. Cereb. Blood Flow Metab.* **2012**, *32* (11), 1959–1972. https://doi.org/10.1038/jcbfm.2012.126.
(14) Wu, D.; Chen, Q.; Chen, X.; Han, F.; Chen, Z.; Wang, Y. The Blood–Brain Barrier: Structure, Regulation, and Drug Delivery. *Signal Transduct. Target. Ther.* **2023**, *8* (1). https://doi.org/10.1038/s41392-023-01481-w.
(15) Calias, P.; Banks, W. A.; Begley, D.; Scarpa, M.; Dickson, P. Intrathecal Delivery of Protein Therapeutics to the Brain: A Critical Reassessment. *Pharmacol. Ther.* **2014**, *144* (2), 114–122. https://doi.org/10.1016/j.pharmthera.2014.05.009.
(16) Bottros, M. M.; Christo, P. J. Current Perspectives on Intrathecal Drug Delivery. *J. Pain Res.* **2014**, *7*, 615–626. https://doi.org/10.2147/JPR.S37591.
(17) Kim, T. K.; Eberwine, J. H. Mammalian Cell Transfection: The Present and the Future. *Anal. Bioanal. Chem.* **2010**, *397* (8), 3173–3178. https://doi.org/10.1007/s00216-010-3821-6.
(18) Chong, Z. X.; Yeap, S. K.; Ho, W. Y. Transfection Types, Methods and Strategies: A Technical Review. *PeerJ* **2021**, *9*, 1–37. https://doi.org/10.7717/peerj.11165.
(19) Gräslund, A.; Madani, F.; Lindberg, S.; Langel, Ü.; Futaki, S. Mechanisms of Cellular Uptake of Cell-Penetrating Peptides. *J. Biophys.* **2011**, *2011*. https://doi.org/10.1155/2011/414729.
(20) Stanzl, E. G.; Trantow, B. M.; Vargas, J. R.; Wender, P. A. Fifteen Years of Cell-Penetrating, Guanidinium-Rich Molecular Transporters: Basic Science, Research Tools, and Clinical Applications. *Acc. Chem. Res.* **2013**, *46* (12), 2944–2954. https://doi.org/10.1021/ar4000554.
(21) Zhou, P.; Wang, M.; Du, L.; Fisher, G. W.; Waggoner, A.; Ly, D. H. Novel Binding and Efficient Cellular Uptake of Guanidine-Based Peptide Nucleic Acids (GPNA). *J. Am. Chem. Soc.* **2003**, *125* (23), 6878–6879. https://doi.org/10.1021/ja029665m.
(22) Najjar, K.; Erazo-Oliveras, A.; Mosior, J. W.; Whitlock, M. J.; Rostane, I.;

Cinclair, J. M.; Pellois, J. P. Unlocking Endosomal Entrapment with Supercharged Arginine-Rich Peptides. *Bioconjug. Chem.* **2017**, *28* (12), 2932–2941. https://doi.org/10.1021/acs.bioconjchem.7b00560.

(23) Puckett, C. A.; Barton, J. K. Fluorescein Redirects a Ruthenium-Octaarginine Conjugate to the Nucleus. *J. Am. Chem. Soc.* **2009**, *131* (25), 8738–8739. https://doi.org/10.1021/ja9025165.

(24) Sepp-Lorenzino, L.; Ruddy, M. K. Challenges and Opportunities for Local and Systemic Delivery of SiRNA and Antisense Oligonucleotides. *Clin. Pharmacol. Ther.* **2008**, *84* (5), 628–632. https://doi.org/10.1038/clpt.2008.174.

(25) Shoji, Y.; Akhtar, S.; Periasamy, A.; Herman, B.; Juliano, R. L. Mechansism of Cellular Uptake of Modified Oligodeoxynucleotides Containing Methylphosphonate Linkages. *Nucleic Acids Res.* **1991**, *19* (20), 5543–5550. https://doi.org/10.1093/nar/19.20.5543.

(26) Lysik, M. A.; Wu-Pong, S. Innovations in Oligonucleotide Drug Delivery. *J. Pharm. Sci.* **2003**, *92* (8), 1559–1573. https://doi.org/10.1002/jps.10399.

(27) Loke, A. S. L.; Stein, C. A.; Zhang, X. H.; Mori, K.; Nakanishi, M.; Subasinghe, C.; Neckers, L. M. Characterization of Oligonucleotide Transport into Living Cells Source : Proceedings of the National Academy of Sciences of the United States of America , Published by : National Academy of Sciences Stable URL : Https://Www.Jstor.Org/Stable/33895 Characte. **2023**, *86* (10), 3474–3478.

(28) Juliano, R. L.; Ming, X.; Carver, K.; Laing, B. Cellular Uptake and Intracellular Trafficking of Oligonucleotides: Implications for Oligonucleotide Pharmacology. *Nucleic Acid Ther.* **2014**, *24* (2), 101–113. https://doi.org/10.1089/nat.2013.0463.

(29) Hyjek-Składanowska, M.; Vickers, T. A.; Napiórkowska, A.; Anderson, B. A.; Tanowitz, M.; Crooke, S. T.; Liang, X. H.; Seth, P. P.; Nowotny, M. Origins of the Increased Affinity of Phosphorothioate-Modified Therapeutic Nucleic Acids for Proteins. *J. Am. Chem. Soc.* **2020**, *142* (16), 7456–7468. https://doi.org/10.1021/jacs.9b13524.

(30) Letsinger, R. L.; Mungall, W. S. Phosphoramidate Analogs of Oligonucleotides. *J. Org. Chem.* **1970**, *35* (11), 3800–3803. https://doi.org/10.1021/jo00836a048.

(31) Kandasamy, P.; McClorey, G.; Shimizu, M.; Kothari, N.; Alam, R.; Iwamoto, N.; Kumarasamy, J.; Bommineni, G. R.; Bezigian, A.; Chivatakarn, O.; Butler, D. C. D.; Byrne, M.; Chwalenia, K.; Davies, K. E.; Desai, J.; Shelke, J. D.; Durbin, A. F.; Ellerington, R.; Edwards, B.; Godfrey, J.; Hoss, A.; Liu, F.; Longo, K.; Lu, G.; Marappan, S.; Oieni, J.; Paik, I. H.; Estabrook, E. P.; Shivalila, C.; Tischbein, M.; Kawamoto, T.; Rinaldi, C.; Rajão-Saraiva, J.; Tripathi, S.; Yang, H.; Yin, Y.; Zhao, X.; Zhou, C.; Zhang, J.; Apponi, L.; Wood, M. J. A.; Vargeese, C. Control of Backbone Chemistry and Chirality Boost Oligonucleotide Splice Switching Activity. *Nucleic Acids Res.* **2022**, *50* (10), 5443–5466. https://doi.org/10.1093/nar/gkac018.

(32) Kandasamy, P.; Liu, Y.; Aduda, V.; Akare, S.; Alam, R.; Andreucci, A.; Boulay, D.; Bowman, K.; Byrne, M.; Cannon, M.; Chivatakarn, O.; Shelke, J. D.; Iwamoto, N.; Kawamoto, T.; Kumarasamy, J.; Lamore, S.; Lemaitre, M.; Lin, X.; Longo, K.; Looby, R.; Marappan, S.; Metterville, J.; Mohapatra, S.; Newman, B.; Paik, I. H.; Patil, S.; Purcell-Estabrook, E.; Shimizu, M.; Shum, P.; Standley, S.; Taborn, K.; Tripathi, S.; Yang, H.; Yin, Y.; Zhao, X.; Dale, E.; Vargeese, C. Impact of Guanidine-Containing Backbone Linkages on Stereopure Antisense Oligonucleotides in the CNS. *Nucleic Acids Res.* **2022**, *50* (10), 5401–5423. https://doi.org/10.1093/nar/gkac037.

(33) Michel, T.; Debart, F.; Vasseur, J. J. Efficient Guanidination of the Phosphate Linkage towards Cationic Phosphoramidate Oligonucleotides. *Tetrahedron Lett.* **2003**, *44* (35), 6579–6582. https://doi.org/10.1016/S0040-4039(03)01694-0.

(34) Skakuj, K.; Bujold, K. E.; Mirkin, C. A. Mercury-Free Automated Synthesis of Guanidinium Backbone Oligonucleotides. *J. Am. Chem. Soc.* **2019**, *141* (51), 20171–20176. https://doi.org/10.1021/jacs.9b09937.

(35) Dempcy, R. O.; Almarsson, Ö.; Bruice, T. C. Design and Synthesis of Deoxynucleic Guanidine: A Polycation Analogue of DNA. *Proc. Natl. Acad. Sci. U. S. A.* **1994**, *91* (17), 7864–7868. https://doi.org/10.1073/pnas.91.17.7864.

(36) Mirkin, C. A.; Letsinger, R. L.; Mucic, R. C.; Storhoff, J. J. A DNA-Based Method for Rationally Assembling Nanoparticles into Macroscopic Materials*. *Spherical Nucleic Acids* **2020**, *382* (August), 3–11. https://doi.org/10.4324/9780429200151-2.

(37) Cutler, J. I.; Auyeung, E.; Mirkin, C. A. Spherical Nucleic Acids. *J. Am. Chem. Soc.* **2012**, *134* (3), 1376–1391. https://doi.org/10.1021/ja209351u.

(38) Cutler, J. I.; Zhang, K.; Zheng, D.; Auyeung, E.; Prigodich, A. E.; Mirkin, C. A. Polyvalent Nucleic Acid Nanostructures. *J. Am. Chem. Soc.* **2011**, *133* (24), 9254–9257. https://doi.org/10.1021/ja203375n.

(39) Teplensky, M. H.; Evangelopoulos, M.; Dittmar, J. W.; Forsyth, C. M.; Sinegra, A. J.; Wang, S.; Mirkin, C. A. Multi-Antigen Spherical Nucleic Acid Cancer Vaccines. *Nat. Biomed. Eng.* **2023**, *7* (July). https://doi.org/10.1038/s41551-022-01000-2.

(40) Radovic-Moreno, A. F.; Chernyak, N.; Mader, C. C.; Nallagatla, S.; Kang, R. S.; Hao, L.; Walker, D. A.; Halo, T. L.; Merkel, T. J.; Rische, C. H.; Anantatmula, S.; Burkhart, M.; Mirkin, C. A.; Gryaznov, S. M. Immunomodulatory Spherical Nucleic Acids. *Proc. Natl. Acad. Sci. U. S. A.* **2015**, *112* (13), 3892–3897. https://doi.org/10.1073/pnas.1502850112.

(41) Kumthekar, P.; Ko, C. H.; Paunesku, T.; Dixit, K.; Sonabend, A. M.; Bloch, O.; Tate, M.; Schwartz, M.; Zuckerman, L.; Lezon, R.; Lukas, R. V.; Jovanovic, B.; McCortney, K.; Colman, H.; Chen, S.; Lai, B.; Antipova, O.; Deng, J.; Li, L.; Tommasini-Ghelfi, S.; Hurley, L. A.; Unruh, D.; Sharma, N. V.; Kandpal, M.; Kouri, F. M.; Davuluri, R. V.; Brat, D. J.; Muzzio, M.; Glass, M.; Vijayakumar, V.; Heidel, J.; Giles, F. J.; Adams, A. K.; James, C. D.;

Woloschak, G. E.; Horbinski, C.; Stegh, A. H. A First-in-Human Phase 0 Clinical Study of RNA Interference-Based Spherical Nucleic Acids in Patients with Recurrent Glioblastoma. *Sci. Transl. Med.* **2021**, *13* (584). https://doi.org/10.1126/scitranslmed.abb3945.

(42) Wu, X. A.; Choi, C. H. J.; Zhang, C.; Hao, L.; Mirkin, C. A. Intracellular Fate of Spherical Nucleic Acid Nanoparticle Conjugates. *J. Am. Chem. Soc.* **2014**, *136* (21), 7726–7733. https://doi.org/10.1021/ja503010a.

(43) Bellettato, C. M.; Scarpa, M. Possible Strategies to Cross the Blood-Brain Barrier. *Ital. J. Pediatr.* **2018**, *44* (Suppl 2), 1DUNNY. https://doi.org/10.1186/s13052-018-0563-0.

(44) Beaucage, S. L.; Iyer, R. P. Advances in the Synthesis of Oligonucleotides by the Phosphoramidite Approach. *Tetrahedron* **1992**, *48* (12), 2223–2311. https://doi.org/10.1016/S0040-4020(01)88752-4.

(45) Vlaho, D.; Damha, M. J. Synthesis of Chimeric Oligonucleotides Having Modified Internucleotide Linkages via an Automated H-Phosphonate/Phosphoramidite Approach. *Curr. Protoc. Nucleic Acid Chem.* **2018**, *73* (1), 1–15. https://doi.org/10.1002/cpnc.53.

(46) Liu, J.; Lu, Y. Preparation of Aptamer-Linked Gold Nanoparticle Purple Aggregates for Colorimetric Sensing of Analytes. *Nat. Protoc.* **2006**, *1* (1), 246–252. https://doi.org/10.1038/nprot.2006.38.

(47) Beaucage, S. L.; Caruthers, M. H. Deoxynucleoside Phosphoramidites-A New Class of Key Intermediates for Deoxypolynucleotide Synthesis. *Tetrahedron Lett.* **1981**, *22* (20), 1859–1862. https://doi.org/10.1016/S0040-4039(01)90461-7.

(48) Kraszewski, A.; Stawinski, J. H-Phosphonates: Versatile Synthetic Precursors to Biologically Active Phosphorus Compounds. *Pure Appl. Chem.* **2007**, *79* (12), 2217–2227. https://doi.org/10.1351/pac200779122217.

(49) Beardsley, R. L.; Reilly, J. P. Optimization of Guanidination Procedures for MALDI Mass Mapping. *Anal. Chem.* **2002**, *74* (8), 1884–1890. https://doi.org/10.1021/ac015613o.

(50) Al Temimi, A. H. K.; Amatdjais-Groenen, H. I. V.; Reddy, Y. V.; Blaauw, R. H.; Guo, H.; Qian, P.; Mecinović, J. The Nucleophilic Amino Group of Lysine Is Central for Histone Lysine Methyltransferase Catalysis. *Commun. Chem.* **2019**, *2* (1), 1–14. https://doi.org/10.1038/s42004-019-0210-8.

(51) Deglane, G.; Abes, S.; Michel, T.; Prévot, P.; Vives, E.; Debart, F.; Barvik, I.; Lebleu, B.; Vasseur, J. J. Impact of the Guanidinium Group on Hybridization and Cellular Uptake of Cationic Oligonucleotides. *ChemBioChem* **2006**, *7* (4), 684–692. https://doi.org/10.1002/cbic.200500433.

(52) Aldewachi, H.; Woodroofe, N.; Gardiner, P. Study of the Stability of Functionalized Gold Nanoparticles for the Colorimetric Detection of Dipeptidyl Peptidase IV. *Appl. Sci.* **2018**, *8* (12). https://doi.org/10.3390/app8122589.

(53) Hurst, S. J.; Lytton-Jean, A. K. R.; Mirkin, C. A. Maximizing DNA Loading on a Range of Gold Nanoparticle Sizes. *Anal. Chem.* **2006**, *78* (24), 8313–8318.

https://doi.org/10.1021/ac0613582.
(54) Bhowmik, A.; Khan, R.; Ghosh, M. K. Blood Brain Barrier: A Challenge for Effectual Therapy of Brain Tumors. *Biomed Res. Int.* **2015**, *2015*. https://doi.org/10.1155/2015/320941.
(55) Dong, X. Current Strategies for Brain Drug Delivery. *Theranostics* **2018**, *8* (6), 1481–1493. https://doi.org/10.7150/thno.21254.
(56) Achar, A.; Ghosh, C. Multiple Hurdle Mechanism and Blood-Brain Barrier in Epilepsy: Glucocorticoid Receptor-Heat Shock Proteins on Drug Regulation. *Neural Regen. Res.* **2021**, *16* (12), 2427–2428. https://doi.org/10.4103/1673-5374.313046.
(57) Nagata, T.; Dwyer, C. A.; Yoshida-Tanaka, K.; Ihara, K.; Ohyagi, M.; Kaburagi, H.; Miyata, H.; Ebihara, S.; Yoshioka, K.; Ishii, T.; Miyata, K.; Miyata, K.; Powers, B.; Igari, T.; Yamamoto, S.; Arimura, N.; Hirabayashi, H.; Uchihara, T.; Hara, R. I.; Wada, T.; Bennett, C. F.; Seth, P. P.; Rigo, F.; Yokota, T. Cholesterol-Functionalized DNA/RNA Heteroduplexes Cross the Blood–Brain Barrier and Knock down Genes in the Rodent CNS. *Nat. Biotechnol.* **2021**, *39* (12), 1529–1536. https://doi.org/10.1038/s41587-021-00972-x.
(58) Liu, X. Clinical Trials of Intranasal Delivery for Treating Neurological Disorders a Critical Review. *Expert Opin. Drug Deliv.* **2011**, *8* (12), 1681–1690. https://doi.org/10.1517/17425247.2011.633508.
(59) Huo, S.; Jin, S.; Ma, X.; Xue, X.; Yang, K.; Kumar, A.; Wang, P. C.; Zhang, J.; Hu, Z.; Liang, X. J. Ultrasmall Gold Nanoparticles as Carriers for Nucleus-Based Gene Therapy Due to Size-Dependent Nuclear Entry. *ACS Nano* **2014**, *8* (6), 5852–5862. https://doi.org/10.1021/nn5008572.
(60) Jana, N. R.; Gearheart, L.; Murphy, C. J. Seeding Growth for Size Control of 5-40 Nm Diameter Gold Nanoparticles. *Langmuir* **2001**, *17* (22), 6782–6786. https://doi.org/10.1021/la0104323.
(61) Brust, M.; Walker, M.; Bethell, D.; Schiffrin, D. J.; Whyman, R. 0864.Chem.Commun.1994,801.Pdf. **2000**, 801–802.
(62) Xia, N.; Wu, Z. Controlling Ultrasmall Gold Nanoparticles with Atomic Precision. *Chem. Sci.* **2021**, *12* (7), 2368–2380. https://doi.org/10.1039/d0sc05363e.
(63) Lahnsteiner, M.; Kastner, A.; Mayr, J.; Roller, A.; Keppler, B. K.; Kowol, C. R. Improving the Stability of Maleimide–Thiol Conjugation for Drug Targeting. *Chem. - A Eur. J.* **2020**, *26* (68), 15867–15870. https://doi.org/10.1002/chem.202003951.
(64) Renault, K.; Fredy, J. W.; Renard, P. Y.; Sabot, C. Covalent Modification of Biomolecules through Maleimide-Based Labeling Strategies. *Bioconjug. Chem.* **2018**, *29* (8), 2497–2513. https://doi.org/10.1021/acs.bioconjchem.8b00252.
(65) Dmitrenko, O.; Thorpe, C.; Bach, R. D. Mechanism of SN2 Disulfide Bond Cleavage by Phosphorus Nucleophiles. Implications for Biochemical Disulfide Reducing Agents. *J. Org. Chem.* **2007**, *72* (22), 8298–8307.

https://doi.org/10.1021/jo071271w.

(66) Getz, E. B.; Xiao, M.; Chakrabarty, T.; Cooke, R.; Selvin, P. R. A Comparison between the Sulfhydryl Reductants Tris(2- Carboxyethyl)Phosphine and Dithiothreitol for Use in Protein Biochemistry. *Anal. Biochem.* **1999**, *273* (1), 73–80. https://doi.org/10.1006/abio.1999.4203.

(67) Choi, C. H. J.; Hao, L.; Narayan, S. P.; Auyeung, E.; Mirkin, C. A. Mechanism for the Endocytosis of Spherical Nucleic Acid Nanoparticle Conjugates. *Proc. Natl. Acad. Sci. U. S. A.* **2013**, *110* (19), 7625–7630. https://doi.org/10.1073/pnas.1305804110.